INVESTIGATION OF THE FATIGUE BEHAVIOUR OF METALLIC COMPONENTS USED IN PLATE HEAT EXCHANGERS UNDER VARIABLE DYNAMIC LOADS

A Thesis Submitted to
the Graduate School of Engineering and Sciences of
İzmir Institute of Technology
in Partial Fulfilment of the Requirements for the Degree of

MASTER OF SCIENCE

in Mechanical Engineering

by

Yiğit HAYTA

July 2020
İZMİR

ACKNOWLEDGMENTS

I would like to extend my sincerely gratitude to my supervisor Assoc. Prof. Dr. Sinan Kandemir. He always supported me during my master thesis study and gave me the chance to work on this cooperative study with Bosch Thermotechnology. I am thankful to him for his guidance.

I would like to express my deepest appreciation to Mr. Remzi Acar, Bosch Thermotechnology Manisa Engineering Product Quality Manager and Mr. Aydın Doğu Yıldırım, Reliability Expert in Engineering Product Quality Department for giving me the opportunity to proceed this study by supporting me both in technical and managerial aspects. This study could not be finished without their support.

I am also deeply indebted to Mehmet Deniz Güneş for his precious help during experimental study and to Yiğit Gürler for his valuable support during finite element analysis.

Finally, I would like to thank to my parents and extend my appreciation to them for always supporting and encouraging me through all my life.

ABSTRACT

INVESTIGATION OF THE FATIGUE BEHAVIOUR OF METALLIC COMPONENTS USED IN PLATE HEAT EXCHANGERS UNDER VARIABLE DYNAMIC LOADS

Plate heat exchanger (PHE) is a component that provides heat to be transferred from hot water to domestic cold water without mixing of them with a high efficiency. Over the lifetime of the PHE, cyclic pressures act on the brazing points and the plates, and this may lead to fatigue failure. The fatigue behaviours of the PHEs which are designed by using copper brazed 316L and 304L stainless steels, were investigated in this thesis by performing strain based fatigue tests to also seek the feasibility of the use of 304L stainless steel in PHE production to reduce the cost. Besides, the microstructural investigation of the brazed regions was conducted and, the tensile tests for both non-brazed and brazed steel specimens were performed in order to determine the mechanical properties of the samples. The fatigue tests were carried out with twelve specimens for each sample groups at four different load levels as displacement (strain) controlled with a stress ratio of R=0 and 5 Hz frequency. Finite Element Analysis (FEA) was performed to determine the strain distribution on the plates of PHEs during their operation to estimate the lifetime of PHEs by using the generated lifetime curves based on the fatigue tests. Consequently, it was obtained that the ultimate tensile strength and fracture strain of non-brazed steel specimens are higher than those of the brazed specimens. The Scanning Electron Microscopy (SEM) analysis shows that; copper can diffuse into 316L easier than 304L and the use of copper foil with 50 μm thickness results in more defect at brazing regions compared to 100 μm thickness. Hereunder the fatigue test results, Weibull Analysis was performed and the fatigue life curves were generated. It was found that 316L brazed joint has approximately 33 times greater fatigue life than 304L brazed joint and filler metal thickness is more likely to have a linear relationship with fatigue life. Finally, fatigue lives of each sample group were calculated based on the loads determined by FEA. The results suggest that either 316L or 304L stainless steels can be used as PHE material as both materials satisfy the lifetime requirement of 15 years which was preliminarily defined by Bosch Thermotechnology (TT).

ÖZET

PLAKALI EŞANJÖRLERDE KULLANILAN METALİK KOMPONENTLERİN DEĞIŞKEN DINAMIK YÜKLER ALTINDA YORULMA DAVRANIŞININ INCELENMESI

Yüksek ısı transfer verimine sahip olan plakalı eşanjörler, plakaların bakır kullanılarak birbirine lehimlenmesi ile üretilir ve kullanımları sırasında oluşan basınç çevrimleri lehim noktalarında ve plakalar üzerinde çevrimsel yükler oluşturur. Bu çalışmada, plakalı eşanjörlerde kullanılan bakır ile lehimlenmiş 316L ve 304L paslanmaz çeliklerin yorulma davranışı uzama kontrollü yorulma testleri gerçekleştirilerek incelenmiştir ve 316L'ye göre daha ucuz olan 304L'nin plakalı eşanjörlerde kullanımı değerlendirilmiştir. Yorulma testleri her test numunesi grubu için on ikişer numune ile R=0 gerilme oranı ve 5 Hz çevrim frekansında gerçekleştirilmiştir. Yorulma testlerinin yanında, malzemelerin mekanik özelliklerini tespit etmek için hem lehimlenmemiş çelik hem de bakır ile lehimlenmiş test numunelerinin çekme testleri de yapılmıştır. Lehimli numunelerin mikro yapı incelemeleri de optik mikroskop ve taramalı elektron mikroskobu kullanılarak gerçekleştirilmiştir. Plakalı eşanjörlerin üzerinde oluşan yük dağılımları sonlu elemanlar analizi yapılarak belirlenmiş, yorulma testleri sonucunda oluşturulan ömür eğrileri kullanılarak belirlenen yüklerin eğride karşılık geldiği kopma süreleri tespit edilmiştir. Çekme testleri lehimsiz çeliğin, lehimlenmiş çelikten daha yüksek çekme mukavemetine ve kopma uzamasına sahip olduğunu göstermiştir. Mikro yapı incelemesi, bakırın 316L paslanmaz çeliğine 304L'ye göre daha iyi nüfuz ettiğini ve 50 µm bakır folyo kalınlığının 100 µm'ye göre lehim bölgesinde daha fazla boşluklar oluşmasına sebep olduğunu göstermiştir. Yorulma test sonuçları kullanılarak Weibull Analizi gerçekleştirilmiş ve malzemelerin farklı yüklerdeki yorulma dayanımlarının belirlenebilmesi için ömür eğrileri oluşturulmuştur. Sonuçlar; bakır ile lehimlenmiş 316L'nin 304L'ye göre yaklaşık 33 katı kadar uzun ömürlü olduğunu, bakır lehim malzemesi kalınlığının da büyük oranda ömür süresi ile doğru orantılı olduğunu işaret etmektedir. Sonlu elemanlar analizi kullanılarak belirlenen yüklere ve oluşturulan ömür eğrilerine göre, analizin yapılmış olduğu plakalı eşanjör dizaynı için 316L ve 304L paslanmaz çeliklerin ikisinin de, Bosch Termoteknik tarafından tanımlanan 15 yıllık ömür kriterini sağladığı ve kullanılabilir olduğu görülmüştür.

TABLE OF CONTENTS

LIST OF FIGURES

Figure **Page**

Figure **Page**

Figure **Page**

Figure **Page**

LIST OF TABLES

Table **Page**

CHAPTER 1

INTRODUCTION

In today's world, energy efficiency is very important in heating systems. It means that, ratio of generated heat to used energy has to be as high as possible according to people's demand. Using an energy efficient heating system massively reduces the needed energy amount for heating purposes in properties. Although the use of insulation materials in buildings have dramatically improved energy efficiency in recent years, there is also significant potential to further contribute to energy efficiency in heating processes. Therefore, there could be a big impact on protecting the environment by reducing the carbon foot print and this can help complying with environmental regulations and financial saving [1].

There are different types of heating techniques such as furnaces, boilers, heat pumps, electrical heaters, air conditioning units and fireplaces. General expectation from all of them is that the heating must be fast enough with high efficiency. Considering domestic use for both heating property and providing hot tap water, combinational boiler, also commonly known as combi boiler, is one of the widely used devices for such applications because of the several advantages such as saving space in properties with combining both domestic water heating and central heating (CH) into one single unit, supplying the domestic hot water (DHW) directly with its mains pressure and their relatively lower cost compare to conventional heating systems like furnaces, wood-burning stoves and gas-fired heaters [2]. Combi boilers and PHEs as the topic of this thesis are discussed in details in the following section.

1.1. Definition of Combi Boiler

Combi boiler is a combination of CH and a high efficiency domestic water heater in an assembled single compact unit which generally uses the energy generated by mostly combustion of natural gas. All heating demand can be met by one combi boiler inside a property as illustrated in Figure 1.1. Combi boilers produce hot water to be fed into radiators in a closed loop circuit for heating purposes and they also heat the domestic water directly from the mains water inside of a PHE when hot water is demanded from a tap [3].

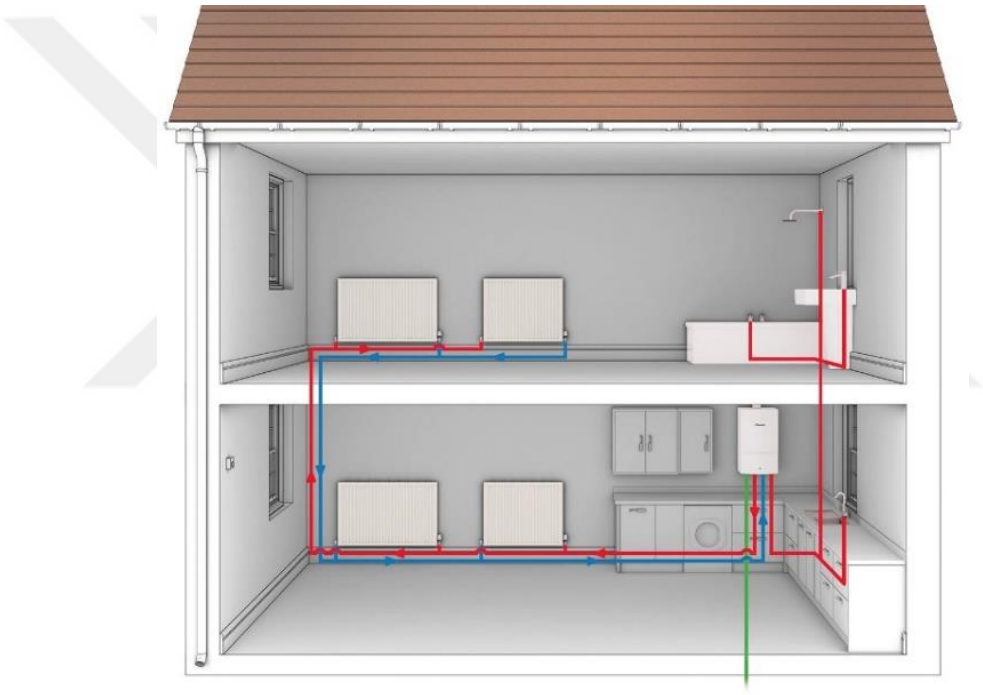

Figure 1.1. Illustration of a heating system which uses a combi boiler [2]

Combi boilers work in two different modes. The first one is CH mode. In this mode, the closed circuit water is heated by means of combi boiler's main (primary) heat exchanger by the burning of a suitable gas. Hot water is then circulated through the radiators with a pump inside the combi boiler. As illustrated in Figure 1.2, PHE inlet gate is closed by three-way valve component to let the water pass through the radiators. By this way, hot CH water is circulated within the radiators to warm a property. The water

that is cooled down due to the heat loss in radiators returns to the primary heat exchanger to be reheated.

The second one is the DHW mode. It is activated when hot water is demanded from a tap. When the water flows from the tap, a signal which is created by flow sensor, is sent to three way valve component and DHW circuit is opened (hot CH water pass through the PHE inlet) and CH circuit is closed. It means that, in such conventional combi boilers, CH is closed during DHW demand by the system. During DHW mode operation, closed circuit water is heated by primary heat exchanger and circulated by pump throughout the first inlet of the PHE. From the second inlet of the PHE, domestic cold water (DCW) enters with the opposite flow direction compare to hot CH water and DCW is heated up with natural heat transfer. After this heat exchange is occurred, DHW proceeds to flow through the opened tap as shown in Figure 1.3.

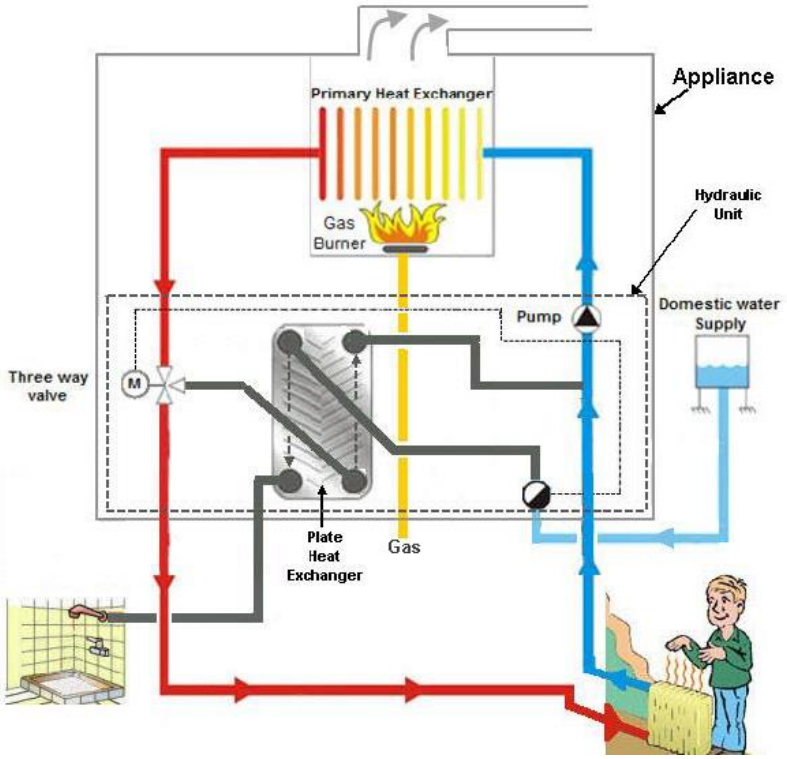

Figure 1.2. Illustration of CH working principal of combi boilers [4]

(Source: Gurler Yigit, 2018)

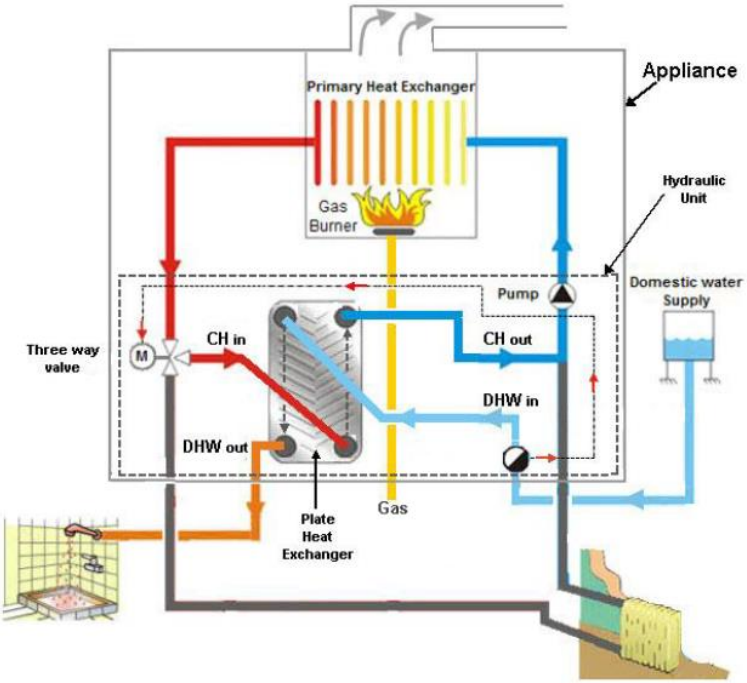

Figure 1.3. Illustration of DHW working principal of combi boilers [4]

(Source: Gurler Yigit, 2018)

1.2. Definition of Plate Heat Exchanger

Plate heat exchanger is a component which enables heat to be transferred from hot CH water to DCW without mixing both fluids (Figure 1.4). Total heat transfer surface of channel plates in PHE is very large and that makes the heat transfer quite efficient up to 97%. It is known that thickness of channel plate, water flow rate, number of channel plates, thermal conductivity of plate material and pattern on plates affect the heat transfer efficiency of PHE [5].

Figure 1.4. Compact brazed plate heat exchanger produced by Bosch TT

PHEs are generally produced by brazing method in order to join the channel plates to each other by using a filler material which is usually copper due to its ease of diffusion ability to steels, good wetting ability and corrosion resistance. In the production of PHEs, stainless steel plates and copper foils having the same shape and pattern which is shown in Figure 1.5, are stamped together. The commonly used materials for PHE production are 316L and 304L stainless steels. Currently, 316L is used in Bosch TT's PHE production due to its superior corrosion resistance compare to 304L stainless steel. However, 304L has also satisfactory corrosion resistance and it can also be used in PHE production once the endurance of it is proved by testing and analysis.

Figure 1.5. Stainless steel channel plate (a) and copper foil as filler material for brazing in production of PHEs for combi boilers (b)

After the forming of the pattern, the plates with foils are placed on the top of each other at the specified number as seen in Figure 1.6 (note that increasing plate number increases the heat transfer efficiency of PHE since it determines the operative heat transfer surface). In the final production stage; the stainless steel channel plates which are previously integrated with copper foils, are placed in the vacuum furnace and heated to a certain temperature where copper starts melting. Under vacuum conditions, molten

copper is accumulated around the peak points (closest points between two channel plates) of stainless steel plates by capillary motion and solidifies at those points which are called brazing points. A cross sectional view of a brazed compact PHE can be seen in Figure 1.11.

Figure 1.6. Copper foil between two stainless steel channel plates

Hot water heated to temperature up to 80 °C by primary heat exchanger (CH water) and DCW with a temperature higher than 0 °C enter the PHE from its inlets, respectively, as indicated in Figure 1.7. They flow in the opposite directions in order to increase heat transfer efficiency. DCW is heated up to 60 °C temperature and leaves the PHE as DHW.

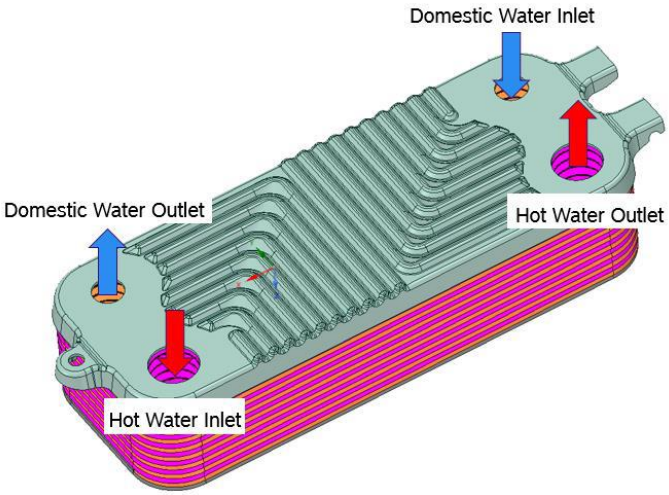

Figure 1.7. Computed Aided Design (CAD) model of PHE with inlets and outlets [6]

(Source: Gurler Yigit, 2018)

During the water flow inside the PHE (both DHW and CH), those two different water circuits do not mix since plates on PHE are brazed to each other in a way to separate them. Figure 1.8 schematically illustrates the exploded image of a PHE that also shows the directions of water flow between plates. Figure 1.9 shows a closed up image of the PHE indicating domestic water and CH water flows without mixing.

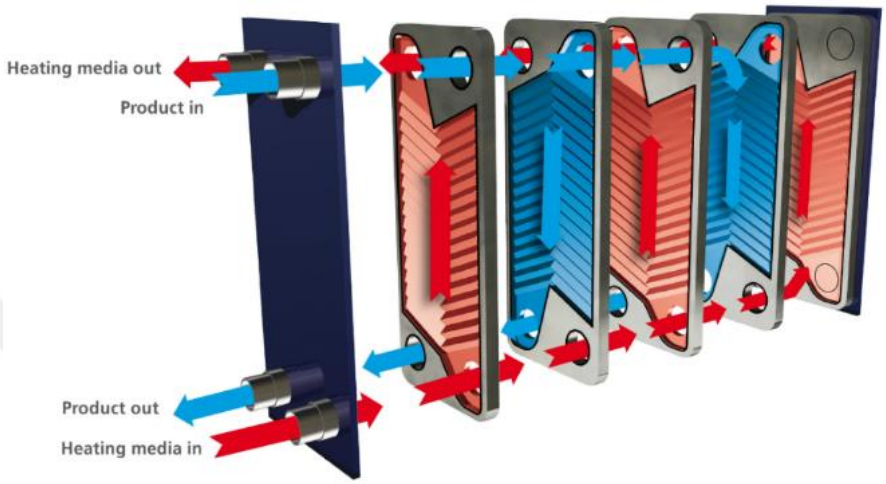

Figure 1.8. Exploded image of a PHE [7]

(Source: GEA Group Aktiengesellschaft, 2019)

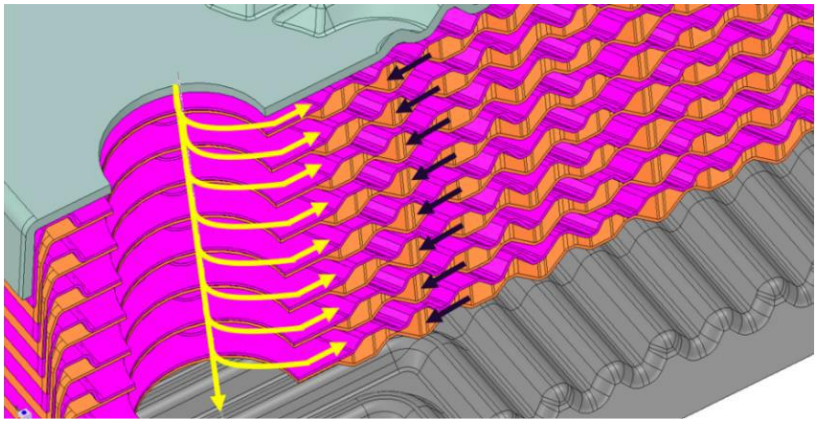

Figure 1.9. CAD model of PHE showing the water flows [6]

(Source: Gurler Yigit, 2018)

1.3. Problem Definition and Aim of the Study

Even if there is not tap water demand, stagnant domestic water which is fed from the mains, always stays inside the PHE. When the tap is opened for hot water demand in a property, stagnant domestic water inside the PHE starts flowing. After that, domestic water continuously flows inside the channels of the PHE through the tap and is heated up until it leaves the PHE. Cross sectional view of those channels and the flow diagram are illustrated in Figure 1.10.

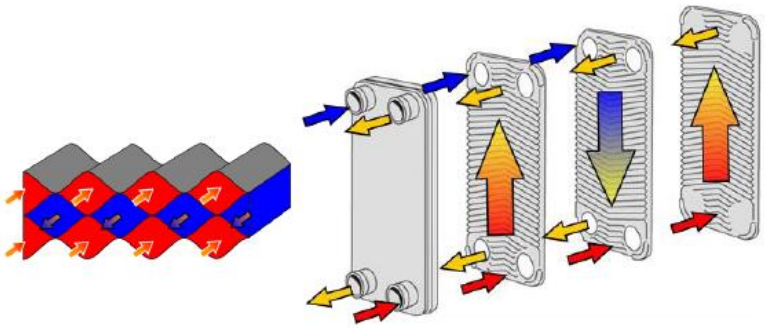

Figure 1.10. Directions of water flow inside the PHE. (Red represents hot CH water and blue represents DCW) [8]

(Source: Uhlig T et al., 2017)

Channel plates of a PHE are stamped together from the brazing points and the separation of channels are provided by means of such brazing junctions, those brazing points can be seen in Figure 1.11. Operational loads occurred on the channel plates, such as fluctuating pressures created when the tap is shortly opened and closed, are carried by those brazing points. Central heating side of the PHE generally has 1 – 1.5 bar as the system pressure which is widely accepted to be the optimum working pressure of the combi boilers to supply sufficient water amount to the closed circuit CH line. On the other hand, pressure of the domestic water side of the PHE changes based on the mains water line pressure level. When the tap valve is closed, static pressure of the water inside the PHE which is fed from mains, is generally accepted as 10 bar. If the tap valve is opened, that static pressure turns into dynamic pressure which is around 0.5 – 1 bar.

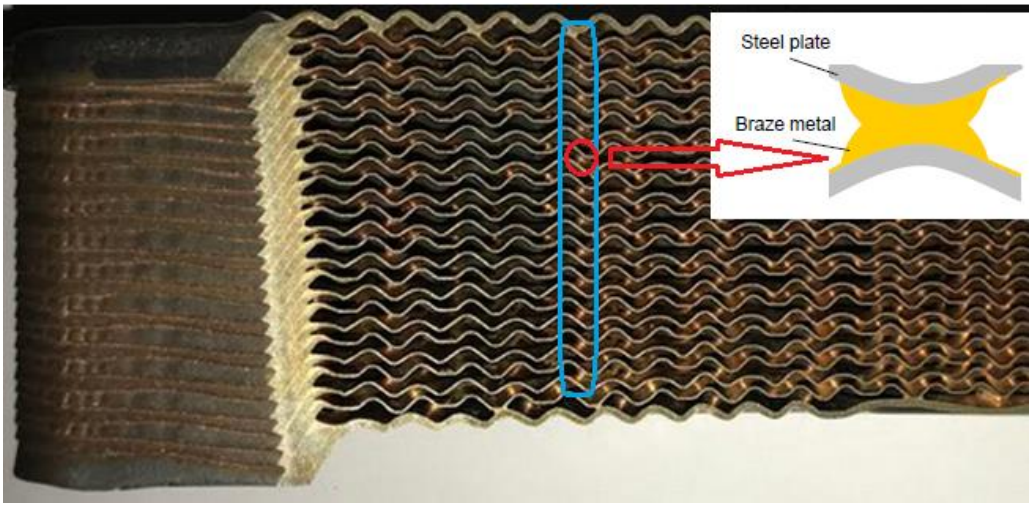

Figure 1.11. A cross-sectional view of a compact brazed PHE produced by Bosch TT indicating the brazing points

The flow rate of DHW inside the PHE ranges from 1 – 2 l/min to 14 – 16 l/min depending on the tap valve opening rate, flow rate limiter inside the combi boiler and mains pressure level. When the tap valve is suddenly closed after the end of a hot water demand, volume of water which flows in high velocity, hits the tap valve quickly and stops. The kinetic energy is transferred into a pressure wave when the flowing water hits to closed valve and this leads to the formation of a sudden pressure peak on the all domestic hot water circuit. This phenomena is called as water hammer [9].

Water hammer pressure peaks can deviate based on the flow rate of tap water, mains water pressure, pipe length in the system and tap valve closing time. General mains water pressure is accepted as 10 bar based on the field research and water hammer pressure peaks can generally be in the range of 10 – 16 bar accordingly. Whenever the tap valve is closed significantly fast, the water pressure in the system sharply peaks up to 16 bar and it is balanced at the mains pressure level which is around 10 bar. Water hammer pressure peak is calculated by using the Equation (1.1),

$$P_{(peak)} = \frac{(0.070).V.L}{t} + P_i\,[10] \qquad (1.1)$$

where P_i states mains pressure, V states water velocity when the tap is opened, L states the piping length from PHE to tap valve and t states the tap valve closing time.

The water hammer pressure peaks act on PHE brazing points as cyclic. According to Gaskeur which is an international certification brand for heating appliances, the number of DHW tapping (opening-closing) per day is defined as 49 in application category no 2. Category no 2 represents the usage of a combi boiler by a family which has four people [11]. It is accepted as standard tapping number per day for a boiler by Bosch TT. For a period of one year operation, PHE is exposed to about 20000 cycles of water hammer pressure peaks and it must withstand those loads at least 15 years as its defined minimum lifetime by Bosch TT. The total number of cyclic loads for 15 years lifetime of PHEs is defined by Bosch TT according to collected pressure loads from the field; these are 180000 and 120000 cycles for 10 bar and 16 bar pressure peaks respectively [9]. It is well known that cyclic loads can induce fatigue damage or failure of engineering components due to crack initiation and propagation [12]. The brazing points of PHEs which are subjected to water hammer cyclic loading, are prone to fatigue failure. Figure 1.12 shows an example of the 16 bar water hammer pressure peak after the tap is closed.

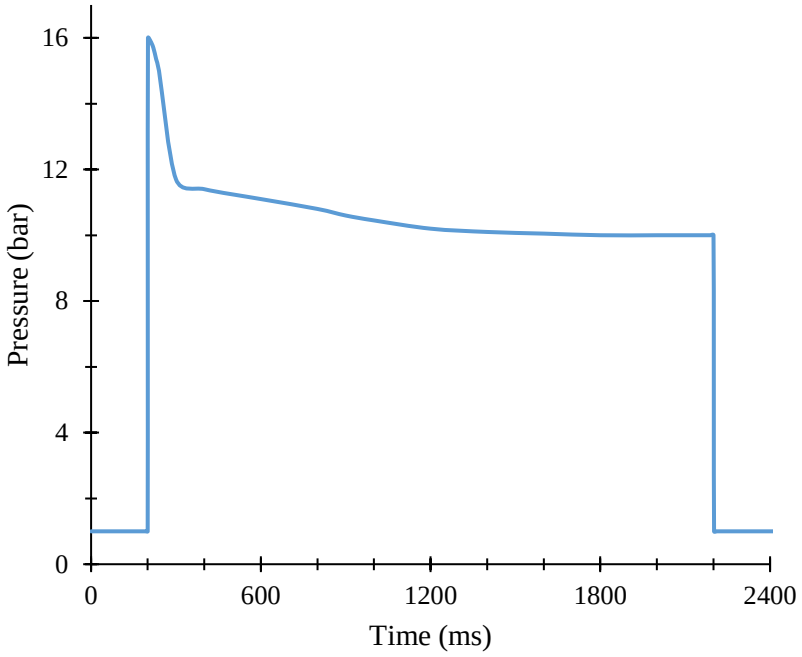

Figure 1.12. Water hammer pressure peak [9]

(Source: Bosch Thermotechnology Ltd, 2010)

It is obvious that there is a high water pressure difference between CH (1-1.5 bar) and DHW (up to 16 bar) sides of PHE. As illustrated in Figure 1.13, the water pressure acts as tensile load on the brazed region in PHEs since the DHW pressure is higher than the CH pressure. It is considered that the acting forces can rupture the brazing points and that resulting in the crack formation on the channel plates. Consequently, internal water leakage may be observed within those cracks and this leads to a massive failure of PHEs. The acting separation forces on the brazing points are also illustrated in the section view of PHE in Figure 1.14.

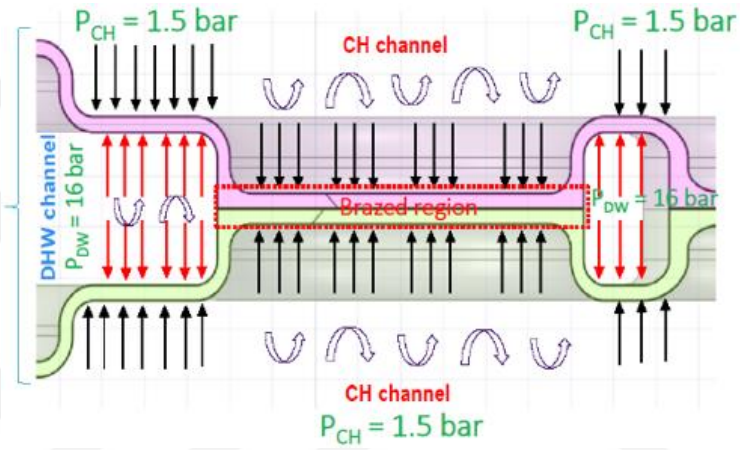

Figure 1.13. Acting loads on the brazing point of the PHE during water hammer [6]

(Source: Gurler Yigit, 2018)

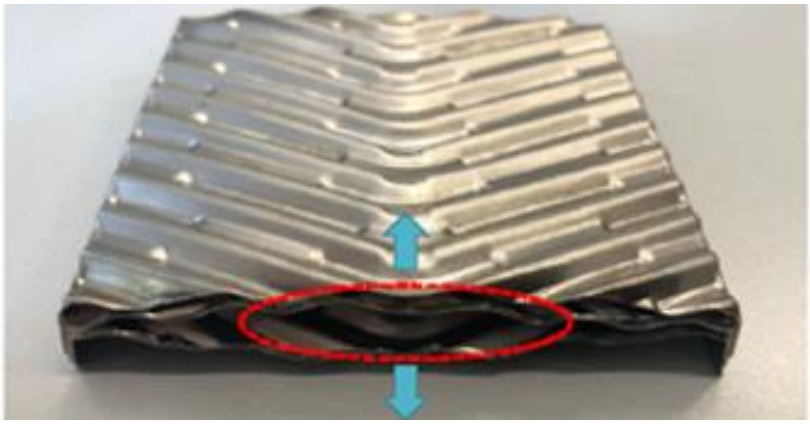

Figure 1.14. Separation forces acting on the PHE brazing points [6]

(Source: Gurler Yigit, 2018)

The pressure peaks create stress on the each brazing point in tension – tension direction. That stress depends on the design of the channel plates and the number of brazing points on them. In order to evaluate the endurance and lifetime of the produced PHEs, water hammer test is performed for the end products. However, the evaluation which is provided by water hammer testing is design depended because the load which is carried by each brazing point can be changed for different PHE designs. In order to make endurance evaluation independent from the design of the product and provide an overall endurance limit for brazed joint material, lifetime of the brazed stainless steel joint must be evaluated based on the examinations of material itself.

Finally, as mentioned in previous section, 304L stainless steel could be an alternative material for the PHE production with relatively lower cost compare to currently used 316L also by having a satisfactory corrosion resistance. This study aims to seek the feasibility of using 304L stainless steel for the production of combi boiler PHEs by determining the fatigue resistance of 304L copper brazed joints and comparing it with the examined fatigue life of 316L copper brazed joint stainless. Additionally, effect of filler material thickness on fatigue life of the copper brazed 316L stainless steel is also aimed to be determined by the performed fatigue tests. In this framework, fatigue life curves (strain versus failure cycle) of both copper brazed 316L and 304L stainless steels were obtained by performing fatigue tests for comparison. The results are used to estimate lifetime of new PHE design of Bosch TT by performing FEA. Therefore, the obtained data can also be used in future PHE designs as an endurance limit criterion to satisfy 15 years lifetime of the product during the design phase.

CHAPTER 2

THEORETICAL BACKGROUND AND LITERATURE REVIEW

This chapter mentions about the theoretical information which are used in this study for both experimental and numerical evaluations. Mechanical properties, testing of 316L and 304L stainless steels and vacuum brazing are briefly explained. Moreover, previously conducted studies about the fatigue behaviour of metallic components are also mentioned and evaluated in literature review section at the end of the chapter.

2.1. Mechanical Properties

Due to variety of acting forces, materials are exposed to different type of loads. Especially for the components under compressive or tensional forces, stress and strain are the affecting parameters on the lifetime of the products. Figure 2.1 illustrates the different types of loadings.

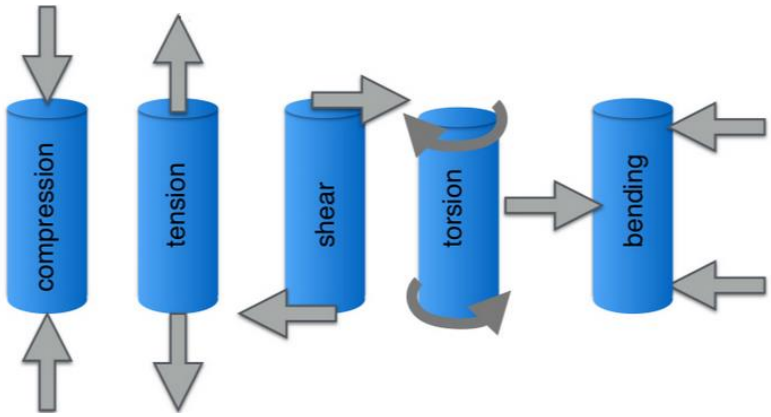

Figure 2.1. Types of loadings on components [13]

(Source: Collins Danielle, 2019)

Stress is a measure that can be calculated by the ratio of applied force to the cross sectional area of part where the load acts and strain is the amount of deformation or displacement on the material which is caused by the acting stress [13].

Engineering stress can be calculated by applied load divided to initial cross sectional area of the specimen as shown below in Equation 2.1.

$$\sigma = F/A_0 \tag{2.1}$$

Engineering strain can be defined by the length change of the specimen divided by the initial length and it is calculated by using the original specimen length [14].

$$\in = \Delta L/L_0 \tag{2.2}$$

If the material is exposed to loads that can plastically deform it, it starts necking after a certain point. That changes the cross sectional area of the part. This causes to a decrease in endurance and maximum load capacity of the part. Engineering stress does not take the instantaneous change in cross-sectional area into account. That's why, true stress is defined as load divided to instantaneous cross sectional area of the specimen [14].

$$\sigma_{true} = F/A_i \tag{2.3}$$

This is also similar for true strain. It can be calculated as;

$$\in_{true} = \ln(l_i/l_0) \tag{2.4}$$

The relation between engineering stress and strain to true stress and strain can be found in below [13].

$$\sigma_{true} = \sigma(1+\in) \tag{2.5}$$

$$\in_{true} = \ln(1+\in) \tag{2.6}$$

Figure 2.2 illustrates the comparison of engineering stress – strain and true stress – strain. Figure 2.3 demonstrates the deformation of a test specimen during a tensile test and designates the M point as ultimate tensile strength (UTS) which is the maximum stress that the test specimen can carry before the failure [14].

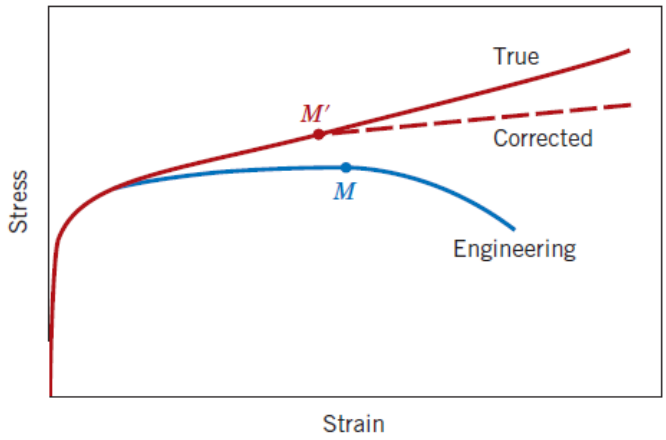

Figure 2.2. Comparison of engineering stress – strain and true stress – strain [14]

(Source: Callister William D., 2007)

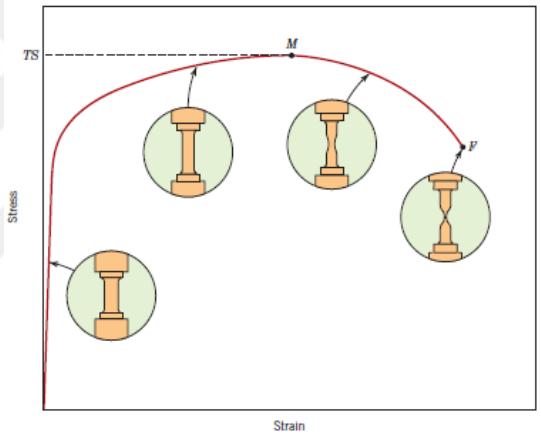

Figure 2.3. Deformed test specimens at different stages of the tensile test [14]

(Source: Callister William D., 2007)

The most common method for obtaining a stress – strain curve, the relation between them, is tensile test. Tensile test is performed in order to determine several mechanical properties such as yield strength, ultimate tensile strength, fracture stress and Young's modulus of the material. In a tensile test, a specimen is deformed until its fracture point by a constantly increasing load applied as uniaxial along the longer axis of the test specimen by using a tensile test machine which is schematically illustrated in Figure 2.4. This specimen is generally shaped as dog-bone in order to narrow the centre for locating the higher stress. During the test, the applied stress and strain can be calculated based on

known initial cross sectional area, applied load, initial length of specimen and elongation of it [14]. A stress – strain curve of a ductile material which has extensive plastic deformation and energy absorption before fracture, is illustrated in Figure 2.5 [15].

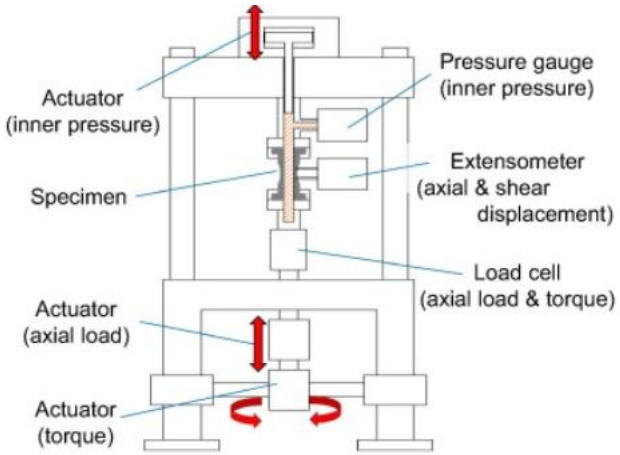

Figure 2.4. Schematic illustration of a tensile test device [16]

(Source: Takahiro Morishita et al., 2016)

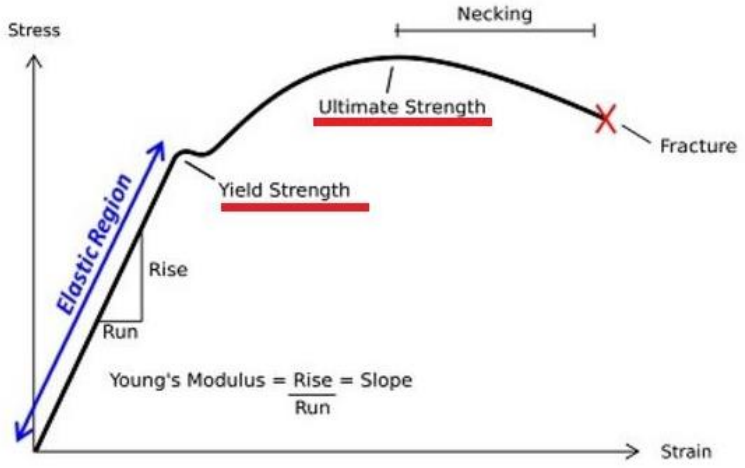

Figure 2.5. Stress – Strain curve of a ductile material [15]

(Source: Shukla Amit, 2018)

Ductility is a measure of the degree of plastic deformation until fracture. A material with opposite characteristic which has less plastic deformation until fracture, is called as brittle. Brittle materials also have low energy absorption before fracture compare

to ductile materials. Comparison of ductile and brittle materials' stress – strain curves are shown below in Figure 2.6 [14].

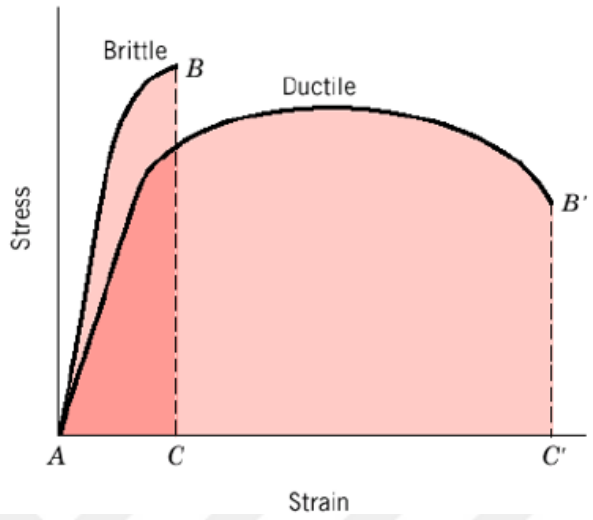

Figure 2.6. Brittle vs ductile material stress – strain graph [14]

(Source: Callister William D., 2007)

For most of the metals, there is a linear relationship between stress and strain at relatively lower stress levels. This is called as Hook's law. The value of that proportionality is known as Young's modulus or modulus of elasticity, E. Young's modulus is calculated by dividing the rise to run (slope) as shown in Figure 2.5. The deformation when the stress and strain have linear relationship is named as elastic deformation and it can also be seen in Figure 2.5 as elastic region. Elastic deformation is not permanent. It means that if the applied load is removed in elastic region, the material returns to its initial position and shape [14].

Generally for the metallic materials, elastic deformation is only acts up to strains about 0.5%. After that point, the stress is no longer linearly proportional to strain and plastic deformation which is permanent, starts after that point. Every metal and alloy comprise dislocations which are generated during solidification or rapid cooling processes. Movement of these dislocations due to increased stress triggers and starts the plastic deformation. During that, bonds are broken and atoms or molecules move respectively. After releasing the stress, they do not come back to initial position and shape. Representation of dislocation motion is given in Figure 2.7. The point that the

deformation turns from elastic to plastic is called as yield point and the phenomenon is called as yielding [14].

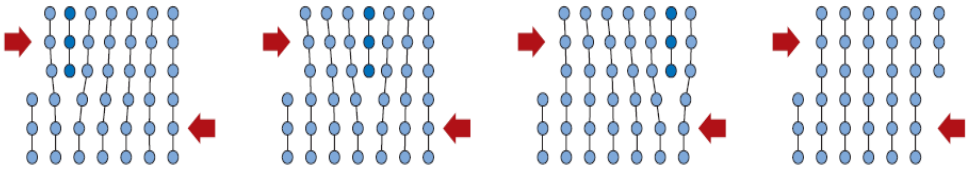

Figure 2.7. Representation of dislocation motion [14]

(Source: Callister William D., 2007)

For some materials, the proportional limit where the deformation is changed from elastic to plastic may not be easily determined. In these circumstances, the yield strength can be detected by applying strain offset method. For that purpose, a line is drawn parallel to the elastic portion of the stress-strain curve with an offset by 0.002 (0.2%) from its origin. Consequently, the yield strength can be obtained by intersecting the constructed 0.002 offset line with the stress versus strain curve as illustrated in Figure 2.8 [17].

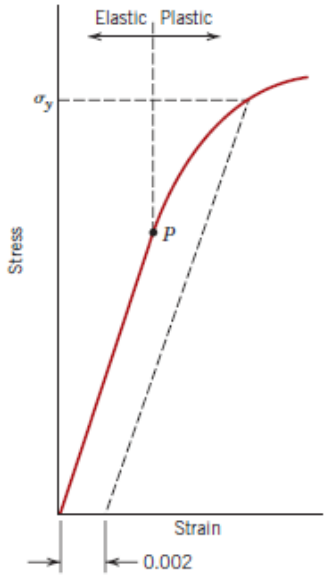

Figure 2.8. The proportional limit P and the yield strength of the material which is determined by using the 0.2% strain offset method [14]

(Source: Callister William D., 2007)

2.2. Fatigue and Fatigue Testing

Fatigue is a type of failure that can act on structures such as planes, bridges and plate heat exchangers which are exposed to cyclic stresses. It may results in failure at stress levels lower than the yield strength of the material due to long period of repeated load cycling. Fatigue is very important since 90% of the all metallic failures are triggered by it. It can suddenly occur without any sign and the fatigue phenomenon must be seriously considered when the components subjected to cycling loading are designed. Fatigue damage mechanism is specified by three stages which are crack initiation, crack propagation and failure. Crack is initiated at a point where the stress highly concentrated. Discontinuities are generated due to dislocation glide during stress cycling and they increase the stress at crack initiation sites. Then, they move and grow gradually with each stress cycle. Finally, failure occurs instantly when the crack size is increased to a critical value. The fracture surface of a fatigue failure can be described by two marks which are named as beachmarks and striations. They designate the location of the crack tip and seem as concentric blisters which sprawl from crack initiation sites. Beachmarks can usually be seen by naked eye and each beachmark line designates a duration of operation time when crack growth is occurred. Besides, striations have micro sizes and can only be investigated by using microscope [14].

Commonly, there are three different cycling stress types which can be seen in Figure 2.9. In Figure 2.9a, the stress is regularly sinusoidal with an amplitude of zero mean stress level. For that type, amplitudes of max and min applied stresses are equal to each other. That is called reversed stress cycle. Second one is represented in Figure 2.9b and it is also cyclic as sinusoidal but maximum and minimum stresses are not symmetrical relative to zero stress level. The mean stress is not equal to zero and that type is called as repeated stress cycle. Random stress cycle is the third one and it is illustrated in Figure 2.9c. It indicates that the stress level may vary randomly in terms of frequency and amplitude [14].

There are four parameters which characterize the stress cycles. First one is mean stress and it is calculated as in Equation 2.7.

$$\sigma_m = (\sigma_{max} + \sigma_{min})/2 \tag{2.7}$$

Second one is the stress range and can be calculated as in Equation 2.8.

$$\sigma_r = (\sigma_{max} - \sigma_{min}) \quad (2.8)$$

Third one is stress amplitude σ_a can be defined as the half of the range stress and can be calculated as in Equation 2.9.

$$\sigma_a = \sigma_r/2 \quad (2.9)$$

Lastly, the stress ratio R is the ratio of min stress to max stress on the material and can be calculated as in Equation 2.10 [14].

$$R = \sigma_{min}/ \sigma_{max} \quad (2.10)$$

Based on the operating conditions of the PHE, R is considered to be almost equal to zero due to acting stresses during water hammer fatigue cycles. When the tap is opened, the dynamic pressure on the DHW side of the PHE is around 1 bar during water flow. The opposite pressure on the brazing point from the CH water can range from 1 to 1.5 bar since it is accepted as the optimum working pressure of combi boilers. Consequently, they cancel each other during the tap water flow and that means the σ_{min} is equal to zero. On the other hand, max stress is eventuated during the instant closing of the tap. This means that the stress level fluctuates between zero and σ_{max}. So, cycling stress type during the working conditions of PHE can be defined as the repeated asymmetrical stress cycle.

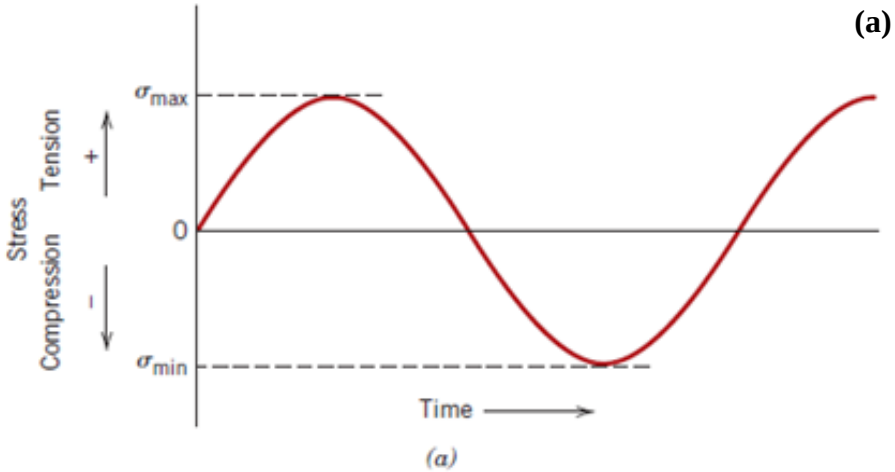

(cont. on next page)

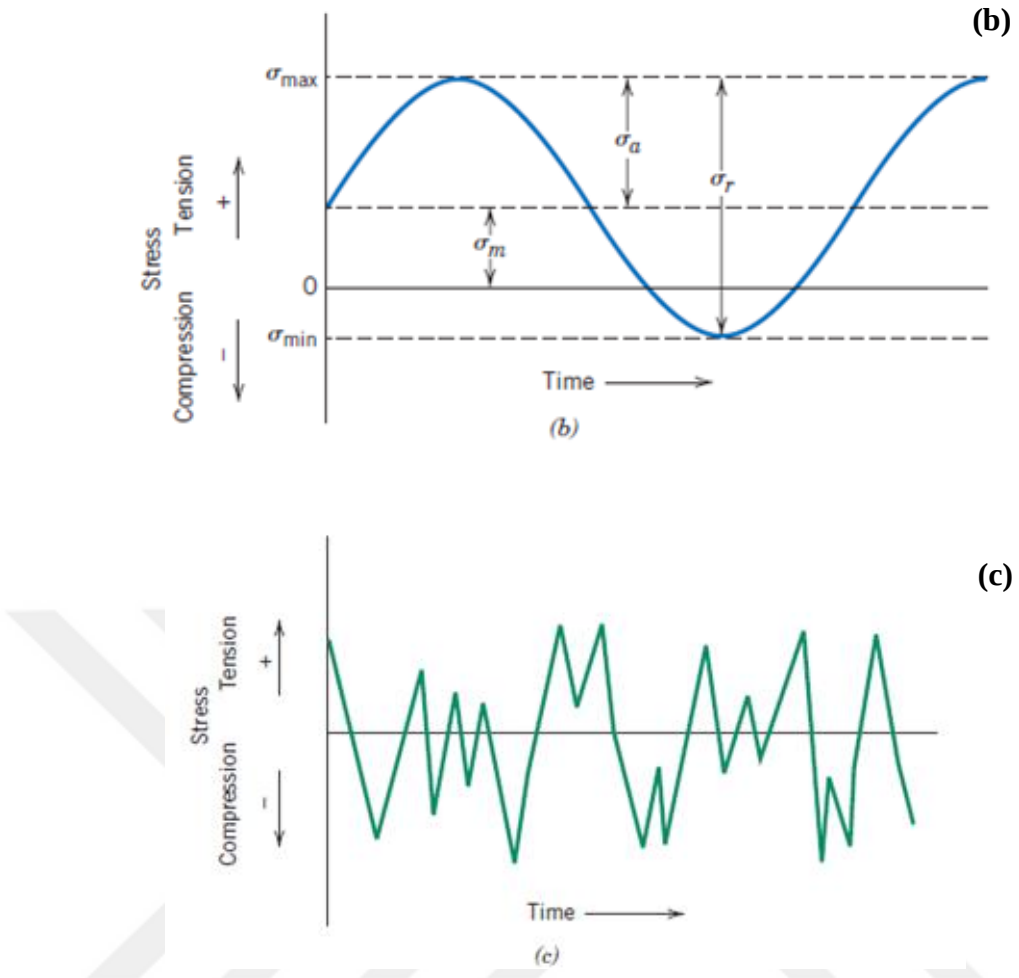

Figure 2.9. Acting stress types during fatigue: Reversed stress cycle (a), repeated stress cycle (b) and random stress cycle (c) [14]

(Source: Callister William D., 2007)

There several parameters which can affect fatigue behaviour of materials. These are mean stress level, part design, surface roughness on brazing surface and environmental conditions.

At first, mean stress effect is explained as increasing the mean stress, decreases the fatigue life of the material. Second is the design of the material and part. Notches or geometrical discontinuities can influence fatigue life by increasing the stress level. Smaller radius of curvature with less rounded fillets or grooves and threads can also increase stress resulting in a less fatigue life of the component [14]. Thirdly, for evaluating the surface roughness effect of brazed region on fatigue life, fatigue tests were performed by Yoshifumi Suezawa [18] with using a mild steel (SS41) as the base metal and Bag_8 eutectic alloy (Silver-Copper) as the filler material. The results showed that,

fatigue life of the material having a relatively rough brazing surface (ground with 60 and 120 mesh emery paper) is better than the one with smoother brazing surface (ground with 240, 400 and 600 mesh emery paper). So, it can be concluded that increasing surface roughness of brazing region also increases the fatigue life of the material since it gives opportunity to the filler material to deeply penetrate into the metals to be joint due to the higher asperities and deeper valleys [18]. Finally, due to environmental conditions, thermal fatigue and corrosion fatigue may operate. Thermal fatigue is caused by immediate temperature changes which is called thermal shock. Sudden and big temperature changes have an impact on the fatigue life, and mechanical load is not necessarily required for the thermal fatigue. The corrosion fatigue emerges when there is any chemical attack along with cyclic stresses [14]. Especially, pitting corrosion has a big impact on reducing the fatigue life since the corrosion pits behave like nucleation site to start fatigue crack. Stress concentration is increased on pit-rich regions and this results in a crack formation [19].

There are two types of fatigue based on the number of applied cycles until failure. These are high cycle fatigue and low cycle fatigue. Parts which are exposed to stresses lower than yield stress do not have plastic deformation. As a result of that, they have a longer fatigue lifetime. This is called as high cycle fatigue. For ductile metals, high cycle fatigue is considered as higher than 100000 cycles of fatigue life [20].

The parts which are exposed to stresses higher than yield point, have plastic deformation. As a result of that, they have short fatigue lifetime. This type of fatigue is called as low cycle fatigue. For ductile metals, low cycle fatigue is considered as lower than 100000 cycles of fatigue life [20].

Fatigue test is performed in order to determine the lifetime of a material which is exposed to cycling loading. The lifetime of those materials is determined by applying repetitive loading and unloading in tension, compression, bending, torsion or combinations of them. In order to perform a fatigue test, a specimen is tested with a fatigue test machine in predetermined test conditions such as the applied load, stress or strain ratio and frequency of the cycles. Test is stopped when the specimen is fractured. The fracture cycle is noted as the fatigue limit of that material regarding to applied load level [21].

Loadings during the fatigue test can be applied as rotating – bending or axial. During the rotating bending loading, the specimen is rotated by a motor at a constant revolutionary speed. In order to trigger a failure, a constant force is loaded on the specimen which creates a bending moment. This constant bending moment on a rotating test specimen generates stress. This stress starts from zero to a maximum tension stress, comes back to zero and then compressive stress acts cyclically as illustrated in Figure 2.10. [22]. In axial loading, specimen is not subjected to bending but tension and compression forces act during loading. Specimen is fixed from two ends and loaded cyclically with tensional or compressive loads [22]. Test machine is mostly the same with the tensile testing machine which is shown in Figure 2.4.

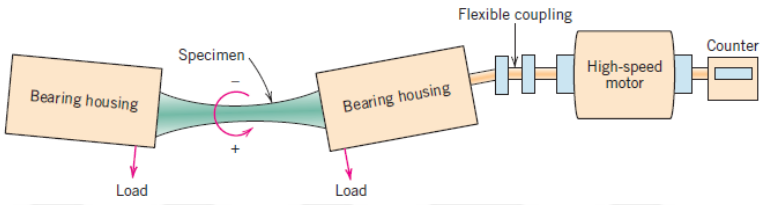

Figure 2.10. Illustration of rotating bending test [14]

(Source: Callister William D., 2007)

2.2.1. Fatigue Testing Methods

There are two types of fatigue testing methods which are stress life and strain life.

Stress life method is an analytical method which is used for estimating the lifetime of the material. In this method, the elastic stress range of the material is determined with a stress versus cycle curve (S-N) as illustrated in Figure 2.11. It designates the lifetime cycles of the material subjected to different stress levels according to the performed fatigue tests. Such tests are conducted as stress controlled. During the test, a specified stress level is applied to the specimen until the failure occurs and this is called as stress controlled fatigue test. The cycle of failure is specified as the fatigue life of the material for specified stress level. However, the use of stress life method is limited to high cycle fatigue applications which the applied stress is below yield stress. Since components are not subjected to plastic deformation, the applied stress during the test can be kept as

constant by means of negligible cross sectional area change with elastic deformation. Otherwise, cross – sectional area change during the test affects the acting stress on test specimen because the applied stress during the test is calculated according to applied constant force and initial cross – sectional area of the specimen when the test is started. Because of that, test data may be saved with a deviation than the real one [20] .

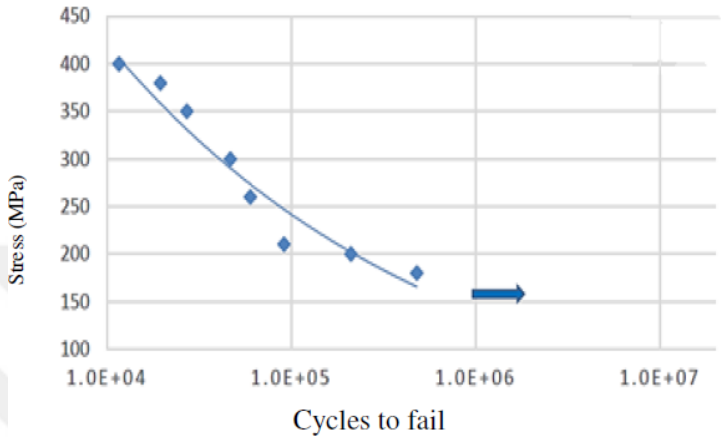

Figure 2.11. S-N curve for mild steel (ST 37) which has been tested with rotating bending load type having a stress ratio of R= -1 [23]

(Source: Ameed Ahmet, 2018)

On the other hand, strain life method considers the actual stress – strain data of the plastically deformed material due to cyclic loading. The effect of plastic strain can be precisely modelled compared to stress life method since the change in the cross sectional area does not have an effect on the saved strain data during the test. During the test; strain or displacement can be selected as the controlled parameter. The strain on the test specimen is measured by an extensometer or the test machine itself based on displacement of specimen. Thus, constant strain or displacement can be applied. Strain life method can be used also for the parts which have complicated geometries. It is applicable for both high cycle fatigue and low cycle fatigue since the applied strain which is the controlled parameter during the test, is independent from plastic deformation and can be constantly applied during the test [24].

The selection of appropriate method to carry out depends on the application and the loads. If the part is exposed to cycling stresses higher than yield strength, then strain

life method is required. If the part is under cycling stresses less than its yield point, both stress and strain life method can be applied to estimate fatigue life. Figure 2.12 shows a representative fatigue strain life curve, where the strain amplitude is defined as half of the difference between max and min applied strain during the test, reversal is number of change in direction of applied load which is twice of the failure cycle number [25].

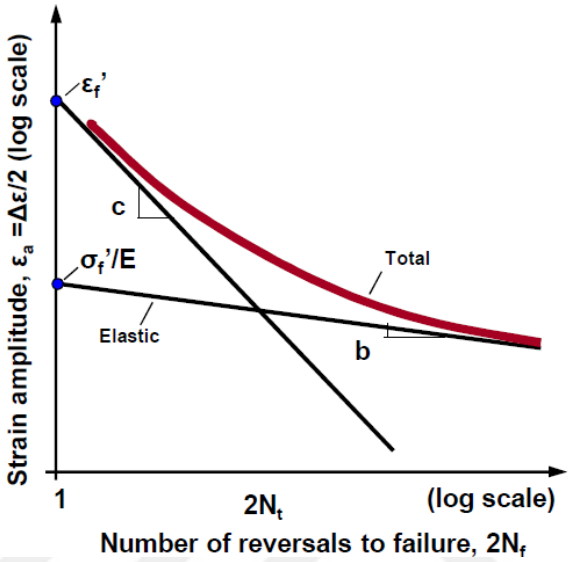

Figure 2.12. A representative fatigue strain-life curve [25]

(Source: Glinka Grzegorz, 2010)

Strain amplitude on a component can be calculated by using both Basquin's and Coffin-Manson equations to consider both elastic and plastic deformations together as given in equation 2.11. Equation 2.12 and 2.13 are used to calculate strain life parameters to determine fatigue behaviour of the materials.

$$\frac{\Delta\varepsilon}{2} = \frac{\sigma_f'}{E}(2N_f)^b + \varepsilon_f'(2N_f)^c \tag{2.11}$$

$$n' = \frac{\mathrm{b}}{\mathrm{c}} \tag{2.12}$$

$$H' = \frac{\sigma_f'}{(\varepsilon_f')^{n'}} \tag{2.13}$$

where, E is modulus of elasticity, σ_f' is strength coefficient, ε_f' is ductility coefficient, c is ductility exponent, b is strength exponent, n' is cyclic strain hardening exponent and H' is cyclic strength coefficient [26].

2.3. Properties of 316L and 304L Stainless Steels

In this section, the properties of 316L and 304L stainless steels are compared.

316L grade stainless steel is an austenitic stainless steel and one of the commonly used grades due to its high strength, high corrosion resistance with high concentrations of chromium, nickel and molybdenum. Its melting temperature is around 1380 °C and its maximum working temperature is around 800 °C. The addition of molybdenum improves its resistance to acids and chloride pitting [27].

304L grade stainless steel is also an austenitic stainless steel which is very frequently used due to its high strength, high durability, good corrosion and oxidation resistance with relatively high concentration of chromium. Its melting and working temperatures which are 1420 °C and 870 °C, are slightly higher than 316L stainless steel. It is widely used in wheel covers, storage tanks, electrical enclosures and kitchen equipment. The only weakness of 304L stainless steel is its resistance to pitting corrosion which can be triggered by chloride presence in the environment [27].

The presence of molybdenum and a larger amount of nickel in 316L stainless steel makes it a bit expensive than 304L stainless steel. However, they increase corrosion resistance and resistance against chlorides. Therefore, 316L stainless steel is favourable for applications which have to operate under potential chemical and corrosive conditions; such as marine parts, outdoor electrical enclosures, medical-surgical equipment, pharmaceutical instruments and chemical equipment [27].

The most important difference between 316 and 304 L stainless steel is that 316L has relatively more nickel and molybdenum in alloying content. Although they have similar mechanical properties, increased nickel content and addition of molybdenum make 316L more resistant to corrosion compared to 304L, especially to chlorides and salt. As a result of this, favourable corrosion resistance makes 316L stainless steel expensive than 304L stainless steel as 1.3 times higher [28]. If the working condition is very corrosive or contains chlorides, 316L stainless steel can be preferred to be used with higher cost. Yet, if the environment has milder acids or salt is not a concern, 304L stainless steel can also be used [27]. The mechanical properties and chemical composition of 316L stainless steel and 304L stainless steel are shown in Table 2.1 and 2.2.

Table 2.1. Mechanical properties of 316L and 304L stainless steels [29, 30]

(Source: ASM Aerospace Specification Metals Inc., 2020)

Property	316L	304L
Yield strength (MPa)	205	210
Ultimate tensile strength (MPa)	515	564
Fracture Strain	60 %	58 %
Modulus of Elasticity (GPa)	193	200
Vickers hardness	155	159

Table 2.2. Chemical composition of 316L and 304L stainless steels [29, 30]

(Source: ASM Aerospace Specification Metals Inc., 2020)

Element	wt%	
	316L	304L
C	0.03	0.03
Cr	17	18-20
Mn	2	2
Mo	2.5	-
Ni	12	8-12
P	0.045	0.045
Si	1	1
Fe	Bal.	Bal.

2.4. Vacuum Brazing

There are several applications which have high geometric complexity and specific material properties. That makes harder to have the final product with a single manufacturing process. Using conventional manufacturing processes such as milling, die sinking or drilling, increase the production duration and cost. In order to manufacture highly complex components, vacuum furnace brazing is performed to joint parts by using a precise and well defined heat treatment recipe [31].

Brazing is a metal jointing process that uses melted filler material in order to bond together two or more metals by containing a filler material with lower melting point than the base metal. It is different from welding because base metal is not melted during brazing. The filler material is suctioned through the gap between adjoining metals under vacuum by capillary action. Temperature is raised slightly above of the liquidus (melting)

temperature of the filler material. Then it flows between base metals which is known as wetting. Finally the product is cooled to unite the work pieces together. Brazing supplies considerably high strength than the filler metal but most likely to have less strength than base metal at the end of the process. Although joint strength is considered as less than welded joints, brazing operation provides a big advantage over welding as ability to joint dissimilar metals which have complex shapes easily [32].

Vacuum brazing is jointing process which is accomplished at high temperatures usually between 930 °C and 1230 °C by using nickel base alloy or pure copper as filler material. The benefit of vacuum brazing is that the vacuumed atmosphere can be precisely controlled. By this way, less residual oxygen level inside the vacuum is achieved and contamination of part is prevented. The naturally formed oxide layers on the base metals can be decomposed in a vacuum atmosphere at high temperature and it provides a better joint property such as high strength and less porosity by enhanced wetting. The distortion of the part is minimized by the help of precisely controlled heating and cooling rates. Additionally, vacuum brazing is favourable for lean and agile manufacturing due to repeatability and reliability of brazed joints [33]. An example of vacuum brazing furnace system is shown in Figure 2.13.

Figure 2.13. Vacuum brazing furnace system [33]

(Source: Kowalewski Janusz, 2006)

In order to have a high quality brazed joints, the parts must be closely fitted and the base metal's surface must be well cleaned. Ideal joint clearance is defined as between 0.03 mm and 0.08 mm in most cases in order to have a good capillary action which is explained as the ability of a liquid to flow in small gaps without external forces [34]. Brazing surface cleanliness is very important since contaminations on the surface can lead to not sufficient wetting. Chemical or mechanical cleaning can be applied in order to provide a proper surface for brazing. During the mechanical cleaning, it is important to have proper surface roughness since wetting can occur easily and be more effective on a rough surface than a smooth one [34].

The uniform capillary action can occur only if the all contaminants including any oil, oxide, grease and dirt are removed from the base metal and filler metal interface before the brazing operation. Water-base alkaline cleaners, solvent cleaning in mineral, alcohol, acetone and chlorinated hydrocarbons are the examples of agents used in chemical cleaning methods. Mechanical cleaning methods include grit blasting, machining and grinding operations [33].

The most critical factor during the process is most likely to be the brazing cycle. Brazing cycle is comprised of initial vacuum pump down, initial heating ramp, cement burn-off, stabilizing soak, heating ramp to brazing temperature, brazing soak and cooling down. The initial heating ramp should be 20 to 30° F/min (10 – 16° C/min) since higher rates may lead to distortion on the parts. For critical materials with complex designs, a cement burn off soak is included in the brazing cycle in order to prevent a high pressure rise. The soak supply the temperature to be equally distributed so the parts can reach brazing temperature uniformly. The final heating rate for brazing temperature is very important. It must be fast in order to prevent extremely high liquation of the filler material. The rates between 35 – 75° F/min (20 - 40° C /min) are considered to be the most optimum values to have sufficient brazing [33]. The brazing temperature time should be long enough to reach the required temperature on all parts. This duration mostly depends on the applied brazing technique, filler metal, base metal and it can be varied between 1 to 45 minutes [34]. A representative brazing cycle illustration can be seen in Figure 2.14.

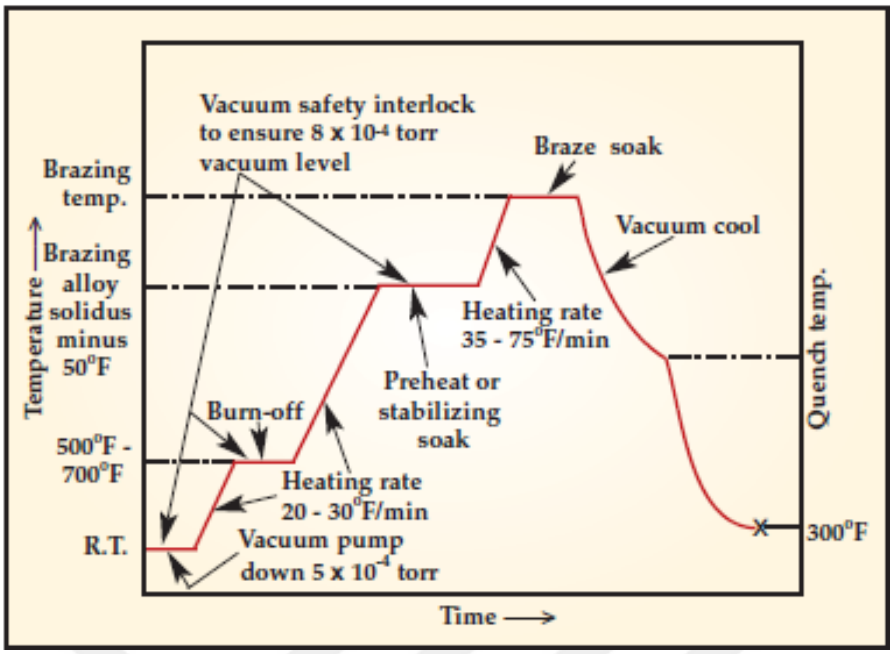

Figure 2.14. Illustration of a typical brazing cycle [33]

(Source: Kowalewski Janusz, 2006)

Filler material is selected based on applications to satisfy requirements which are withstand to servicing conditions, ability to wet and melt at a lower temperature than the base metals. Brazing filler material can be applied as in rod, ribbon, paste, wire or foil forms. Filler material is mostly placed on the brazing location before the process, especially in vacuum furnace brazing since the process is automated. The most common types of filler metals are; nickel alloy, pure copper, copper – silver, gold – silver and silver [34].

Proper vacuum level is another important parameter to have good wetting. Oxide amount in brazing environment can be decreased by vacuum, so brazing filler material can wet and flow over the surfaces of joining metal easily. 8 x 10^{-4} torr (0.1 Pa) is recommended for metal brazing applications [33].

During vacuum cooling, cooling gases are mostly used to shorten the brazing cycle and acquire good metallurgical properties. Argon or nitrogen can be used as cooling gas. Cooling must be done in two steps as shown in Figure 2.14 in order to prevent parts from being more brittle by minimizing thermal shocks, hence formation of cracks [33].

2.5. Literature Review

The previously conducted studies have been reviewed in this section in order to document the fatigue behaviour of the raw steel, welded and the brazed samples.

The fatigue behaviour of 316L stainless steel was studied via stress controlled fatigue tests by K.A. Mohammad et al. [35]. The fatigue tests were conducted with constant stress amplitude, 5 Hz frequency and a stress ratio of R = 0.1. After the test, microstructural analysis of fractured specimens was carried out by using SEM. It was seen that crack propagation presents a transgranular fracture mode. At the end of the tests, fatigue life curve (S-N) of the 316L stainless steel was determined and the fatigue limit from the results was constructed as 146.45 MPa at 3946882 cycles which means part reaches to its infinite life at a stress level below 146.45 MPa [35]. Room temperature fatigue properties of 316L stainless steel in tension and characteristics of fracture surface were studied by Xiao Zhao [36]. In the study, stress controlled fatigue tests were performed with a stress ratio of R = 0. The conducted fracture surface analysis showed that fatigue striations are present at the crack propagation region and cracks were initiated mostly from defects on the specimen surface. S-N curve shows that fatigue life of 316L stainless steel decreases linearly in low cycle regime [36]. The effect of various frequencies, i.e. 20 kHz, 140, 20, 2 and 0.2 Hz, on the fatigue behaviour of JIS S15C low carbon steel was investigated by Benjamin Guennec et al. [37]. The fatigue tests were conducted at room temperature with a stress ratio of R = -1 meaning that tests were done in tension-compression. It was shown that fatigue strength inclines to rise by increasing testing frequency which can be explained by the work hardening mechanism due to increased number of dislocations act as obstacle to other dislocation lines and make the dislocation motion harder. Besides, fatigue limits at the testing frequencies between 2 and 140 Hz are very close to each other and the differences are regarded as insignificant [37].

The fatigue behaviour of laser welded T-joint 304L stainless steel under tension-tension was studied by Søren Heide Lambertsen et al. [38]. In this investigation, the fatigue experiments were conducted with 36 specimens which have 1 mm sheet thickness. Three sample groups in which two of them are non-welded and one is welded with a transverse welding (T – Joint), were tested. Non-welded samples were produced by milling cutter and plasma cutter. The fatigue tests were performed as load controlled with a stress ratio of 0.1 and a testing frequency between 2-12 Hz at room temperature. It was

found that; cutting methods of the non-welded samples as milling cut or plasma cut do not have an effect on the fatigue life of the samples and fatigue life of the non-welded specimens is higher than the welded T-joints specimens due to produced welding defects which generate high stress concentrations on welding region [38]. Jiunn-Yuan Huang et al. studied to determine the effects of the temperature, specimen orientation, stress ratio (R), specimen size and welding on the fatigue life of the 316L stainless steel [39]. Welding of the specimens was made by a manual "Gas Tungsten Arc Welding" using ER316L (stainless steel weld filler wire) as filler metal. Fatigue tests were performed as stress controlled at 20 Hz frequency with various testing parameters such as specimen size, stress ratio (0.8, 0.2, -0.2 and -1.0) and temperature (room temperature and 300 °C). The fatigue limit of the specimens tested at 300°C was found as to be lower than of specimens tested at room temperature. It was also shown that the welded specimens have better fatigue life than the non-welded ones at 300°C but they have very similar results at room temperature. The fractures were observed both from the base metal and welding. The fatigue limit of the sub-sized specimens was found to be similar with that of the standard testing specimen sizes at both room temperature and 300°C. Additionally, increasing the stress ratio enhanced the fatigue limit of the material [39].

The effect of filler metal thickness on the tensile strength of 304 stainless steel which is used in plate-fin heat exchangers, was studied by Wenchun Jiang et al. [40]. Brazing of the metal was made in a vacuum furnace and BNi_2 (Nickel based brazing alloy) was used as filler material which has melting point suppressors such as boron and silicon to decrease the brazing temperature and provide better wetting. Six different filler material thicknesses which are 35 μm, 50 μm, 70 μm, 105 μm, 140 μm and 180 μm were tested. Room temperature tensile tests show that the tensile strength is increased with an increase of the filler material thickness up to 105 μm. Between 105 μm and 140 μm thickness values, the tensile strength is stabilized and tends to remain constant. Yet, after 140 μm, increasing the filler material thickness decreases the tensile strength rapidly. The use of thinner filler material creates a low quality of fillet and thicker filler material produces more brittle phase and cracks. It was shown that the 304 steel sample with 105 μm filler material thickness has the highest UTS value [40]. Characterization of microstructure and fatigue behaviour of 304L stainless steel brazed joints was studied by Y. Li et al. [41]. In the study, 304L stainless steel samples brazed with pure copper were subjected to fatigue testing. Fatigue tests were performed as stress controlled with stress

ratio R = 0.1 and 20 Hz frequency. Two different stress amplitudes of 135 MPa and 180 MPa were applied during the fatigue testing. Also, the tensile tests were performed for the samples having different interface surface roughness values changing from P80 (0.963 μm) to OPS (0.005 μm) in order to determine the effect of surface roughness on tensile properties of the samples. According to the tensile results, the surface roughness of brazing interface does not have a remarkable impact on the UTS of the samples. UTS values for all specimens were determined as very close to each other between 500 and 540 MPa. It was observed that all specimens were fractured from the brazed region. However during post-test examination of fractured specimens by using SEM, it was found that some specimens have joint defects on brazing regions which might be occurred during brazing process. Consequently, stress amplitude versus failure cycle graphs were plotted with both defected and not defected samples. Failure cycles were specified as; average $7x10^4$ cycles for defect free samples at 180 MPa, $2x10^4$ cycles for samples have defect at 180 MPa, $10x10^6$ cycles for defect free samples at 135 MPa and $2x10^5$ cycles for samples have defect at 135 MPa [41]. The impact of surface roughness on the fatigue behaviour of brazed steels was studied by Yoshifumi Suezawa [18]. SS41 mild steel was used as the base metal and BAg_8 eutectic alloy (Silver-Copper) was used as the filler material in the study. Every test specimen's brazing surface was grinded with different emery papers and different machining techniques such as 60 (15 μm), 120 (11 μm), 240 (5 μm), 400 (1 μm), 600 (0.6 μm) emery papers, machining by milling cutter (14 μm), electrolytic polishing (0.7 μm) and 60 (1.6 μm), 80 (0.8 μm), 240 (0.6 μm) grits grinding wheels. The fatigue tests were performed for each specimen as rotary bending type stress controlled at room temperature. It was determined that the specimens with having rougher surface finish have better fatigue strength compare to those having smoother surface based on the fatigue life curves. Rough surface results in larger area and facilitates bonding since it gives opportunity to the filler material to deeply penetrate into the metals to be joint due to higher asperities and deeper valleys [18]. Fatigue behaviour of grade 1.4313 stainless steel and its brazed joints was studied by M. Koster et al. [42]. Stress controlled fatigue tests were performed at a stress ratio of R=0.1. Gold – Nickel (Au 18wt% Ni) alloy foil was used as the filler metal with 100 μm thickness and the brazing was conducted in a shielding gas furnace. For low cycle failures, it was shown that the strength values of the both brazed and non-brazed joints against applied loads are very similar. However, for the high cycle failures, it was seen that the brazed joints were failed at stress levels below than those of non-brazed specimens. It was suggested that

introducing a braze layer causes to increased stress accumulation on brazing region due to microstructural changes and possible defects produced during brazing operation [42]. The fatigue and tensile properties of 304L stainless steel brazed with BAu_4 (gold alloy, with thickness of 50 μm) were studied by Anke Schmiedt et al. [43]. The study provides an understanding for the effect of gauge length ranging from 0.5 to 12.5 mm on the produced strain of brazed joints under cyclic and quasi static loads in normal and pre-corroded conditions (6 weeks corrosion aged). The fatigue tests were performed as stress controlled with a stress ratio of R = 0.1 and 10 Hz frequency. During the test, applied stress was gradually increased by 10 MPa after each 10^4 cycles. It was shown that the pre-corroded brazed samples have lower UTS values and fatigue life about (65% and 42%, respectively, compared to non-corroded) samples due to corrosive attack at the brazing interface between the base and filler metals [43]. Yiğit Gürler studied the room temperature fatigue behaviour of 316L stainless steel brazed with 100 μm thick copper by stress controlled fatigue tests (a stress ratio of R=0 and 5 Hz frequency) and tensile properties of the brazing region for the production of PHEs [6]. Additionally, a numerical model analysis was conducted to calculate the acting stresses on PHEs. Based on the test results, it was observed that the strength coefficient (K) which is equal to true stress at a true strain of 1, and strain hardening exponent (n) which is the slope of stress-strain curve in log scale, of the brazed region are different from the 316L stainless steel and copper ($K_{brazed\ int.}$ = 900.8325 MPa, K_{copper} = 420-480 MPa, $K_{stainless\ steel}$ = 525-575 MPa, $n_{brazed\ int.}$ = 0.2075, n_{copper} = 0.35-0.50, $n_{stainless\ steel}$ = 0.40-0.55) which proves the occurrence of an additional brazing phase. Fatigue test results showed that lifetime of the brazed test specimens are higher than 120000 cycles when the part is exposed to 60% of UTS (312,3 MPa) as load [6].

The short literature survey presented here clearly shows that there are a number of studies which evaluate the fatigue behaviour of various metals with or without brazed joints using different filler materials. However, the preferred test method for the majority of studies is stress or load controlled type even for the low cycle fatigue regimes. It is known that strain or displacement controlled fatigue test is proposed to have more reliable results compare to stress or load controlled type if the applied loads during the test are higher than the yield strength of the specimen material. Mostly the stress ratio was selected to be different than R = 0 which is the proper value for acting loads on PHE.

Furthermore, according to the best of our knowledge there is not any report in

literature showing the fatigue life comparison of the copper brazed 316L and 304L stainless steel joints. In addition to that the effect of copper thickness as filler metal on fatigue life of 316L stainless steel has also been evaluated with the current thesis project study which is known as a gap in the literature.

CHAPTER 3

EXPERIMENTAL PROCEDURES

In order to determine the mechanical properties and fatigue behaviour of 316L and 304L copper brazed stainless steels, a series of tests and investigations were performed. This chapter gives the detailed information about test specimen preparation, performed tests, metallurgical analysis and determination of load distribution on PHE plates by FEA.

3.1. Materials and Brazing Operation

Along with the copper foil (Cu 141, 99.90 % of Cu) in 50 μm thickness which has 1085°C melting temperature, four 316L and two 304L stainless steel sheets (500 x 70 x 5 mm) were used as materials for brazing and specimen production. Procured stainless steel sheets are shown in Figure 3.1.

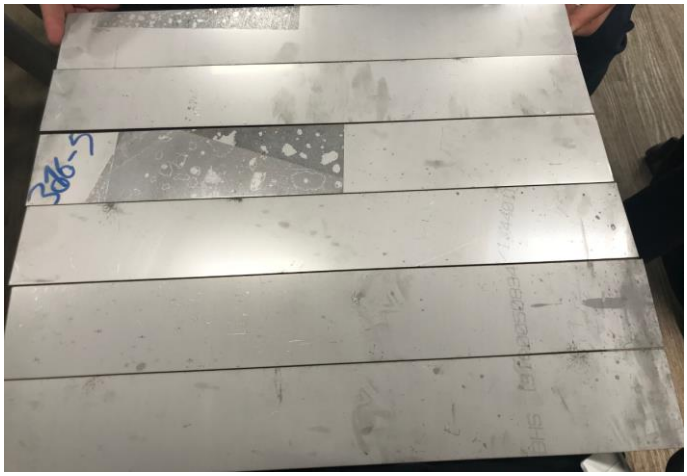

Figure 3.1. 316L and 304L stainless steel sheets

As already mentioned in Section 2.2, based on the study of Yoshifumi Suezawa [18], surface roughness has a remarkable impact on fatigue life of the brazed joints. Therefore, this was taken into consideration during the specimen preparation. Since the

results of the fatigue and tensile tests will be used for evaluating the PHE's fatigue lifetime, the surface roughness of the ordered stainless steel sheets have to be similar with the those of PHE plates. The procured stainless steel sheets were laser cut by the provider based on the requested size of 500 x 70 x 5 mm. The laser cut surface which is presented in Figure 3.2, is the area that brazing of the two sheets occurs. The average surface roughness (Ra) of the as-received laser cut stainless steel sheets was measured by stylus profilometer as 2.44 μm which is shown in Figure 3.3. Figure 3.4 presents those performed measurement results on the laser cut surfaces. Then, the surface roughness of the formed plates of PHEs was measured. Measurements were done on the brazing contact region of the channel plates as presented in Figure 3.5. Consequently, average surface roughness for the PHE plates was calculated as 1.45 μm. Measurement results are presented in Figure 3.6. Finally, as-received stainless steels were grinded by wire erosion machining and surface roughness measurements were repeated for them. Consequently, average surface roughness of the brazing surfaces on the received stainless steel sheets was measured as 1.52 μm. So, the surface roughness of the channel plates of the PHE and the brazing surfaces of the received stainless steel sheets became very close in order to eliminate the effect of surface roughness on brazing strength. Figure 3.7 shows the final measurement results on the received stainless steel sheets.

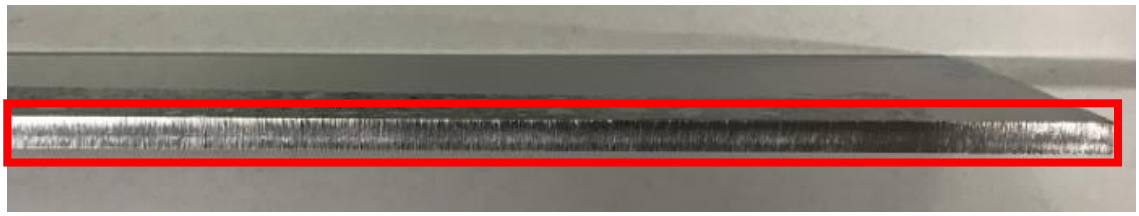

Figure 3.2. Laser cut surface where the stainless steel sheets are brazed

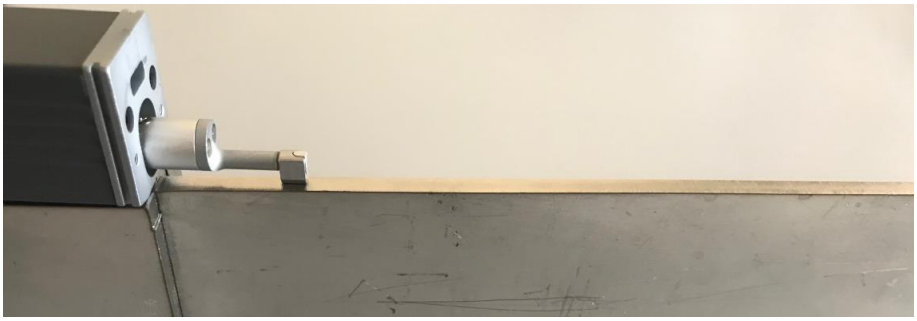

Figure 3.3. Surface roughness measurement of the laser cut stainless steel sheets

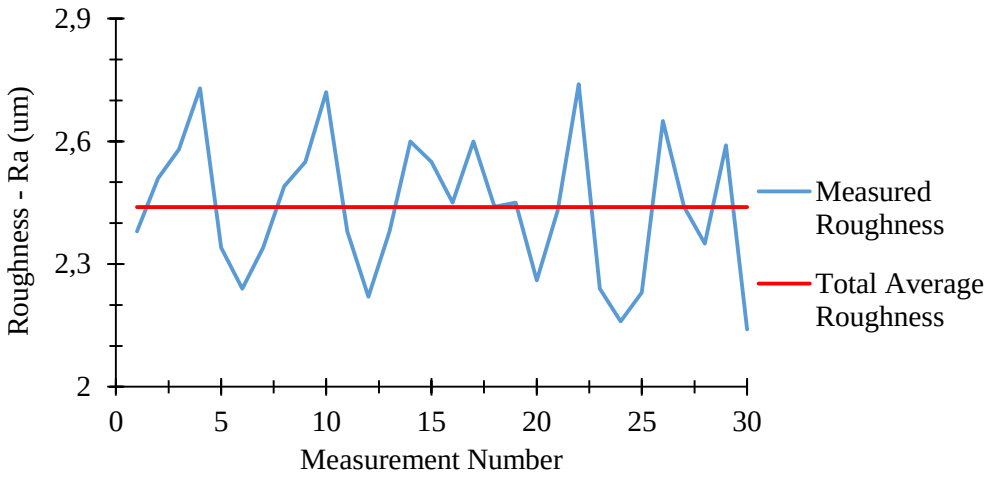

Figure 3.4. Surface roughness (Ra) results of the as-received laser cut surfaces

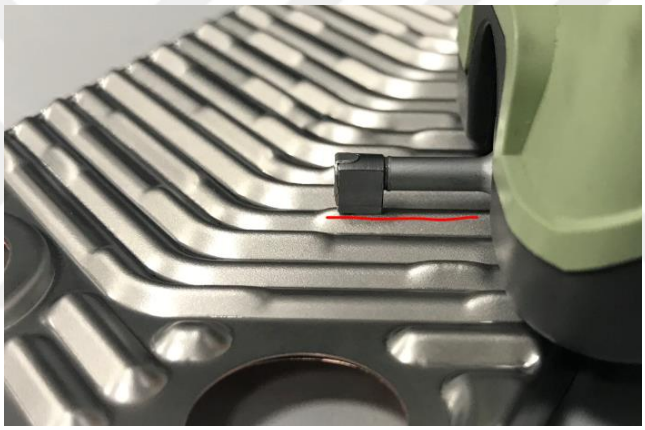

Figure 3.5. Roughness measurement of brazing surface on formed PHE channel plate

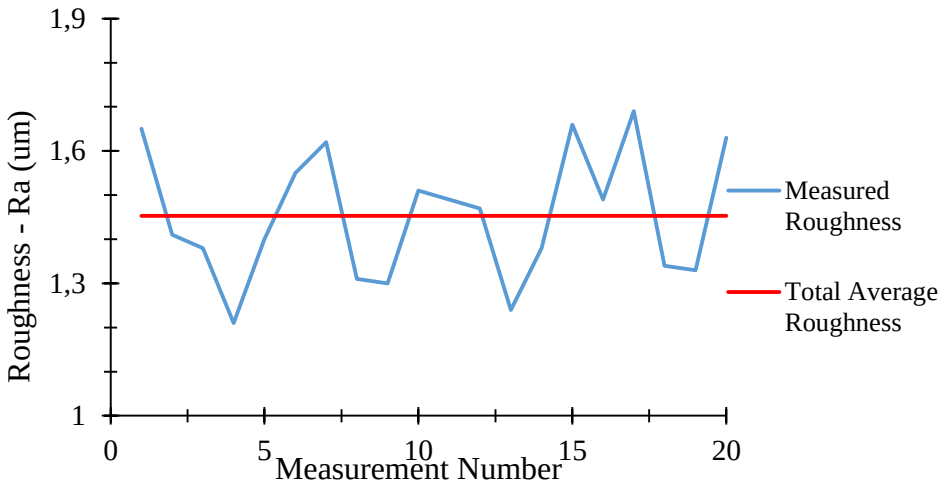

Figure 3.6. Surface roughness of brazing surface on formed PHE plates

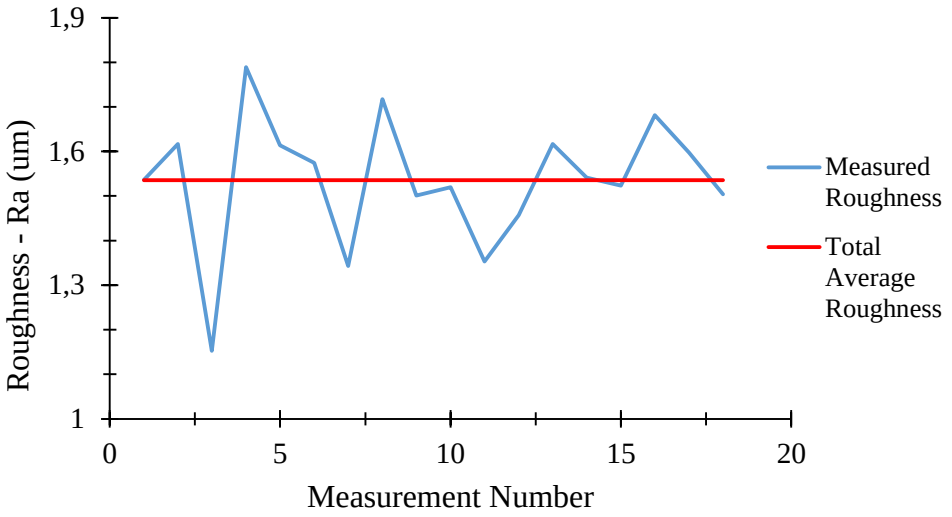

Figure 3.7. Surface roughness results of stainless steels cut by wire erosion

After the surface roughness modifications, the received stainless steel sheets, were cleaned with ethyl alcohol prior to brazing operation. Three sample groups were produced as follows:

a) Sample group 1: 316L stainless steel brazed with 50 µm thick copper foil
b) Sample group 2: 316L stainless steel brazed with 100 thick µm copper foil
c) Sample group 3: 304L stainless steel brazed with 100 µm thick copper foil

Figure 3.8. Inserted copper foil between two stainless steel sheets before brazing

Those metal sheets were placed next to each other with copper foil inserted between them as shown in Figure 3.8 and they were placed in a vacuum furnace for brazing operation by fixing from their edges with ceramic stoppers in order to obtain an intimate contact for successful brazing as shown in Figure 3.9. Those ceramic parts were

also put on the metal sheets in order to prevent any warpage of the metal sheets due to temperature changes during the brazing process.

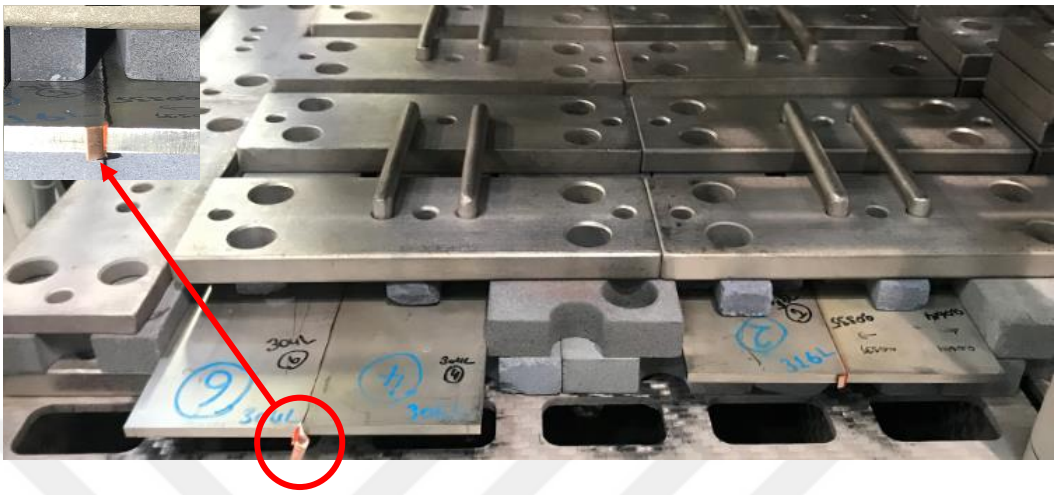

Figure 3.9. Placement of the stainless steel sheets in vacuum furnace before brazing

After placing the samples inside the vacuum furnace, brazing operation was started. The brazing was completed step by step according to instructions which are presented in Figure 2.14. Temperature inside the vacuum furnace was increased gradually under a specific vacuum environment and then it was cooled down progressively. The detailed brazing recipe cannot be given due to confidential data of Bosch TT but it can be shared that the brazing was performed at 1120° C and the total brazing process was completed in 6.5 hours. Figure 3.10 shows a brazed the stainless steel joint as one solid rigid part after the brazing operation. The images of brazed stainless steel sheets for all sample groups are presented in Figure 3.11.

Figure 3.10. Brazed stainless steel sheets after brazing in the vacuum furnace

a)

b)

c)

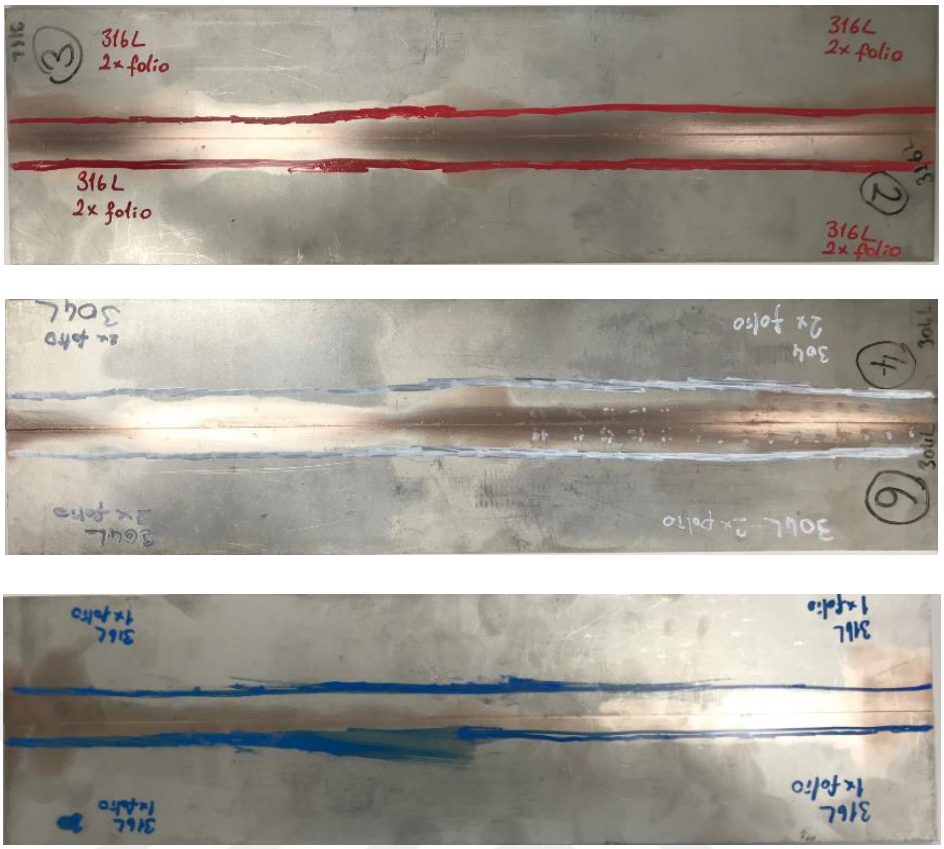

Figure 3.11. 316L stainless steel brazed with 100 µm copper foil (a), 304L stainless steel brazed with 100 µm copper foil (b) and 316L stainless steel brazed with 50 µm copper foil (c)

After brazing the stainless steel sheets, the tensile and fatigue test specimens were prepared. The dimensions of tensile test specimens were determined according to "Standard Test Methods for Tension Testing of Metallic Materials, ASTM E 8/E 8M – 08" [44] as sheet type of flat test specimens since the testing machine fixation apparatus is suitable for test flat type specimens. The dimensions of the tensile test specimens are given in Figure 3.12.

The dimensions of fatigue test specimen were defined according to "Standard Practice for Strain Controlled Fatigue Testing, ASTM E 606 – 92" [45] as seen in Figure 3.13.

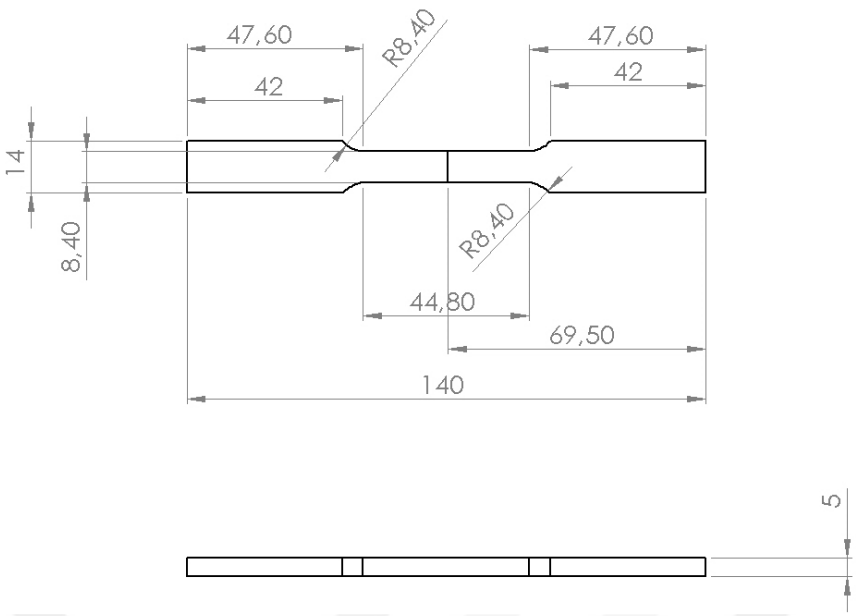

Figure 3.12. Dimensions of the tensile test specimen (in mm)

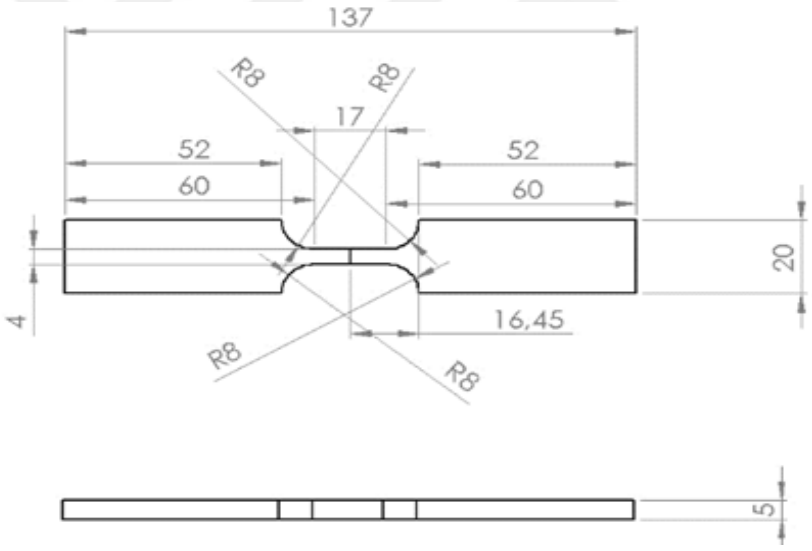

Figure 3.13. Dimensions of the fatigue test specimens (in mm)

Based on the defined specimen dimensions in Figure 3.12 and 3.13, the non-brazed and brazed stainless steel specimens were cut by means of wire erosion machining to produce the tensile and fatigue test specimens. Three non-brazed tensile test specimens, four brazed tensile test specimens and fifteen brazed fatigue test specimens for each sample group of 316L and 304L stainless steels were cut. Non-brazed specimens were produced from the steel region of the brazed sheets which are shown in Figure 3.11, to determine the mechanical properties of the steels also by considering the effect of

annealing during brazing process. Some of the prepared non-brazed tensile test specimens are shown in Figure 3.14 and brazed tensile and fatigue test specimens are presented in Figure 3.15.

Figure 3.14. Non-brazed 316L and 304L stainless steel tensile test specimens

Figure 3.15. Tensile test specimens (1, 3 and 5) and fatigue test specimens (2, 4 and 6)

3.2. Metallographic Sample Preparation and Microstructural Analysis

Microstructural investigations under optical microscope (Leica DM2500 M) and SEM (Zeiss Evo MA10) were carried out in order to examine the interface between the steels and copper, the diffusion of copper into steel and brazing area thicknesses.

Optical microscopy, also known as light microscope, is generally used to investigate microstructure of opaque materials. Light is reflected from the material and reflectivity of the different regions in microstructures creates contrast in the produced image. Magnification up to 2000 times can be achieved with optical microscopy analysis [14].

In SEM analysis, the specimen surface is examined by scanning electron beams and collection of the reflections (back – scattered) of them. Electrons hit to the atoms of the specimen and create different feedbacks which can provide surface topography, morphology and composition information. The specimen under investigation has to be electrically conductive in order to conduct electrons on it and magnification up to 50000 times is possible in SEM [14]. After the electron beams hit to specimen surface, reflected beams of the electrons are distinguished by the three detectors which are backscatter electron detector (BSD), secondary electron detector (SED) and energy dispersive x-ray spectroscopy (EDS) detector. BSD detects the elastically scattered electrons to obtain atomic contrast and the distribution of the different elements in specimen material, SED provides information about the material's surface morphology and EDS can provide information about the number of the elements and types in the specimen material [46].

In order to perform microstructural analysis by using optical microscope and SEM, metallographic samples were prepared. In the sample preparation, the brazed stainless steel coupons were cut from the brazed stainless steel plates as seen in Figure 3.16. Then, those coupons were hot mounted in black phenolic powder resin as given in Figure 3.17.

Figure 3.16. Brazed stainless steel coupons

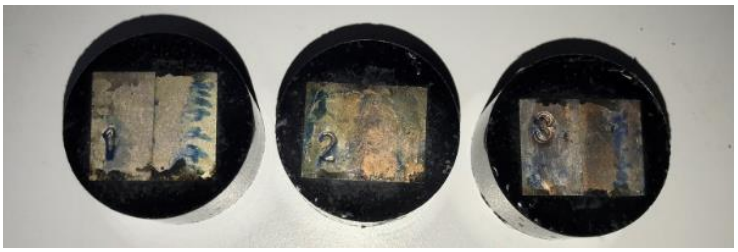

Figure 3.17. Brazed stainless steel coupons from each sample groups inside the hot mounting resin

After preparing the samples in resin, surface treatment of the coupons was started with grinding which is a chip removal process by using abrasive grains as the cutting material. During the process, a grinding wheel or a grinding pad with abrasive grains removes a layer of the material from its surface. After grinding, polishing which is a process that provides perfectly smooth surface finish on the materials, was performed. [47]. Grinding and the polishing of the samples were completed by following the procedure which is presented in Table 3.1, with using the Metkon Forcipol 2V Grinder – Polisher machine. After completing the polishing, samples were placed into an ultrasonic bath (Bandelin Sonorex) in order to remove residual particles on their surfaces. Then, all samples were cleaned by ethanol and dried to complete the polishing process. Grinding of the samples is presented in Figure 3.18 and the ground samples are shown in Figure 3.19. Figure 3.20 shows the mirror like shiny surface finishes of the polished samples.

Table 3.1. Parameters of the grinding and polishing

Operation	**Step**	**Abrasive Baize**	**Coolant**	**Force (N)**	**Speed (rpm)**	**Time (min)**
Grinding	1	SiC 400	Water	20	200	3
	2	SiC 800	Water	20	200	3
Polishing	3	6 µm	Water-based diamond suspension and lubrication	20	250	4
	4	3 µm	Water-based diamond suspension and lubrication	20	250	4
	5	1 µm	Water-based diamond suspension and lubrication	20	250	4

Figure 3.18. Grinding of the samples

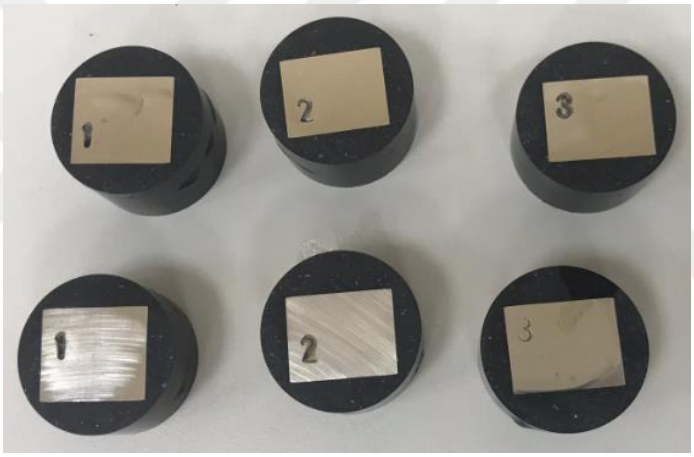

Figure 3.19. Ground samples

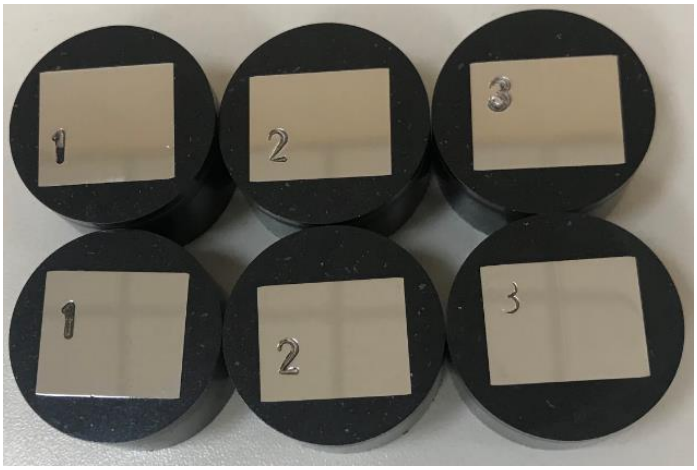

Figure 3.20. Polished samples

After polishing, some samples were etched in order to examine the grain boundaries of the materials and diffusion of copper throughout the microstructure under optical microscope. In etching, chemical solutions which are named as etchants, are used to reveal the grains of the microstructure by corroding the affected elements. The shape and size of grain boundaries, the presence of different phases and potential inclusions in materials can be exposed by etching. Most commonly applied etching technique is the chemical etching and it is explained as the chemically weathering of the sample's surface by a mixture of an acid mostly with alcohol and water [48].

The etched samples were prepared according to "Standard Practice for Microetching Metal, ASTM E407-07" [49]. Etchant number 88 has been selected since it is proposed as proper etchant for the 300 series stainless steels. The etchant is composed of 10 ml HNO_3, 20 ml HCL and 30 ml water. In order to prepare that, 37% hydrochloric acid fuming was mixed with HNO_3 in a plastic pan by considering the defined ratio in etchant number 88 [49]. The etchant was applied to the surface of the coupons about two minutes until the etchant becomes a dark orange colour. Then the coupons were washed by ethanol and dried. Three coupons for each sample group were etched according to the defined procedure as shown in Figure 3.21.

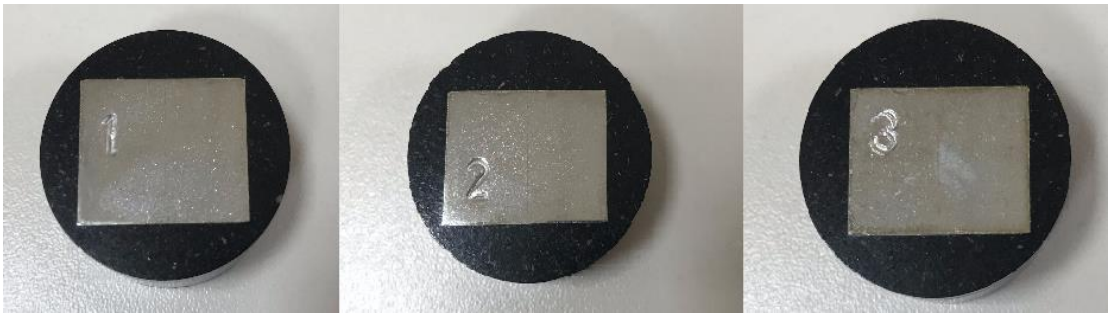

Figure 3.21. Etched brazed stainless steel samples

3.3. Mechanical Tests

At least three tensile specimens were tested for each brazed sample groups along with non-brazed samples which were cut from the steel sections of the brazed sheets, and average data was reported. For tensile testing, a MTS Landmark servo hydraulic test system with 647 hydraulic wedge grip for flat specimens was used as shown in Figure 3.22. Tensile speed was set to 2mm/min during the tests.

Figure 3.22. MTS Landmark servo hydraulic test system with 647 hydraulic wedge grip for flat specimens has been used

Tensile test specimens were fixed between the hydraulic wedges of the test machine. Then, the extensometer (634.31F – 24) was placed on the gauge section of the test specimens in order to save the elongation data during elastic deformation with high resolution and proximity. After reaching the strain of 0.2%, the extensometer was removed from the specimen and tests were resumed to the fracture point. Figure 3.23a and 3.23b present the fixation of the test specimen to the test machine and the fractured of test specimen, respectively.

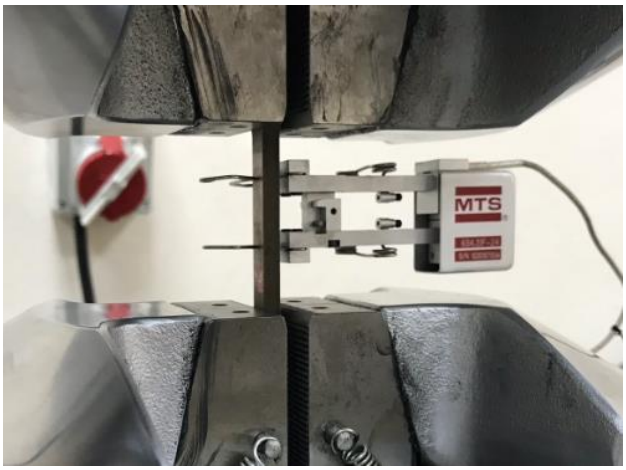

a) Fixation of the test specimen to the test machine

b) Fracture of the brazed test specimen

Figure 3.23. Tensile test of brazed stainless steel specimens

For fatigue testing, as explained in Section 1.3 and illustrated in Figure 1.14; acting loads on the PHE's brazing points during water hammer cycling are considered to be in tension, which means that stress ratio is equal to zero. Therefore, tension – tension fatigue tests were performed at a stress ratio of R = 0. Since the acting loads on the brazing region were selected as higher than the yield strength of the specimens during the test, displacement controlled fatigue test (strain is also calculated) was performed in order to eliminate the deviations on the results caused by cross sectional area reduction of the test specimens because of the plastic deformation. The same machine used for tensile tests was utilized for the fatigue tests as well since the servo hydraulic test systems are capable of performing displacement controlled, load control or strain controlled fatigue tests with high resolution, stability and broad frequency ranges.

In order to determine the testing frequency, the water hammer test bench in Bosch TT Reliability Lab was used for examining the acting duration of the water hammer pressure peak on the PHE. Water hammer pressure peaks were produced on PHEs which were connected to the test rig and pressure peaks up to 16 bar were produced. It was found that 16 bar pressure acts on the PHE for a duration of 40 ms. It means that max frequency of the displacement controlled fatigue test can be selected as 25 Hz (1/0.04=25). Additionally, Benjamin Guennec et al. [37] claims that the difference between 2 and 20 Hz testing frequencies has no impact on the fatigue life of JIS S15C steel [37]. However, the maximum frequency that the test machine can achieve without having deviation

between displacement set value and output one is 5 Hz. Hence, the testing frequency was set to 5 Hz for all specimens.

In the literature, it is suggested that at least 28 specimens should be tested for the reliability of fatigue data (4 specimens for 7 different stress or strain levels) [50]. However, due to the limited testing time and budget, the tests were performed for twelve test specimens for each sample group at four different strain (displacement) levels. So, for each strain level three fatigue specimens were tested. Equation 3.1 is used to determine the needed sample number for testing based on requested reliability and confidence levels [50];

$$n = \frac{\ln\alpha}{\ln(1-P)} \tag{3.1}$$

where; n is test specimen number, $(1 - \alpha)$ is confidence level and P is probability of failure (unreliability level)

Confidence level is explained as the ratio of all possible samples in population that can be expected to have the correct parameter. If all samples are selected from the same population, 90% confidence level implies that 90% of the all population have the calculated or measured population parameter in general. The confidence level represents the frequency of possible confidence intervals that contain the correct value of the required population parameter [50].

Reliability level refers to the ratio of the products which operate successfully without failures for the defined service time. If a test which aims 80% of reliability level is completed successfully for all samples, it implies that 80% of the total population will not fail until the end of their intended operation time [50].

Bosch TT provides 80% reliability level at the end of 15 years of service time of PHEs with 80% confidence level. Therefore, at least 8 samples are required for testing to satisfy these criteria according to Equation 3.1. Despite that, the selected sample number for displacement controlled fatigue tests of brazed specimens is twelve. And this refers to:

P = 17.5%, so the ensured reliability level in the fatigue tests is 82.5% with a 90% of confidence level.

Fatigue tests were conducted at room temperature since the operating temperature range of the PHE is between 0 °C and 80 °C as explained in Section 1.2, and the operational temperature effect on the fatigue life of PHEs is considered to be negligible due to considerably lower thermal load compared to stainless steels' working temperature limit which is around 800 °C [27]. In addition to that, it is known that thermo-mechanical fatigue has an impact on lifetime of the steel parts at temperatures higher than 150 °C, which was also indicated by Omesh Chopra and Gary L. Stevens [51]

Since the displacement value was selected as the controlled parameter during the fatigue test, four different displacement levels were defined to generate a fatigue life curve for all samples. In order to determine the displacement levels for the test, iterations were made to detect the lowest load leading to a failure before 10^6 cycles which is accepted as infinite lifetime. According to tensile test results, the average yield strain value of the parts was calculated around 0.1 %. Therefore, 0.3 % strain was applied at first during the iterations. At the end, failure was not observed up to 0.35 % of strain for 316L brazed with 50 µm thick copper foil specimens, 0.45 % strain for 316L brazed with 100 µm thick copper foil specimens and 0.40 % strain for 304L brazed with 100 µm thick foil specimens. The iterations were stopped at a cycle number of 1500000 if there is no failure. Strain levels to start the tests were determined according to these performed iterations. Table 3.2 shows the corresponding strain and displacement values for each sample group in the fatigue tests. Apart from the applied load and displacement, the test machine saved the number of cycles completed.

Table 3.2. Strain and displacement values used in the fatigue tests for each sample

316L + 50 µm Cu foil			**316L + 100 µm Cu foil**			**304L + 100 µm Cu foil**		
Sample #	Strain (%)	Displacement (µm)	Sample #	Strain (%)	Displacement (µm)	Sample #	Strain (%)	Displacement (µm)
1	0.35	59	1	0.45	77	1	0.4	68
2	0.35	59	2	0.45	77	2	0.4	68
3	0.35	59	3	0.45	77	3	0.4	68
4	0.4	68	4	0.5	85	4	0.45	77
5	0.4	68	5	0.5	85	5	0.45	77
6	0.4	68	6	0.5	85	6	0.45	77
7	0.5	85	7	0.55	93	7	0.5	85
8	0.5	85	8	0.55	93	8	0.5	85
9	0.5	85	9	0.55	93	9	0.5	85
10	0.6	102	10	0.6	102	10	0.6	102
11	0.6	102	11	0.6	102	11	0.6	102
12	0.6	102	12	0.6	102	12	0.6	102

3.4. Finite Element Analysis

FEA was performed in order to determine the maximum strain on the plates of the PHEs under 16 bar and 10 bar pressures which represent the field conditions as determined by Bosch TT (see Section 1.3), to evaluate the PHE's endurance. Static structural analyses were performed for a concept PHE which was designed by using both 316L and 304L stainless steels. The PHE concept design completely belongs to Bosch TT and it is protected due to the ongoing patent approval. During the FEA, all brazing points were designated as contacts between the channel plates. The mechanical properties of brazing points and plates were defined based on the tensile test results of non-brazed and brazed 316L and 304L specimens. During the modelling of the PHE plates, scaling was not applied and plates was modelled based on the original dimensions of the design. A commercial software (ANSYS) was used for the FEA.

In order to perform static structural load analysis of the plates, strain life approach was used. The strain amplitude versus reversals ($2N_f$) graphs in log scale were generated by using the produced failure data from the fatigue tests of brazed stainless steel specimens. The strength coefficient, ductility coefficient, ductility exponent, strength exponent, cyclic strain coefficient and cyclic strength coefficient of the both 304L and 316L brazed stainless steel joints were calculated as input parameters for the FEA. Those parameters were determined by using Equations 2.11, 2.12, 2.13 and the approach shown in Figure 2.12.

Moreover, stress-based lifetime curves (S-N) of the base metals were obtained from the literature and directly used in the FEA as inputs for the fatigue behaviours of 316L and 304L stainless steels (for the non-brazed regions of the plates). Figure 3.24 and 3.25 depict the S-N curves of the pure 316L and 304L stainless steels. It was seen that there is a noticeable difference between the fatigue life of the 316L and 304L stainless steels. It should also be considered that these data were obtained from different sources which may lead to have greater differences. However, the comparison of these fatigue data for the non-brazed 316L and 304L stainless steels are consistent with the comparison of the performed fatigue test results for the copper brazed 316L and 304L stainless steels. Since, the copper brazed 316L stainless steel has better fatigue behaviour than the copper brazed 304L stainless steel based on the conducted fatigue tests, it is logical for the non-

brazed 316L stainless steel to have a better fatigue life than the non-brazed 304L stainless steel.

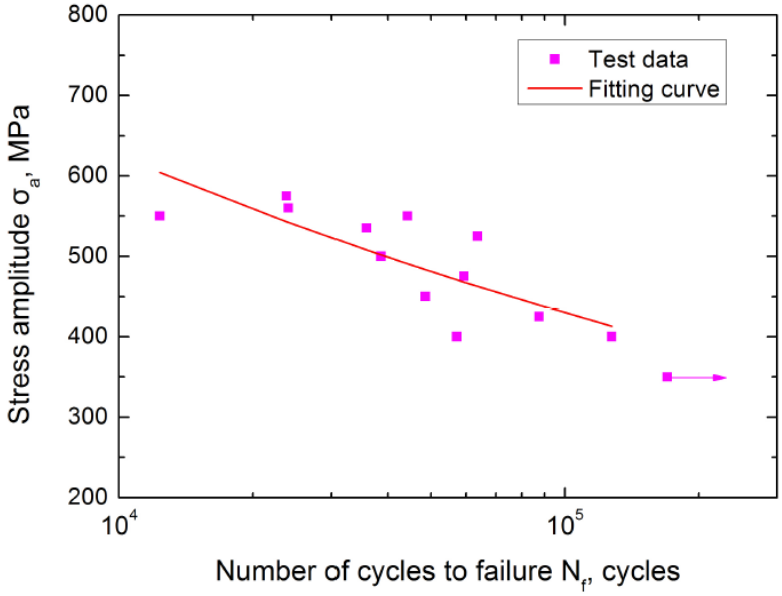

Figure 3.24. S-N curve of pure 316L stainless steel [36]

(Source: Zhao Xiao, 2012)

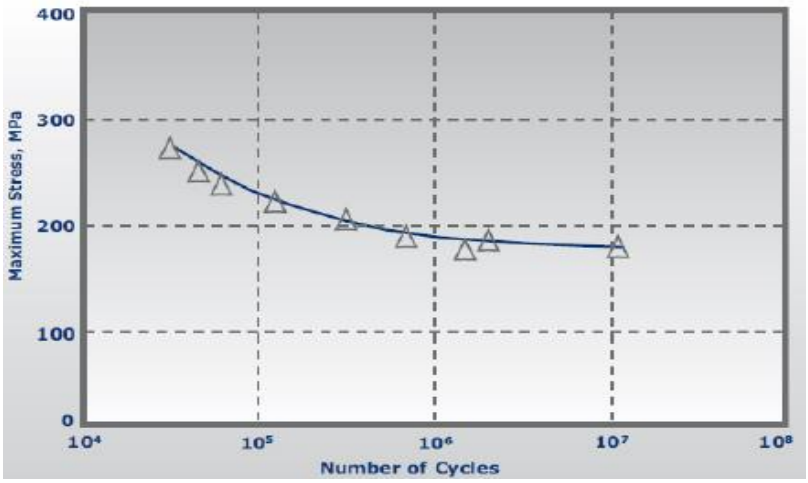

Figure 3.25. S-N curve of 304L stainless steel [52]

(Source: North American Stainless, 2020)

Since the plate thickness, plate material, pattern design of plates and brazing point number have remarkable impact on the load distribution; different PHE designs are

expected to have different fatigue behaviours. Therefore, different PHEs have to be modelled and FEA must be performed to determine the load distribution under different working pressures for different designs. Consequently, by comparing the strain distribution acquired from the FEA with the obtained fatigue test results, an estimation can be made for if the design is robust enough to fulfil the intended lifetime. For this purpose, four different FEA were performed for:

1) 316L stainless steel under 16 bar water pressure
2) 316L stainless steel under 10 bar water pressure
3) 304L stainless steel under 16 bar water pressure
4) 304L stainless steel under 10 bar water pressure

The aim of performing the FEA for both 16 and 10 bar pressures is to determine the ratio between the failure cycles of the PHEs under 16 and 10 bar pressures. As mentioned in Section 1.3, acting loads on the PHE during 15 years of lifetime consist of a combination of 16 and 10 bar pressure cycles according to collected load profiles by Bosch TT (180000 cycles 10 bar and 120000 cycles 16 bar) [9]. However, by using the lifetime curves, failure cycle can only be estimated for just one single load, not a combination of several ones. In accordance with this purpose, that ratio will be used to calculate corresponding failure cycle of 10 bar pressure to 16 bar pressure in order to determine the total cycles which consists of just 16 bar pressure peaks for 15 years. Thereby, required 16 bar pressure cycle number to have 15 years of lifetime can be compared with the determined failure cycle from the generated lifetime curves based on the performed fatigue tests.

Moreover, the performed FEA indicates the load distribution on the plates based on the PHE design, and the deviations which may be occurred during the manufacturing processes such as missing brazing points were not considered. In addition to that, residual stresses on the PHE plates due to forming operation was not taken into consideration during the FEA.

CHAPTER 4

RESULTS AND DISCUSSIONS

In this chapter; results of the microstructural investigations, tensile tests, fatigue tests and FEA are presented and discussed.

4.1. Microstructural Analysis of the Brazing Regions

Metallographic investigations under optical microscope and SEM were made for the brazed stainless steel samples in order to examine the microstructures of the joints.

4.1.1. Optical Microscopy Analysis

First of all, non-etched copper brazed stainless steel coupons were investigated. Based on the investigations, although most of the contact surfaces of steels were brazed properly, gaps were observed in the brazing regions of every sample as shown in Figure 4.1. These gaps at microscale sizes show that brazing could not be performed perfectly. These brazing defects are highly noticeable in 316L brazed with 50 μm copper foil sample. Same defects were also observed in 304L and 316L brazed with 100 μm copper foil samples but less than the 316L 50 μm sample. It could be suggested that copper foil with a thickness of 50 μm cannot provide a sufficient brazing as 100 μm copper foil does.

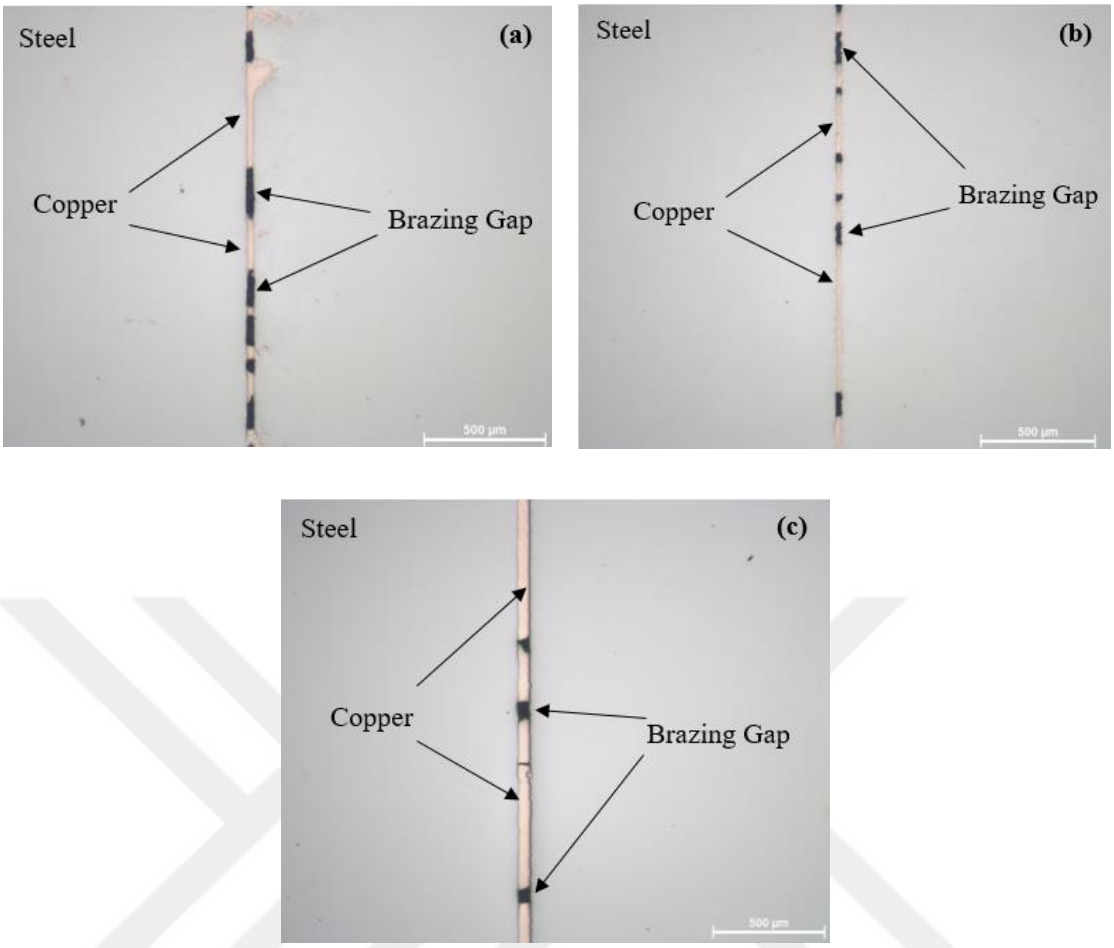

Figure 4.1. Optical microscope images of non-etched 316L stainless steel brazed with 50 thick μm copper foil (a), 316L stainless steel brazed with 100 μm thick copper foil (b) and 304L stainless steel brazed with 100 μm thick copper foil (c)

Then, the etched samples were examined and their images are presented in Figure 4.2. It is seen that copper penetrated into the stainless steels through the grain boundaries. Copper accumulation between the grains is highly seen in Figure 4.2a and 4.2b compare to that in Figure 4.2c. This may imply that copper tends to easily diffuse into 316L stainless steel rather than 304L stainless steel.

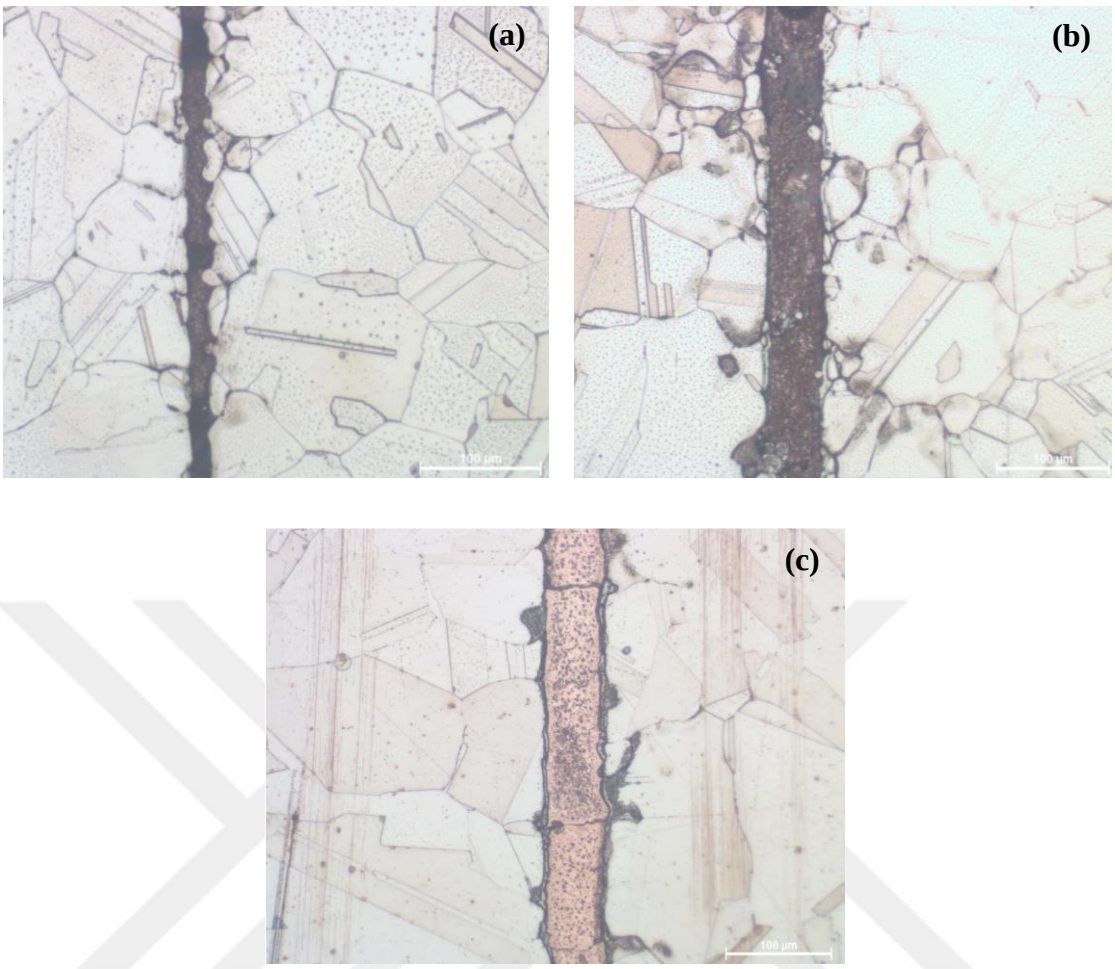

Figure 4.2. Optical microscope images of the etched brazed 316L stainless steel brazed with 50 µm thick copper foil (a), 316L stainless steel brazed with 100 µm thick copper foil (b) and 304L stainless steel brazed with 100 µm thick copper foil (c)

Moreover, the austenitic microstructures of the both 316L and 304L stainless steels were revealed in Figure 4.3. It was observed that the microstructures of both steels contain grains with different sizes and annealing twins. Twins are the arrangements of the atoms in a mirror-image symmetry around one line which is called as twin boundary and they are resultants of the applied mechanical shear forces or heat treatments. The annealing twins were observed in the microstructure because the stainless steels were annealed during the brazing process since the brazing temperature is higher than the annealing temperature of the stainless steel which is in between 1040° C and 1120° C [53]. Mostly similar microstructure with annealing twins was also observed at austenitic stainless steel NF709 by T.Sourmail et al. [54] and in brass by Yuan Jin [55]. Furthermore, because of the moderate cooling rate after brazing, chromium carbide

(Cr_3C_2) is known to precipitate during the recrystallization. This precipitation, also known as sensitization, leads to reduction in the corrosion resistance of the material due to decreasing chromium content in steel. Cooling rate should be fast enough to prevent chromium carbide precipitation, but on the other hand fast cooling may cause distortion of material [53]. The potential chromium carbide rich areas inside the grains of both 316L and 304L stainless steels were marked in Figure 4.3.

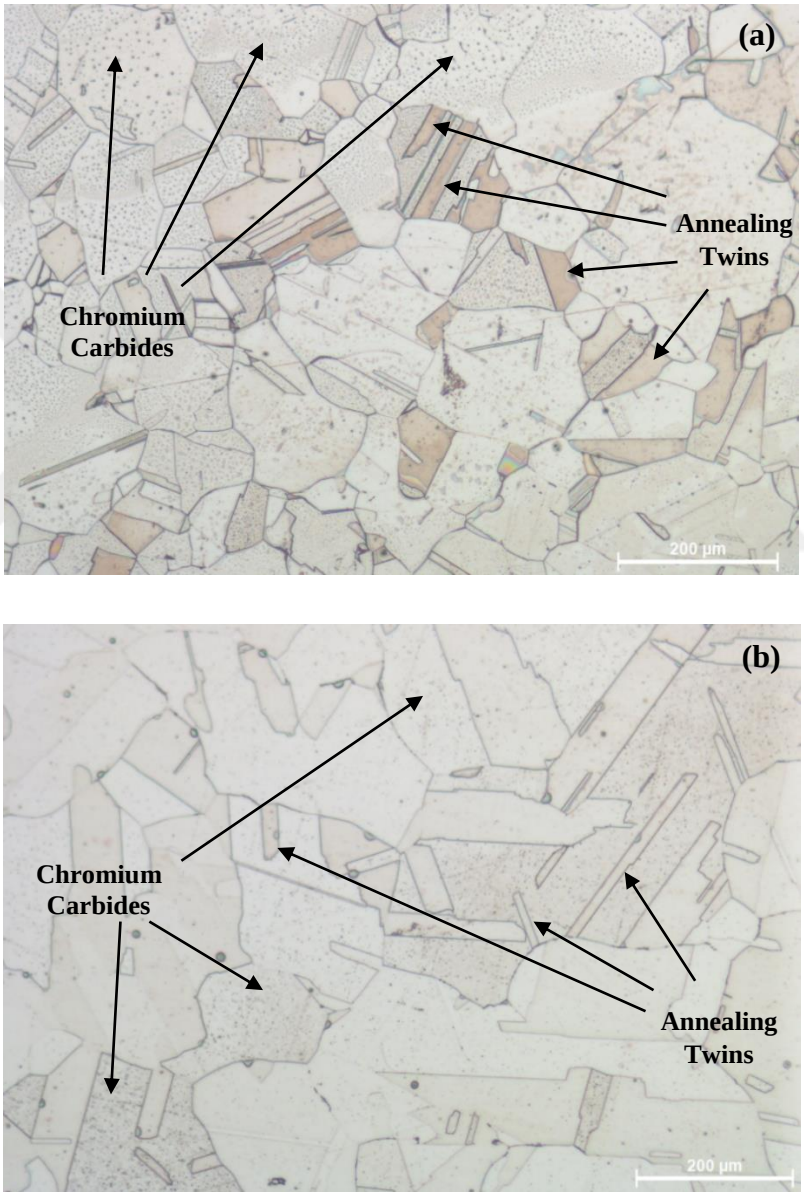

Figure 4.3. Optical micrographs of 316L (a) and 304L (b) stainless steels after brazing operations

4.1.2. Scanning Electron Microscopy Analysis

The SEM analysis was performed with three different brazed stainless steel coupons. It is clearly seen from Figure 4.4a and 4.4b that copper significantly diffused inwards to the 316L stainless steel. In 304L stainless steel, a transition phase was detected (Figure 4.4c). The region containing this phase has a distinct colour implying that a different phase was formed after brazing.

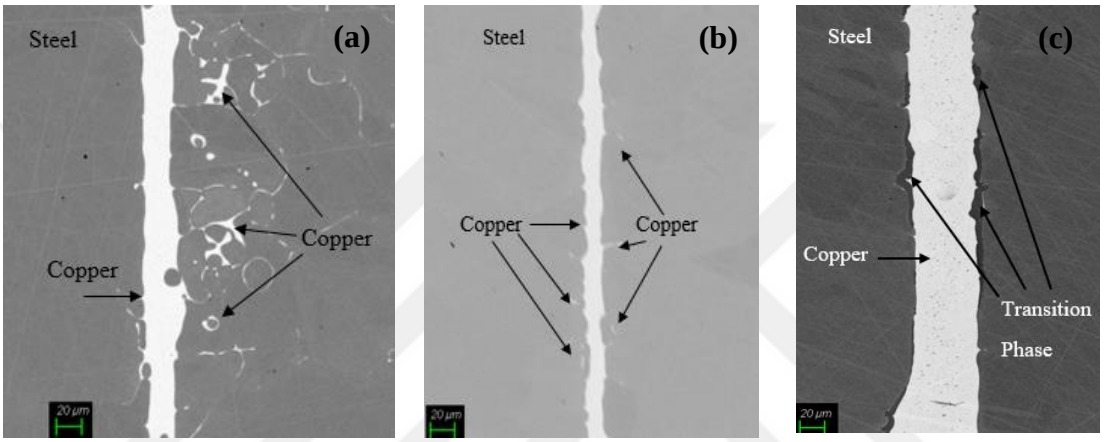

Figure 4.4. SEM images of 316L stainless steel brazed with 50 µm thick copper foil (a), 316L stainless steel brazed with 100 µm thick copper foil (b) and 304L stainless steel brazed with 100 µm thick copper foil (c) taken by back scattered electron detector

Moreover, copper brazing thicknesses of all samples were measured as shown in Figure 4.5. According to the measurements, it can be certainly said that a significant amount of the copper foil which was inserted between the base metals before brazing, was drifted away from the brazing region due to applied vacuum during the brazing process. The average copper brazing thicknesses of 316L stainless steel joints with 50 and 100 µm foil thickness were measured to be around 20 µm. Copper brazing thickness of the 304L stainless steel was measured around 58 µm although the inserted amount of copper was 100 µm before the vacuum brazing.

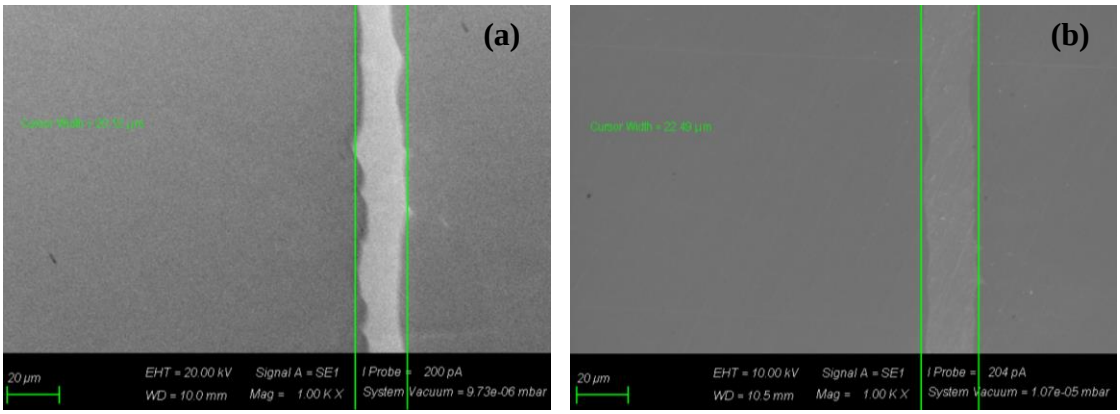

Cursor Width = 20.12 µm

Cursor Width = 22.49 µm

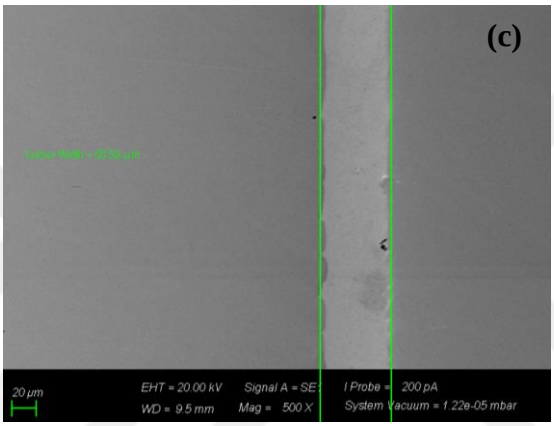

Cursor Width = 58.59 µm

Figure 4.5. Brazing thicknesses of the 316L 50 µm thick copper foil (a), 316L 100 µm thick copper foil (b) and 304L 100 µm thick copper foil (c) joint samples under SEM

The difference of copper brazing thicknesses between the 316L and 304L samples brazed by 100 µm copper foil can be ascribed to the relatively higher diffusion rate of copper into 316L grade than 304L grade stainless steel as shown also in the EDS analyses in Figure 4.6, 4.7 and 4.8. This might be caused by the relatively higher Chromium (Cr) content and absence of Molybdenum (Mo) in 304L compare to 316L stainless steel. Copper was observed in the inner regions of the 316L stainless steels as indicated in EDS spot 4 of Figure 4.6 and EDS spot 2 of Figure 4.7. Approximately 1.5 – 2% of the total composition was found as copper for these spots. Higher copper content in the inner regions of 316L stainless compare to 304L stainless steel was also slightly observed in elemental map scan images of the samples which are shown in Figure 4.9. On the other hand, it was noticed that the average copper region thicknesses of both brazed 316L

samples are nearly the same despite the inserted copper foil thicknesses were different before the brazing. So, it is most likely that using less filler material results in brazing gaps and defects in the brazing region of the 316L sample brazed with 50 µm copper foil, as shown in Figure 4.10. The chemical composition of the detected intermediate region in 304L brazed by 100 µm copper foil was determined by EDS point analysis as presented in Figure 4.8. The results showed that this region contains both Fe and Cu, which shows the formation of an additional phase due to diffusion of copper into the steel.

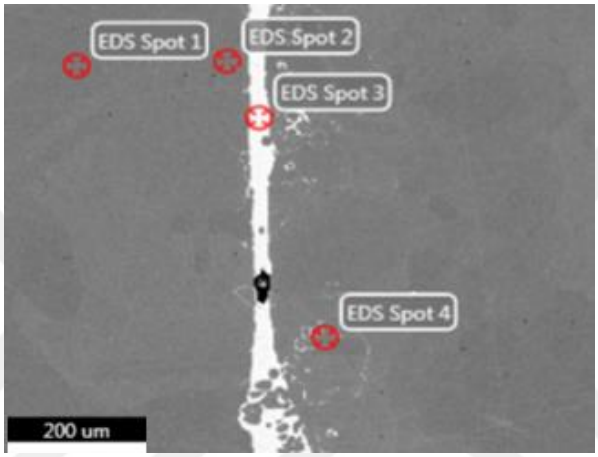

	Element Atomic (%)				
Spot #	Fe	Cu	Cr	Mn	Ni
1	71.34	-	17.74	1.69	-
2	71.44	-	17.68	1.72	9.16
3	7.00	89.29	17.68	-	2.13
4	70.41	1.56	17.92	1.52	8.59

Figure 4.6. EDS point analysis of 316L 50 µm copper brazed sample

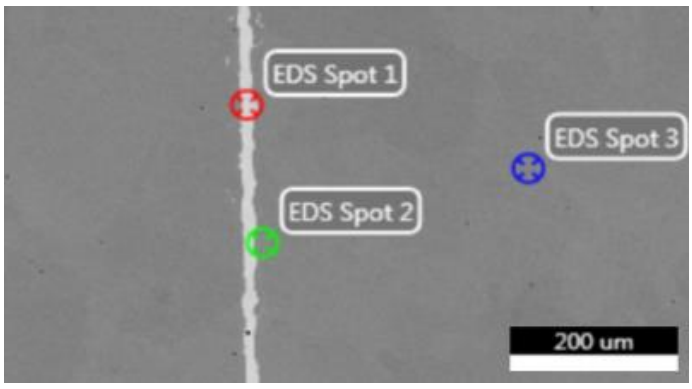

(cont. on next page)

	Element Atomic (%)				
Spot #	Fe	Cu	Cr	Mn	Ni
1 (Red)	2.37	97.63	-	-	-
2 (Green)	70.16	2.12	17.51	1.25	8.97
3 (Blue)	71.09	-	17.79	1.76	9.36

Figure 4.7. EDS point analysis of 316L 100 µm copper brazed sample

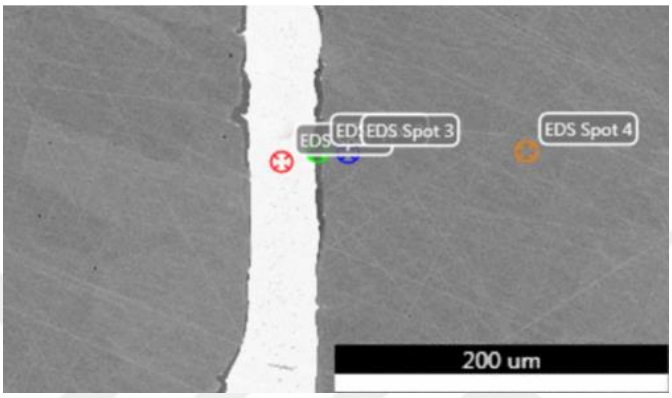

	Element Atomic (%)				
Spot #	Fe	Cu	Cr	Mn	Ni
1 (Red)	-	100.00	-	-	-
2 (Green)	71.69	2.07	23.76	-	2.48
3 (Blue)	71.67	-	19.29	1.85	7.19
4 (Orange)	71.33	-	19.20	2.11	7.36

Figure 4.8. EDS point analysis of 304L 100 µm copper brazed sample

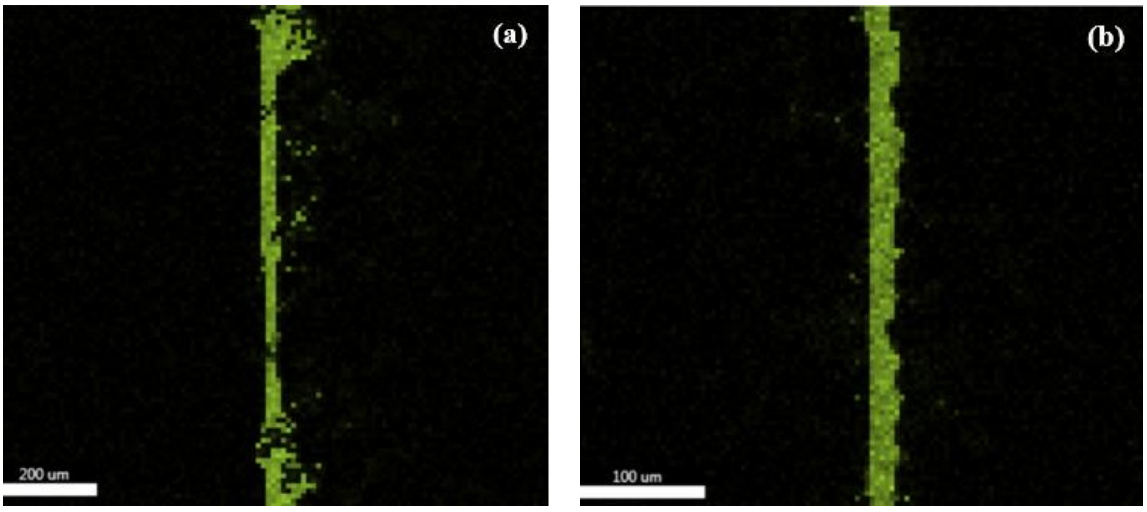

(cont. on next page)

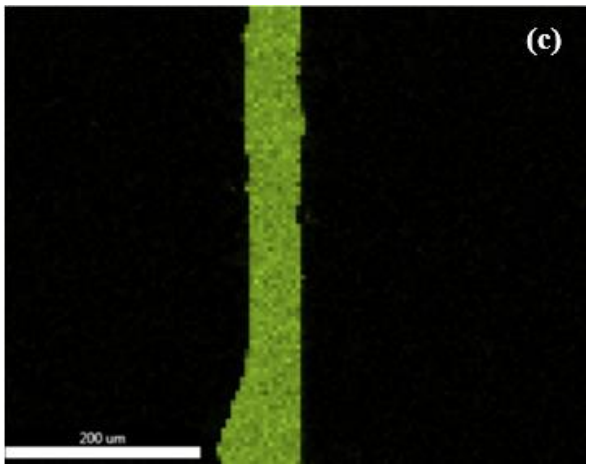

Figure 4.9. Elemental map scan of copper content in the 316L 50 µm thick copper foil (a), 316L 100 µm thick copper foil (b) and 304L 100 µm thick copper foil (c)

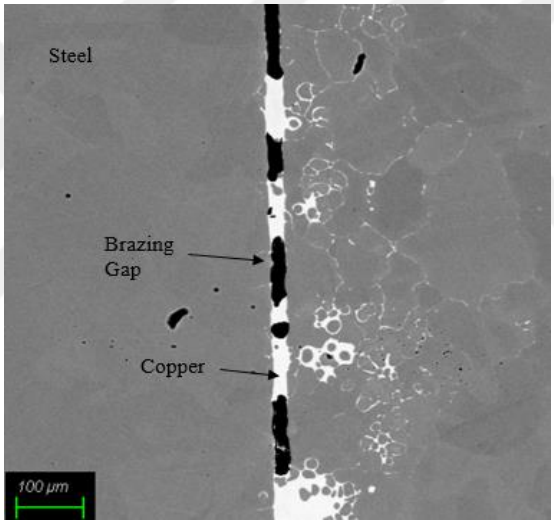

Figure 4.10. SEM image of 316L stainless steel brazed with 50 µm thick copper foil taken by back scattered electron detector

4.2. Tensile Tests

Tensile tests of the non-brazed 316L and 304L stainless steels were conducted with three specimens for each type which were cut from the steel region of the brazed sheets to evaluate mechanical properties of steel in PHE. Results are given in Table 4.1. The majority of the test results are similar to the values in literature as given in Table 1.1 [29, 30]. It is noticed that the fracture strain values of the tested specimens were 87.48% for 316L and 93.05% for 304L in average which are higher than those reported literature

values given in Table 1.1 as 60% for 316L and 58% for 304L. This improved ductility is most likely to be due to the annealing of stainless steels during the brazing.

Table 4.1. Tensile test results of stainless steel dog bone test specimens

	Sample #	Y. Stress (MPa)	UTS (MPa)	Y. Strain (%)	Fracture Strain (%)
316L Stainless Steel	1	216	612	0.4	86.66
	2	216	610	0.43	87.61
	3	214	607	0.44	88.16
	Average	215.33±0.94	609.67±2.06	0.42±0.02	87.48±0.62
304L Stainless Steel	1	210	659	0.53	90.65
	2	204	657	0.48	93.97
	3	205	657	0.5	94.53
	Average	206.33 ± 2.63	657.67±0.94	0.50±0.02	93.05±1.71

Figure 4.11 presents the representative stress versus strain curves for non-brazed pure specimens. 316L grade has slightly higher yield stress in comparison to 304L grade. On the other hand, 304L has slightly higher UTS and strain values.

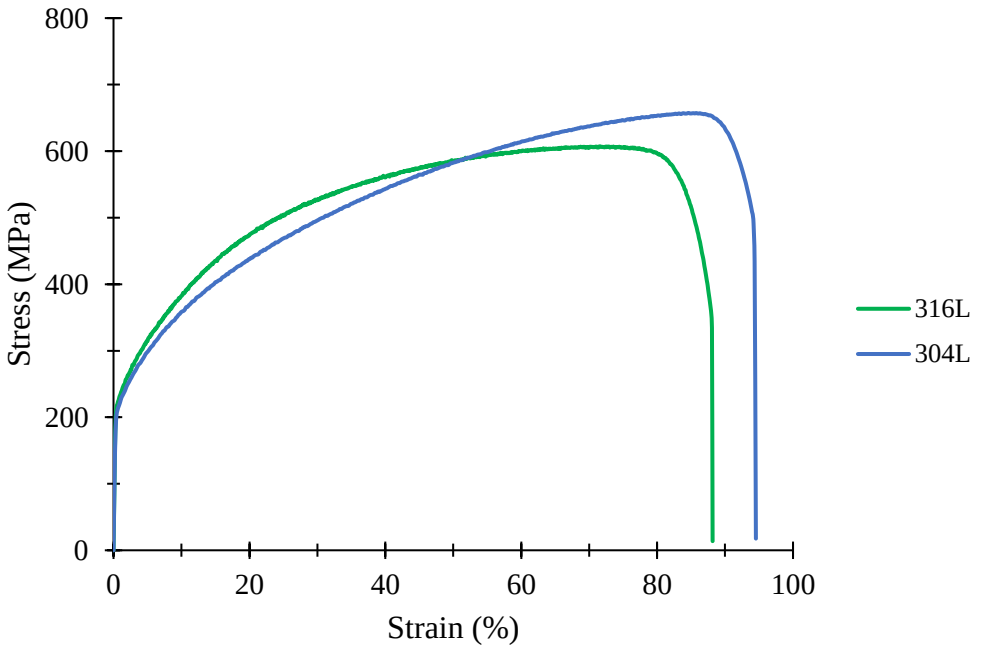

Figure 4.11. Stress vs strain comparison of one tensile test specimen result for 316L and 304L stainless steels

The tensile test results of brazed specimens are given in Table 4.2. The excluded data due to improper brazing of the specimens was highlighted as red. The results showed that the mechanical properties of 316L and 304L 100 µm copper brazed stainless steels are very similar to each other. Just the yield strength and UTS of 100 µm copper brazed 316L grade are slightly higher than those of 100 µm copper brazed 304L grade. On the other hand, the yield strength and the yield strain of 316L 50 µm copper brazed stainless steel are similar to those of the samples with 100 µm copper foil. However, its UTS and fracture strain are significantly lower than those of the others. This means that 50 µm filler material cannot provide a sufficient joint as 100 µm foil thickness provides. Consequently, it can be suggested that filler material thickness has a remarkable impact on the UTS and the fracture strain of the brazed stainless steel joints. Figure 4.12 compares the representative stress versus strain curves of brazed specimens.

Table 4.2. Tensile test results of copper brazed stainless steel specimens

Sample Type	Sample #	Y. Stress (MPa)	UTS (MPa)	Y. Strain (%)	Fracture Strain (%)	Modulus of Elasticity (Gpa)
316L 50 µm Copper	1	197	310	0.1	6.95	174
	2	186	288	0.11	5.61	190
	3	194	359	0.1	11.11	181
	4	203	365	0.11	11.28	194
	Avg	198.5±6.12	362±32.52	0.105±0.005	11.195±2.50	187.50±7.79
316L 100 µm Copper	1	201	480	0.1	25.98	202
	2	201	507	0.1	33.09	203
	3	205	516	0.1	35.95	220
	Avg	202.33±1.89	501±15.30	0.1	31.67±4.19	208.33±8.26
304L 100 µm Copper	1	191	362	0.11	13.66	188
	2	191	466	0.1	30.17	186
	3	189	357	0.1	13.13	171
	4	188	477	0.1	32.2	200
	Avg	189.5±1.30	471.5±56.16	0.1	31.185±8.93	193±10.30

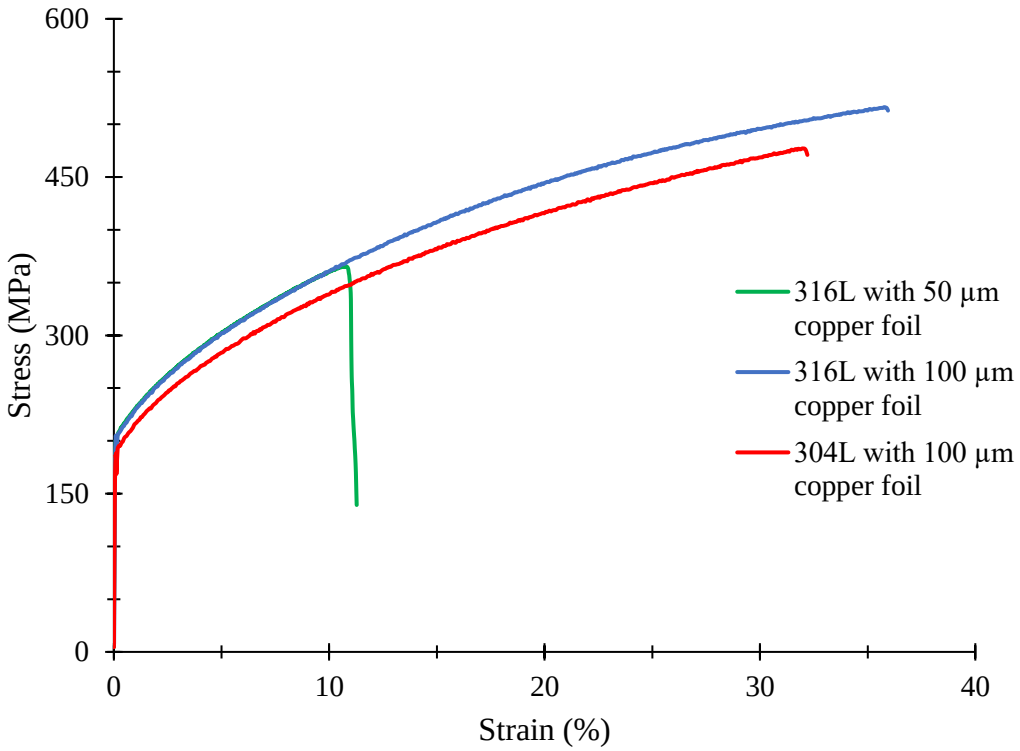

Figure 4.12. The representative stress – strain curves of brazed samples

In comparison of the tensile tests results of the brazed and non-brazed stainless steels; there are slight decreases on the UTS, yield strength and yield strain for brazed samples. That shows us strength of the material is not considerably reduced by brazing, that means brazing is an applicable technique to joint stainless steel materials in complex shapes and designs. Though, fracture strain of the brazed stainless steel joints were remarkably decreased, which shows that ductility of the material was lost after the brazing. Consequently, brazing the stainless steel parts by using copper as filler material reduces the ductility of the joint without changing their strength significantly.

During the tensile tests of the brazed specimens; four of 316L stainless steel brazed with 50 µm copper specimens were tested and the results for two of them were excluded due to early failures caused by improper brazing. It is assumed that the reason of this deviation is the position of the stainless steel inside the vacuum furnace. As shown in Figure 3.9, the plates were brazed to each other in horizontal orientation. Due to vacuum, it was observed that some of the copper was removed from the edges of the brazing surfaces. This is not possible during the production of PHE, since the plates are stamped on top of each other and placed to vacuum furnace vertically with additional

mass positioned above them. Due to dimensional deflections of the plates and stamping process sustainability, missing brazing points may still be observed during the manufacturing of PHE instead of the improper brazing. These process related deviations were not aimed to be investigated during this study, instead of that, the endurance of the design itself was evaluated.

Same defects were also observed for 304L stainless steel 100 µm copper brazed sample group. Four specimens were tensile tested but the results of two of them were excluded. Tensile tests of the 316L stainless steel 100 µm copper brazed samples were completed with three specimens and the results were found to be consistent. Properly and improperly brazed tensile test specimens can be seen in Figure 4.13.

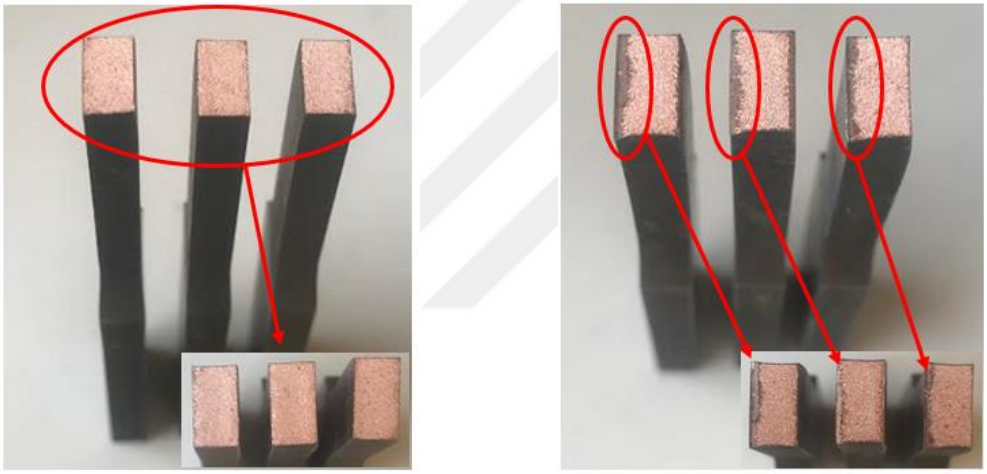

a) Fracture surfaces of the properly brazed tensile test specimens

b) Fracture surfaces of the improperly brazed tensile test specimens

Figure 4.13. Brazing surfaces of fractured tensile test specimens (fractographs)

Fracture surfaces of the tensile test specimens were investigated by SEM as shown in Figure 4.14. As indicated in the EDS point analysis of Spot 1, 3 and 3 show in Figure 4.15, 4.16 and 4.17, all specimens were failed from the brazing regions that the copper content can be clearly seen. No necking was observed before fracture of the brazed stainless steel specimens in contrary to the non-brazed stainless steel tensile test specimens.

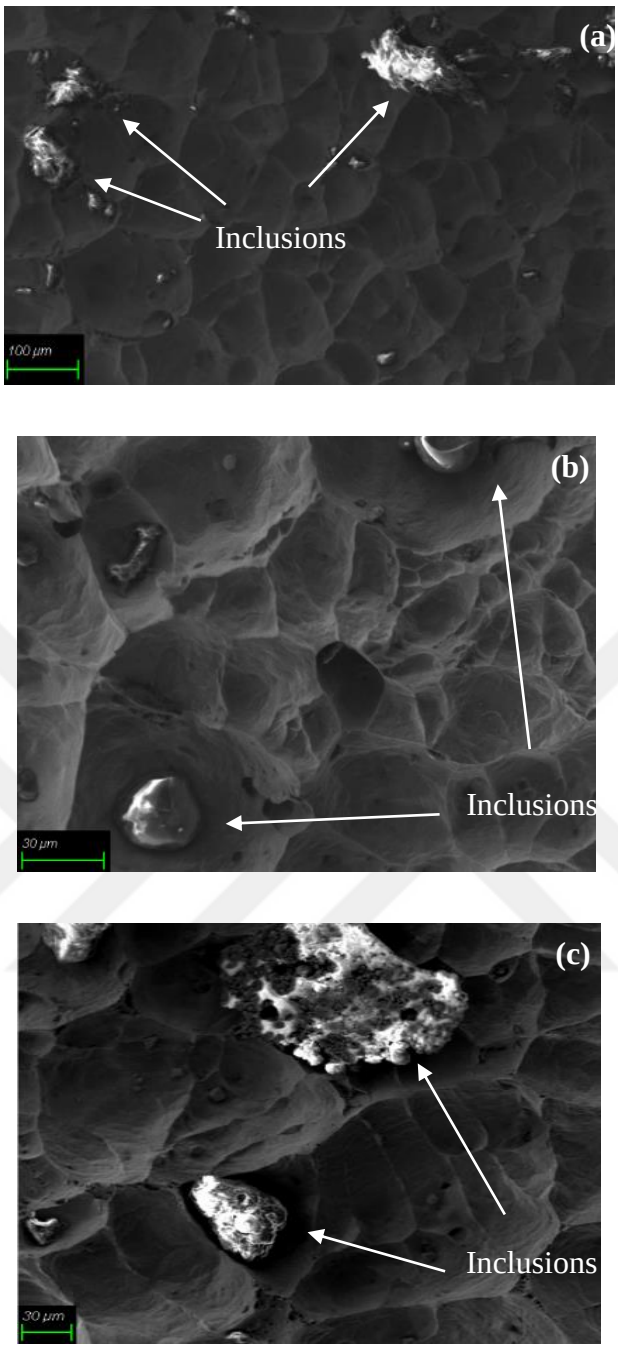

Figure 4.14. SEM images of the fractured tensile test specimens of 316L brazed with 50 (a) and 100 (b) µm copper foil and 304L brazed with 100 µm copper foil (c)

In the SEM and EDS analyses, some particles called as inclusions were detected on the fracture surfaces. The EDS analyses of all fracture surfaces showed that the inclusions contain significant amount of oxygen, carbon, aluminium, zinc, sodium and silicon as given in Figure 4.15, 4.16 and 4.17. It is thought that the fracture was originated from those oxide-based inclusions. These inclusions might be accumulated to brazing

surfaces during the brazing operation due to potential contaminations inside the vacuum furnace.

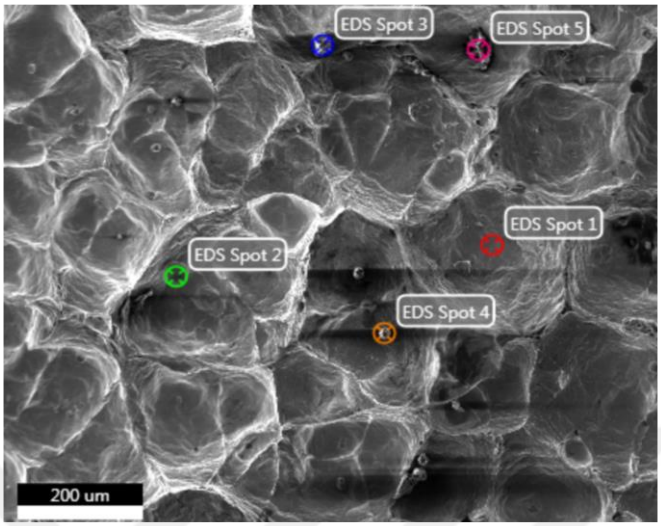

	Element Atomic (%)										
Spot#	Fe	Cu	Cr	Mn	Ni	Zn	O	Al	Si	Na	C
1	-	100.00	-	-	-	-	-	-	-	-	-
2	4.59	2.61	-	-	-	92.8	-	-	-	-	-
3	0.23	-	-	-	-	1.72	34.62	0.83	0.05	-	62.55
4	-	-	0.39	0.61	-	-	59.76	2.36	8.44	-	28.44
5	-	-	-	-	-	-	34.15	-	0.24	1.54	64.07

Figure 4.15. EDS analyses of several spots marked on the fracture surface of 316L 50 μm copper brazed tensile specimen

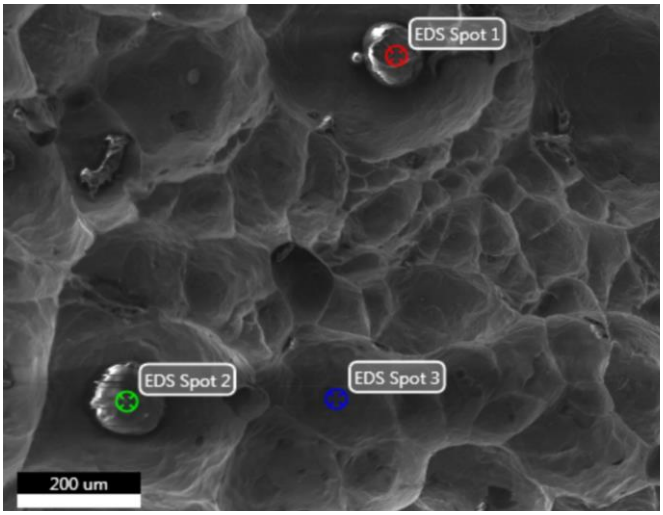

(cont. on next page)

	Element Atomic (%)						
Spot #	Fe	Cu	Mn	Co	O	Si	C
1	-	-	-	-	72.75	11.70	15.55
2	-	-	-	-	86.17	13.83	-
3	9.51	70.62	6.93	8.70	-	-	-

Figure 4.16. EDS analyses of several spots marked on the fracture surface of 316L 100 µm copper brazed tensile specimen

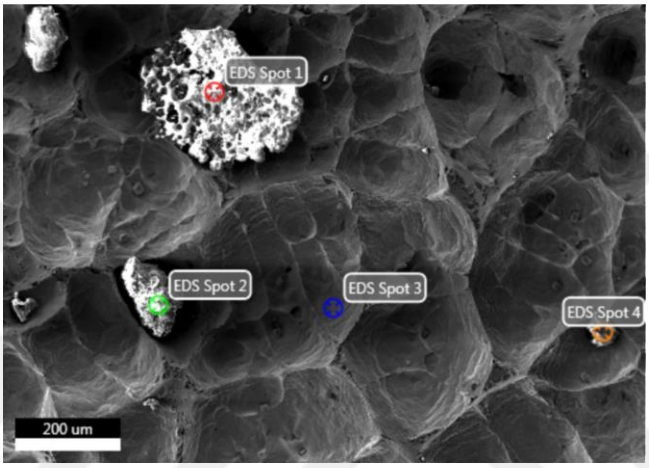

	Element Atomic (%)						
Spot #	Fe	Cu	Zn	Cl	O	Na	C
1	0.45	-	1.26	-	42.17	-	56.13
2	-	56.76	43.24	-	-	-	-
3	-	100.00	-	-	-	-	-
4	-	-	-	0.76	25.73	4.63	68.88

Figure 4.17. EDS analyses of several spots marked on the fracture surface of 304L 100 µm copper brazed tensile specimen

4.3. Fatigue Tests

The displacement controlled fatigue tests of copper brazed stainless steels were performed with twelve specimens at four different load levels for all sample groups which were already given in Table 3.2. Table 4.3, 4.4 and 4.5 show the fatigue test results. The results of two specimens of 316L brazed with 50 µm copper foil and result of one specimen of 316L brazed with 100 µm copper foil specimens were excluded from the

calculations due to premature failures caused by improper brazing of the specimens as also experienced in the tensile tests (those excluded results were highlighted as red in the tables).

Table 4.3. Fatigue test results of 316L brazed with 50 µm copper foil

Sample #	Strain (%)	Displacement (µm)	Failed Cycle	Average
Trial 1	0.3	51	1500000 no fail	-
1	0.35	59	44695	
2	0.35	59	224315	
3	0.35	59	472313	348314
4	0.4	68	277635	
5	0.4	68	44480	
6	0.4	68	314952	212356
7	0.5	85	78920	
8	0.5	85	65170	
9	0.5	85	84296	76129
10	0.6	102	65168	
11	0.6	102	10291	
12	0.6	102	16968	30809

Table 4.4. Fatigue test results of 316L brazed with 100 µm copper foil

Sample #	Strain (%)	Displacement (µm)	Failed Cycle	Average
Trial 1	0.37	63	1500000 no fail	-
Trial 2	0.4	68	1500000 no fail	-
1	0.45	77	55201	
2	0.45	77	606393	
3	0.45	77	597012	601703
4	0.5	85	170759	
5	0.5	85	198417	
6	0.5	85	840675	403284
7	0.55	93	189740	
8	0.55	93	609750	
9	0.55	93	323690	374393
10	0.6	102	35962	
11	0.6	102	78096	
12	0.6	102	29974	48011

Table 4.5. Fatigue test results of 304L brazed with 100 µm copper foil

Sample #	Strain (%)	Displacement (µm)	Failed Cycle	Average
Trial 1	0.3	51	1500000 no fail	-
Trial 2	0.35	60	1500000 no fail	-
1	0.4	77	1111535	
2	0.4	77	1030925	
3	0.4	77	323935	822132
4	0.45	68	257004	
5	0.45	68	307100	
6	0.45	68	194645	252916
7	0.5	85	109105	
8	0.5	85	83005	
9	0.5	85	147025	113045
10	0.6	102	38615	
11	0.6	102	48610	
12	0.6	102	77800	55008

Based on the fatigue test results, a comparison graph was drawn for each sample group as presented in Figure 4.18 and percentage errors of the results are also indicated by error bars for each specimen result. From the graph, it is seen that 316L brazed with 100 µm copper has the highest fatigue life (resistance), 304L brazed with 100 µm copper has the second highest fatigue life and 316L brazed with 50 µm copper has the lowest fatigue life based on the results of the fatigue tests.

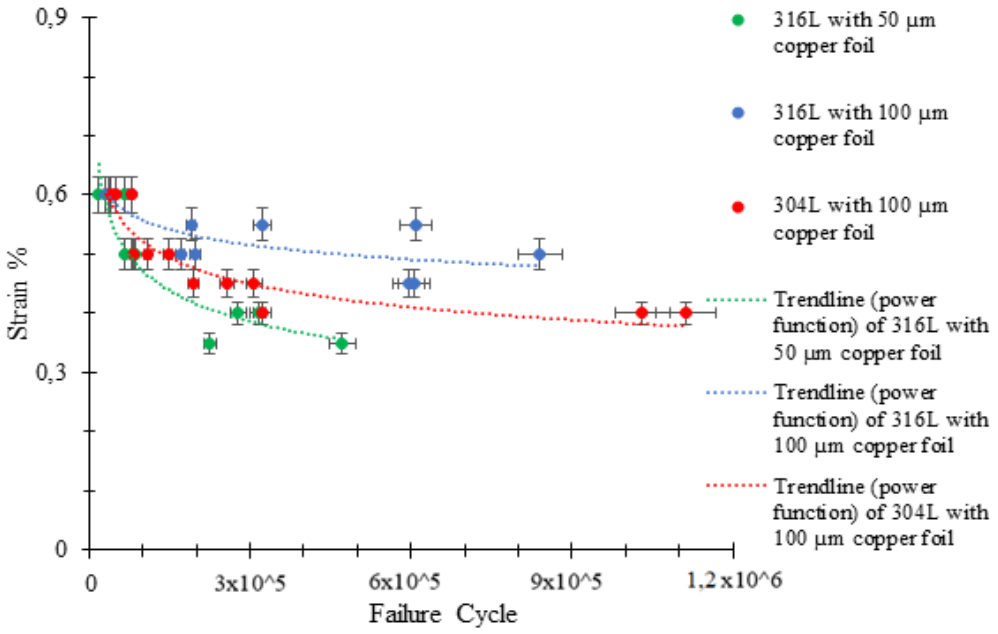

Figure 4.18. Failure cycles of the fatigue test specimens

In order to estimate the fatigue life of the specimens for wider load ranges also by considering suspended test results, Weibull Analyses were performed for each sample group based on the fatigue test results. Weibull Analysis is an approach which is used for conducting life data evaluations based on the measurement or the test results. It is an influential approach for examining the reliability characteristics and trends of a population by using a limited sample size of data which can be taken from a field or laboratory test. It evaluates the life data of the products which contain failures and suspensions. Thereby, trends of the curves can be extrapolated for the wider load levels [56]. In order to perform Weibull Analysis, a commercial software (ReliaSoft Weibull ++/Alta Pro) was used.

In the analysis, Weibull shape parameter of each sample group which is represented by β, were calculated. It defines the types of failure trends. If the value of β is smaller than 1, the behaviour of the failures decreases over the time and increased load level. This indicates an early-failure. If β value is equal to 1, it means that the failure rate is constant over the time and is not affected by applied load level, which is an indication of random failures. Lastly, if β value is higher than 1, it specifies that failure rate increases over the time due to wearing and increased load level [56]. According to the analysis results; β values for 316L stainless steel brazed with 50 and 100 μm copper foil, and 304L stainless steel brazed with 100 μm copper foil were found to be 2.51, 1.40 and 2.75 respectively. Therefore, it can be seen that the failure rate of each sample groups tends to increase over the time and also with increased load levels, which is logical since fatigue failures are time and load dependent.

In the analysis, Inverse Power Law Model was used since it is proposed to model lifetime behaviour of the products which are exposed to non-thermal cyclic stresses. It is used to estimate the lifetime of a product at a load level higher or lower than it is tested. The trend-line of the estimation is shown as a straight line on a log scale graph [57].

The failure cycles and tested loads as % strain were entered as input data to ReliaSoft Weibull Analysis software. Additionally, non-failed specimen data were also included in the analysis as suspensions. After running the analysis, lifetime versus strain plots were generated for each sample group in log scale as shown in Figure 4.19. By using the generated data from those plots, lifetime versus strain % curves were drawn in normal scale as presented in Figure 4.20.

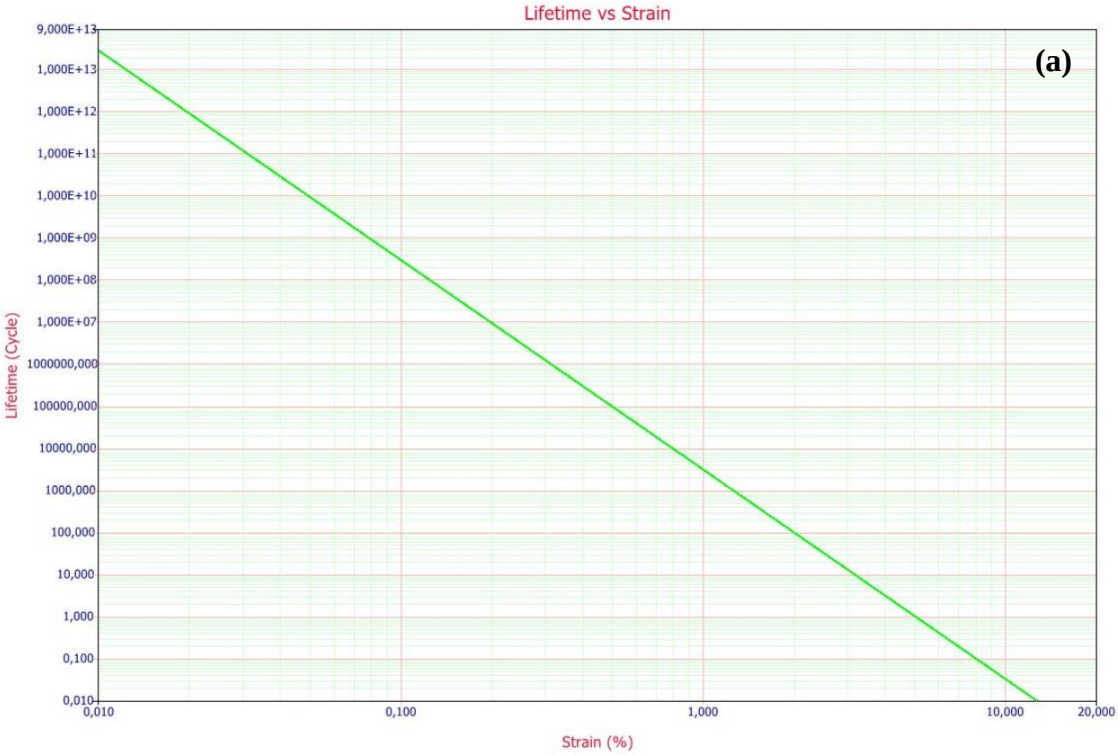

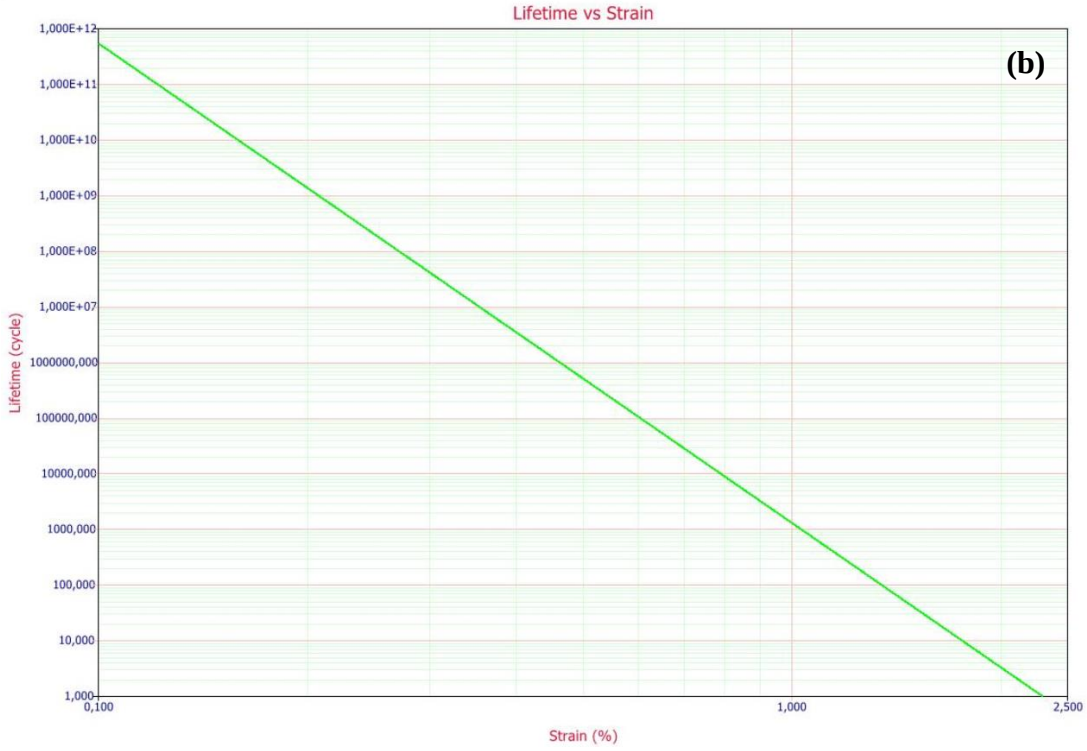

(cont. on next page)

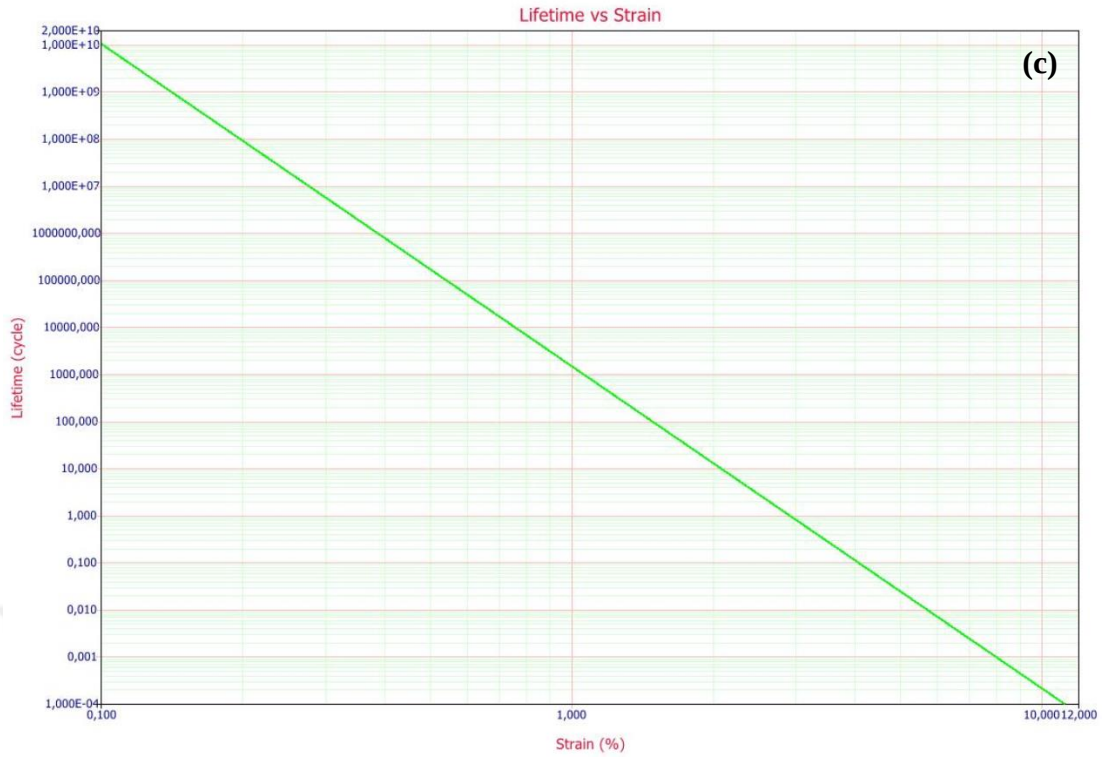

Figure 4.19. Strain vs Lifetime curves of 316L stainless steel brazed with 50 µm copper foil (a), 316L stainless steel brazed with 100 µm copper foil (b) and 304L stainless steel brazed with 100 µm copper foil (c) in log scale

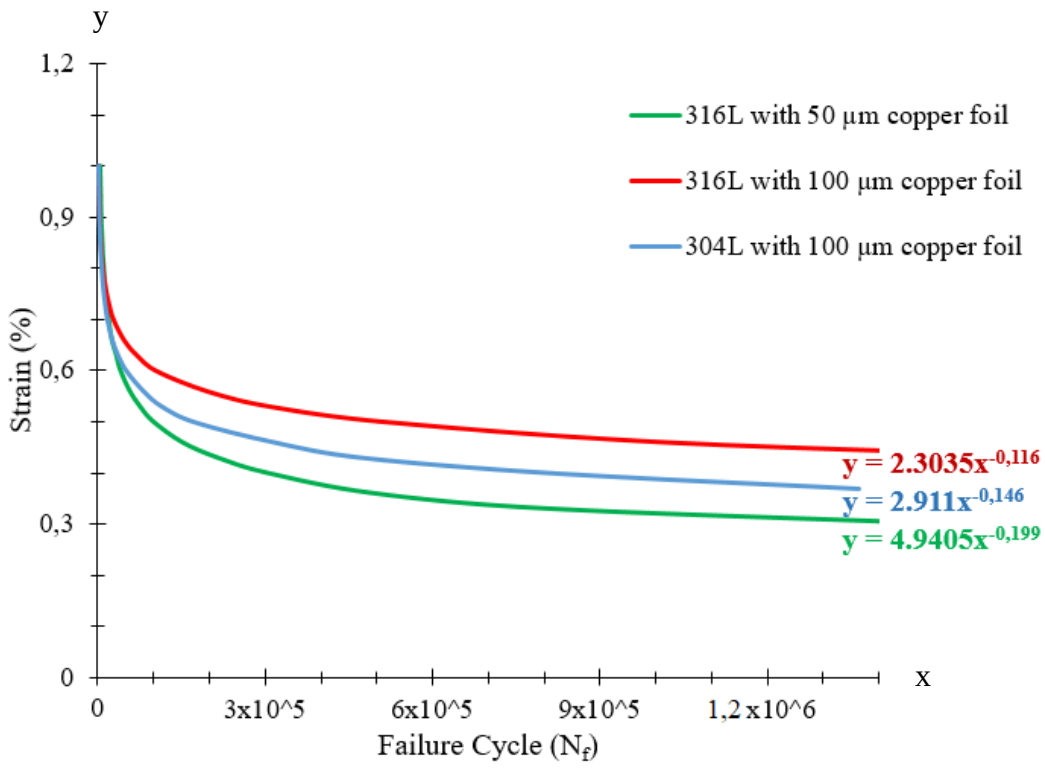

Figure 4.20. Lifetime curves of the tested samples

Overall, the Weibull Analysis results also suggested that 316L has better fatigue life rather than 304L stainless steel joints. On the other hand, it was noticed that brazing filler material thickness has a significant impact on fatigue life since there is a remarkable difference between determined fatigue lives of 316L stainless steels brazed with 50 and 100 μm copper foil samples. Greater brazing metal thickness provides better fatigue life since it is most likely to have less gaps and defects on the brazing region as determined in metallographic investigations.

Fatigue failures are mostly triggered by the dislocation glide in micro structures of materials. During cyclic loading, dislocation motion increases the strain particularly on the critical point of the design, which is the brazing region for the brazed stainless steel specimens. It is most likely that crack was initiated from the inclusions on the brazing region which was detected in the SEM analysis of fractured tensile test specimens as shown in Figure 4.14, and those inclusions are more likely to also be found in fatigue specimens. After the crack was initiated, fracture occurs due to crack propagation. The premature failure of 316L brazed with 50 μm copper foil can be attributed to the insufficient brazing thickness compared to the other sample groups, since the crack growth and propagation reach to a critical state earlier than those of the specimens brazed with 100 μm copper foil. In addition, since it is known that the crack growth rates of AISI 316 and 304 stainless steels are the same at room temperature [58], the diffusion rate of the copper into stainless steels limits the fatigue life of the joints. Thus, premature failure of the 304L compared to that of 316L stainless steel joints brazed with 100 μm copper foil can be ascribed to higher penetration of copper into 316L. This is most likely to be caused by the chemical content differences between 316L and 304L (relatively higher Cr content and absence of Mo in 304L compare to 316L stainless steel).

In Figure 4.20, equations to calculate the % strain on the parts for variable failure cycles are given. By using them, below equations were generated to estimate failure cycles which indicate the fatigue life of parts for given strains, i.e. applied loads.

$$N_f = (3.06).10^3.\varepsilon^{-5.025} \quad (4.1)$$

$$N_f = (1.51).10^3.\varepsilon^{-6.849} \quad (4.2)$$

$$N_f = (1.33).10^3.\varepsilon^{-8.621} \quad (4.3)$$

where, N_f is failure cycle and ε is maximum % strain on the part.

Equation 4.1, 4.2 and 4.3 can be used for estimating the failure cycle of the 316L stainless steel brazed with 50 µm copper foil, 316L stainless steel brazed with 100 µm copper foil and 304L stainless steel brazed with 100 µm copper foil for wider load ranges.

Additionally, the fracture surfaces of the failed fatigue test specimens were investigated after the tests. The fractographs of the tested fatigue specimens are shown in Figure 4.21. Based on the macro investigation by naked eyes, no stretching and necking of the material were observed on the fracture regions of the fatigue specimens. It is obvious that all test specimens were fractured from the brazing joint region where the copper is clearly visible.

a)

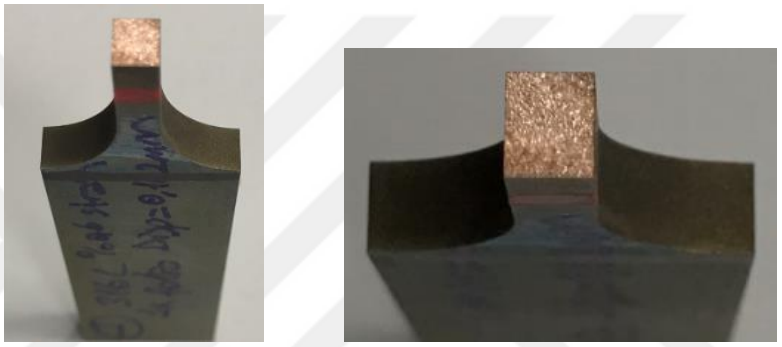

b)

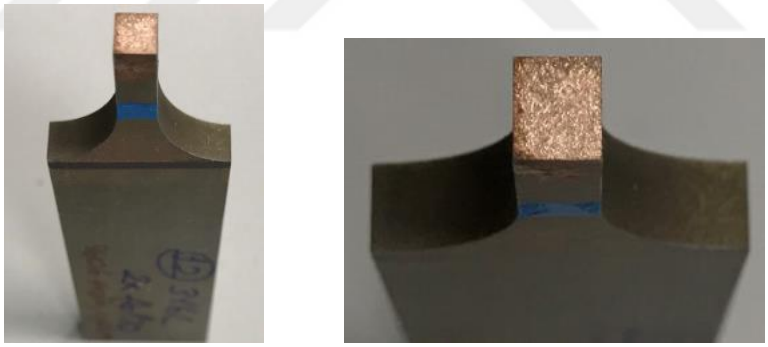

c)

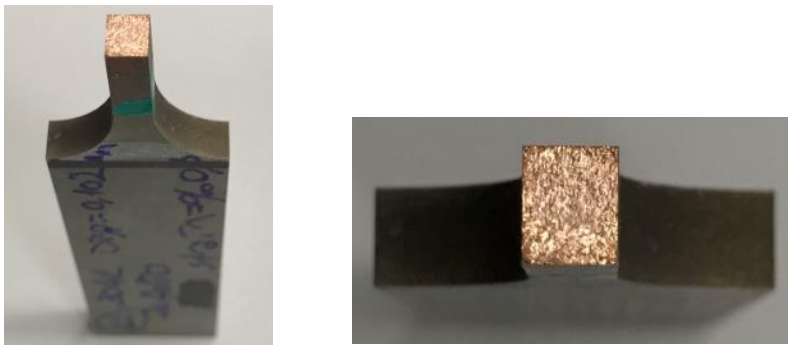

Figure 4.21. Fatigue test specimen fractographs of 316L stainless steel brazed with 50 µm copper (a), 316L stainless steel brazed with 100 µm copper (b) and 304L stainless steel brazed with 100 µm copper (c)

4.4. Finite Element Analysis

In order to model the PHE plates in analysis, the mechanical properties of the both stainless steel plates and brazing points were defined based on the previously determined tensile test results of the non-brazed and brazed specimens, stress based fatigue curves (S-N) of the stainless steels which were obtained from the literature and the strain based fatigue curves of the brazed specimens as input data in FEA. To characterize the fatigue behaviour of the brazed stainless steels, strain life approach was used since the generated lifetime data of brazed specimens are based on the displacement (strain) controlled fatigue test. As explained in Sections 2.2.2 and 3.4; strength coefficient σ_f', ductility coefficient ε_f', ductility exponent c, strength exponent b, cyclic strain hardening exponent n' and cyclic strength coefficient H' were calculated by using Equations 2.11, 2.12, 2.13 and the method which is shown in Figure 2.12.

The strain amplitude versus reversals graphs based on the fatigue test results of the brazed stainless steels were plotted in log scale. The strength coefficient and ductility coefficient were determined from the graphs as shown in Figure 4.22 and 4.23. The ductility and strength exponents for each material were obtained by calculating the slope of the plotted lines. The modulus of elasticity for both 316L and 304L copper brazed stainless steels were calculated previously as given in Table 4.2. Table 4.6 and 4.7 indicate the calculated parameters of the strain life approach for static structural load analysis in ANSYS.

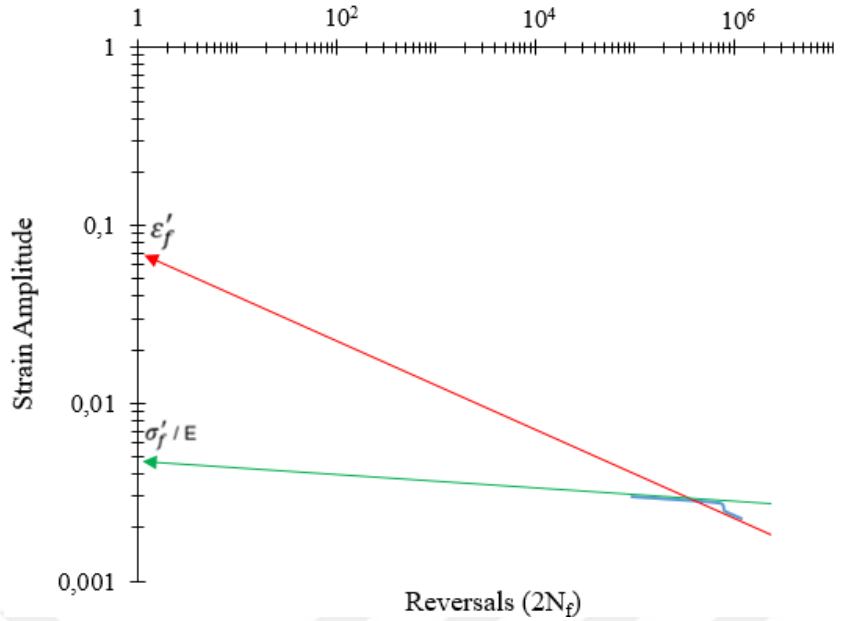

Figure 4.22. Strain amplitude vs reversals graph for 316L 100 µm copper brazed stainless steel based on fatigue test results

Table 4.6. Strain life parameters as inputs to FEA for 316L stainless steel

Parameter	Symbol	Calculation Result
Modulus of Elasticity	E	$(2.08).10^{11}$
Ratio of Strength Coefficient to Modulus of Elasticity	σ_f' / E	0.005
Strength Coefficient	σ_f'	$(9.5).10^{8}$
Ductility Coefficient	ε_f'	0.07
Ductility Exponent	c	-0.39
Strength Exponent	b	-0.09
Cyclic Strain Hardening Exponent	n'	0.23
Cyclic Strength Coefficient	H'	$(1.8).10^{9}$

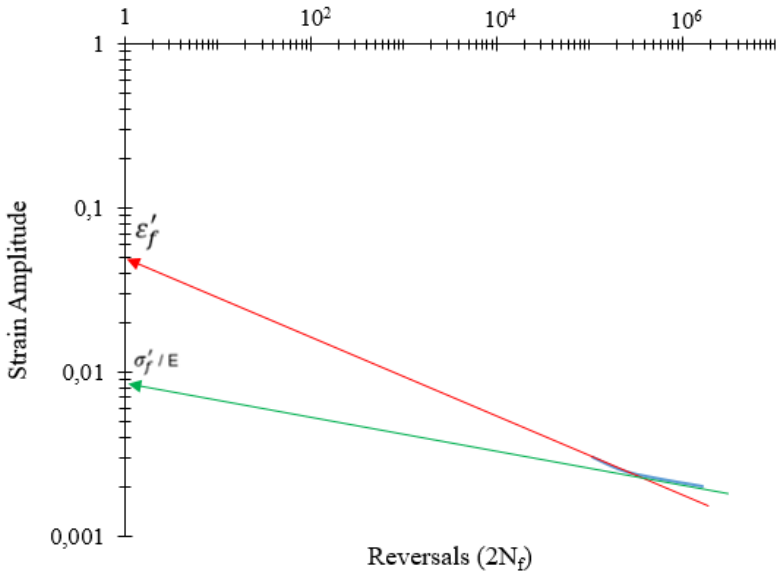

Figure 4.23. Strain amplitude vs reversals graph for 304L 100 µm copper brazed stainless steel based on fatigue test results

Table 4.7. Strain life parameters as inputs to FEA for 304L stainless steel

Parameter	**Symbol**	**Calculation Result**
Modulus of Elasticity	E	$(1.93).10^{11}$
Ratio of Strength Coefficient to Modulus of Elasticity	σ_f' / E	0.0085
Strength Coefficient	σ_f'	$(1.7).10^{9}$
Ductility Coefficient	ε_f'	0.05
Ductility Exponent	c	-0.36
Strength Exponent	b	-0.17
Cyclic Strain Hardening Exponent	n'	0.4
Cyclic Strength Coefficient	H'	$(5.6).10^{9}$

By using these data, FEA to determine the equivalent total strain distribution in brazed 316L and 304L PHE plates were carried out. The simulation results are given in Figure 4.24, 4.25, 4.26 and 4.27. As previously mentioned, the analyses were performed for a concept PHE design of Bosch TT and the pattern on the plates was protected due to ongoing patent approval. Additionally, since the pattern design of the plates is symmetrical, equivalent total strain distribution analyses were performed just for one half of the plates. The other half is accepted to have the same strain distribution result.

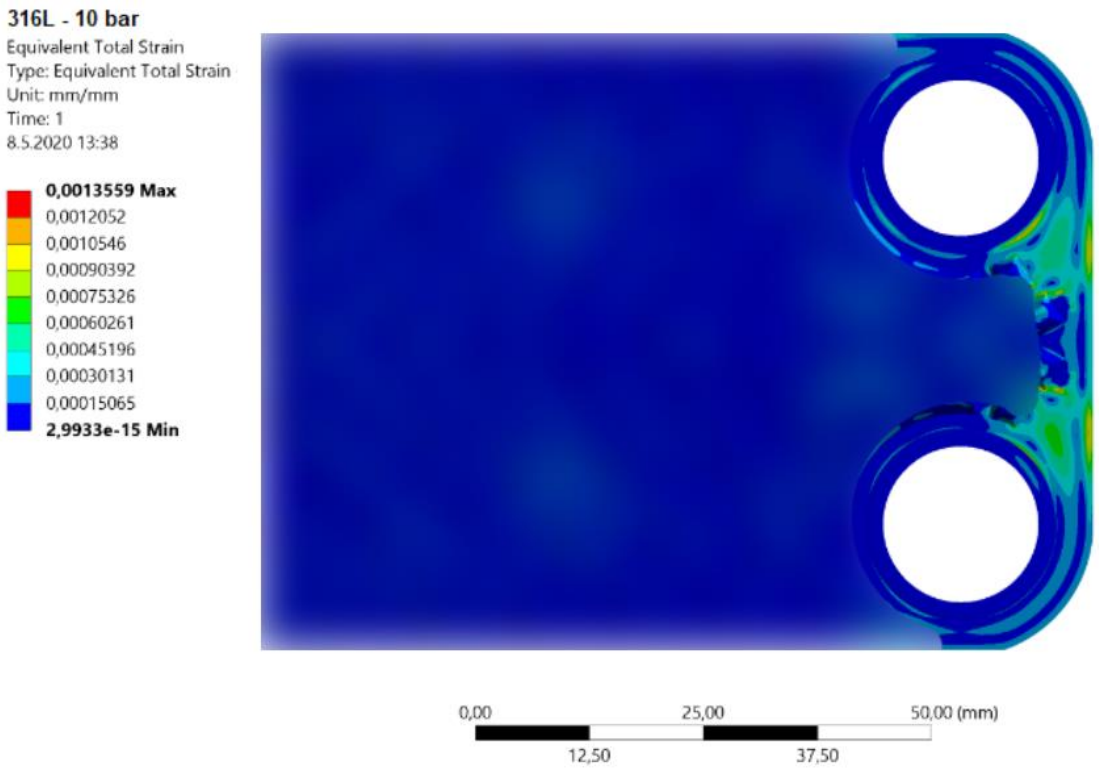

Figure 4.24. Equivalent total strain distribution for 316L stainless steel plate at 10 bar

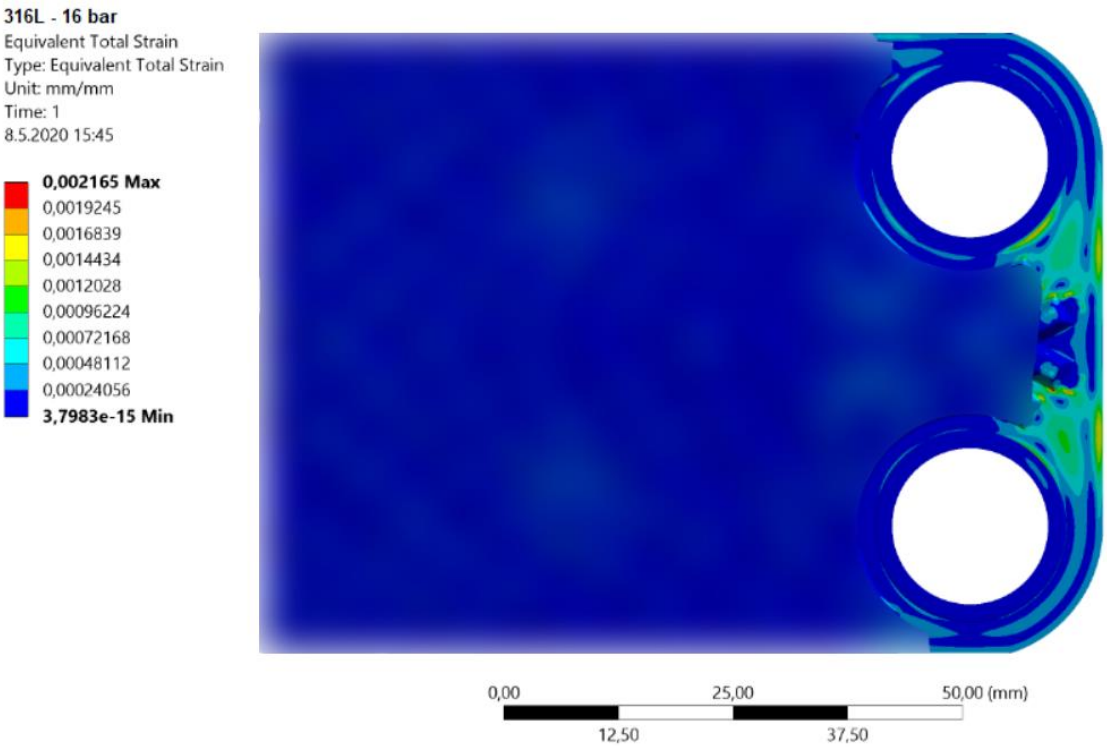

Figure 4.25. Equivalent total strain distribution for 316L stainless steel plate at 16 bar

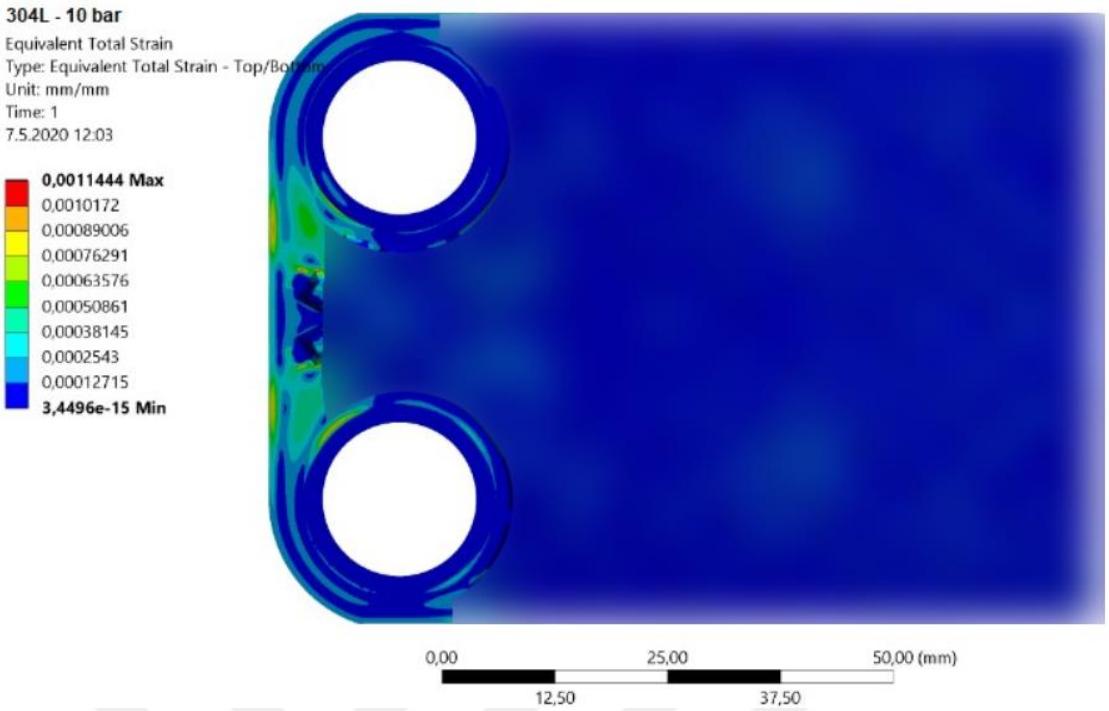

Figure 4.26. Equivalent total strain distribution for 304L stainless steel plate at 10 bar

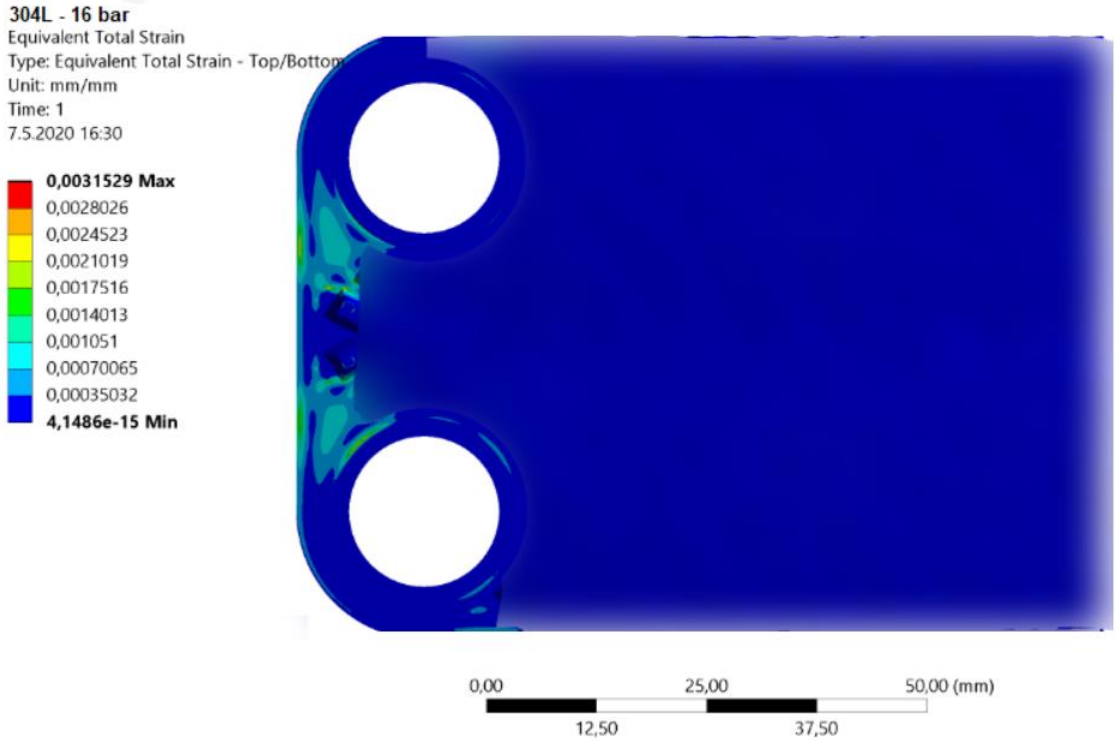

Figure 4.27. Equivalent total strain distribution for 304L stainless steel plate at 16 bar

The equivalent strain distribution on PHE plates were obtained by FEA. The edges of the plates, inlet and outlet holes and the contact points between the plates are the regions where the brazing occurs. These regions were obtained as the areas where the higher strain values were observed. The evaluations of the FEA results were done by considering the sharp edges which were built during modelling of the PHE in ANSYS, and the strain which is located at those points were excluded. The results showed that the determined strain values of both 316L and 304L stainless steel plates are very similar. However, the strain under 16 bar pressure was obtained as slightly higher for 304L compared to 316L brazed stainless steel, which can be ascribed to higher UTS and fatigue life of the 316L brazed stainless steel. The detected maximum strain on the plates are given in Table 5.1.

Table 5.1. Maximum acting strain according to FEA results

Material	Pressure (bar)	Max Strain %
316L	10	0.10
	16	0.19
304L	10	0.10
	16	0.21

Based on the results in Table 5.1, the fatigue lifetimes of the PHEs under 10 and 16 bar pressures were calculated by using Equations 4.1, 4.2 and 4.3. The failure cycles at 10 and 16 bar pressure levels were calculated for 316L stainless steel brazed with 50 μm thick copper foil as $3.24x10^8$ and $1.29x10^7$, for 316L stainless steel brazed with 100 μm thick copper foil as $5.56x10^{11}$ and $2.20x10^9$, and for 304L stainless steel brazed with 100 μm thick copper foil as $1.07x10^{10}$ and as $6.62x10^7$.

The ratio between the failure cycle numbers at 10 and 16 bar pressures for the 316L stainless steel brazed with 50 μm thick copper foil was calculated by dividing them to each other as; $(3.24 \times 10^8) / (1.29 \times 10^7) = 25.12$. Therefore, the impact of 180000 cycles at 10 bar pressure peaks on the fatigue life of the PHE is equal to 180000 / 25.12 = 7167 cycles at 16 bar pressure peaks. Consequently, the required cycle number to fulfil 15 years of lifetime based on 16 bar pressure peak number was estimated to be 120000 + 7167 = 127167 cycles for 316L stainless steel brazed with 50 μm thick copper.

The ratio between the failure cycle numbers at 10 and 16 bar pressures for the 316L stainless steel brazed with 100 μm thick copper foil was calculated by following the same procedure as; $(5.56 \times 10^{11}) / (2.20 \times 10^{9}) = 252.73$. Thus, the impact of 180000 cycles at 10 bar pressure peaks on the fatigue life of the PHE is equal to 180000 / 252.73 = 712 cycles at 16 bar pressure peaks. As a result, the required cycle number to fulfil 15 years of lifetime for 16 bar pressure peak number was estimated to be 120000 + 712 = 120712 for 316L stainless steel brazed with 100 μm thick copper.

Finally, the ratio between the failure cycles at 10 and 16 bar pressures for the 304L stainless steel brazed with 100 μm thick copper foil was calculated as; $(1.07 \times 10^{10}) / (6.62 \times 10^{7}) = 161.63$. Thereby, the impact of 180000 cycles at 10 bar pressure peaks on the fatigue life of the PHE is equal to 180000 / 161.63 = 1114 cycles at 16 bar pressure peaks. To conclude, it was obtained that the required cycle number to fulfil 15 years of lifetime for 16 bar pressure peak number was estimated to be 120000 + 1114 = 121114 for 304L stainless steel brazed with 100 μm thick copper.

Furthermore, if the ratio between the calculated fatigue life of the 316L brazed with 100 and 50 μm copper samples is accepted as an assumption also for 304L copper brazed stainless steel to evaluate the impact of copper foil thickness on 304L fatigue behaviour, the fatigue life estimation for the 304L stainless steel brazed with 50 μm thick copper foil can also be done by applying a linear interpolation. The ratio was calculated by dividing the estimated failure cycles of the 316L specimens at 16 bar pressure as $(2.20 \times 10^{9}) / (1.29 \times 10^{7}) = 170.54$. Thus, the fatigue lifetime of the 304L brazed with 50 μm thick copper can be estimated by diving the defined fatigue life of the 304L brazed with 100 μm thick copper to the calculated ratio as $(6.62 \times 10^{7}) / 170.54 = 388179$ cycles. And, the required 16 bar pressure cycle number which has to be fulfilled to have 15 years lifetime, can also be calculated by following the same approach. Equivalent 16 bar pressure cycle number at 10 bar pressure for the 304L 50 μm thick brazed PHE was calculated to be; 7167 / 712 x 1114 = 11214 cycles. Consequently, the number of 16 bar pressure cycle over 15 years for the 304L 50 μm thick copper brazed PHE was estimated to be 120000 + 11214 = 131214.

As Table 5.2 presents, the calculated failure cycles of the all sample types are much higher than the operating pressure cycles which means that the analysed PHE design is safe to be used against mechanical fatigue. Hence, no failure due to mechanical fatigue is expected during 15 years of lifetime operation of the analysed PHE.

Table 5.2. Required 16 bar water hammer cycles to fulfil 15 years of lifetime and the estimated lifetime of the PHE based on the loads determined by FEA

PHE Material	**Water hammer 16 bar pressure peaks during 15 years (cycle)**	**Calculated lifetime for 16 bar pressure load (cycle)**
316L 50 µm brazed	127167	$1.29x10^7$
316L 100 µm brazed	120712	$2.20x10^9$
304L 100 µm brazed	121114	$6.62x10^7$
304L 50 µm brazed	131214	388179

CHAPTER 5

CONCLUSION

Within the aim of this thesis, the fatigue life of the copper brazed 316L and 304L stainless steels were investigated by testing and analysing three different sample groups which are 316L stainless steel brazed with 50 and 100 μm copper foils, and 304L stainless steel brazed with 100 μm copper foil. Thereby, fatigue lives of the brazed 316L and 304L grade stainless steels were determined and the effect of the filler material thickness on the fatigue life of the PHE was evaluated. The fatigue life curves of the copper brazed 316L and 304L stainless steels were constructed to estimate the lifetime of the PHE designs. These curves can be used for various PHE designs to estimate their lifetime by means of FEA.

1. The microscopic investigation of the brazed samples were carried out by using optical microscope and SEM. It was shown that 50 μm copper foil does not provide a sufficient brazing as 100 μm copper foil provides. This causes the formation of the brazing gaps and those brazing defects affect the fatigue life of the material negatively. It was also suggested that the copper diffuses throughout the grains of 316L stainless steel relatively higher than those of 304L stainless steel.

2. In SEM analysis, it was observed that copper penetrated properly into the steels and formed a brazing layer. The average copper brazing thicknesses of both 316L stainless steel joints produced by using 50 and 100 μm foils were measured to be around 20 μm. On the other hand, it was measured to be around 58 μm for 304L stainless steel joint although the inserted amount of the copper was 100 μm before the brazing. These may imply that a significant amount of copper foil was drifted away from the brazing region during the brazing process due to applied vacuum. Also, the difference of the copper brazing thicknesses of 316L and 304L joints which were brazed by 100 μm copper foil, can be ascribed to relatively higher diffusion rate and penetration of the copper into 316L rather than 304L stainless steel.

3. The mechanical properties of non-brazed and copper brazed 316L and 304L stainless steels were examined by performed tensile tests. Fracture strain of non-brazed test specimens were found as higher than those of reported values in literature as given in Table 1.1, which is most likely the result of the annealing of stainless steels during the brazing. The mechanical properties of the 316L and 304L 100 μm copper brazed stainless steels were detected as mostly similar to each other, just yield strength and UTS values of 316L were slightly higher than those of 304L brazed with 100 μm copper foil samples. On the other hand, 316L stainless steel brazed with 50 μm copper foil has relatively lower UTS and fracture strain. In comparison of the tensile test results of non-brazed and brazed specimens, slight decreases on UTS, yield strength and yield strain were obtained in brazed specimen results. Besides, fracture strain of the brazed stainless steel joints was remarkably lower than those of non-brazed ones which proves that ductility of the materials was lost by brazing.

4. Displacement (strain) controlled fatigue tests were performed for three sample groups with twelve specimens per each. Results of the fatigue tests were evaluated by performing Weibull Analysis, and the fatigue life curves based on % strain were plotted to estimate the failure cycles for loads in wider ranges. It was determined that copper brazed 316L stainless steel has 33 times greater fatigue life than copper brazed 304L stainless steel in average. Also, it was noticed that the brazing filler metal thickness is most likely to have a linear relationship with fatigue life of the material. Decreasing the filler material thickness to half of it has a worse impact on the lifetime of the PHE rather than changing its material from 316L to 304L stainless steel.

5. FEA were performed for a concept PHE which were designed by using both copper brazed 316L and 304L stainless steel plates, in order to examine the equivalent total strain distribution on the plates during water hammer pressure cycling. Failure cycles of each sample group were estimated by using fatigue life curves based on determined strain values by the FEA. Consequently, it was noticed that the estimated failure cycles for each sample group are higher than the required lifetime of the PHE designs since the determined strain values on the PHE plates in FEA are in the portion of infinite lifetime of the generated lifetime curves. All sample groups are safe to be used as PHE material and satisfy the 15

years of lifetime requirement of Bosch TT which means 304L stainless steel can also be used as an alternative PHE material to 316L stainless steel based on the fatigue life estimation.

6. 16 bar pressure level has remarkably high impact on the fatigue life of PHE compare to 10 bar pressure level because the acting loads at 10 bar is respectively low according to FEA results. Therefore, 10 bar pressure cycles can be converted to 16 bar pressure cycles in order to decrease the testing duration of the produced PHEs in Bosch TT (Bosch TT internal lifetime test).
7. As a future work, the effect of the corrosion on the fatigue life of the PHE (corrosion fatigue) can also be investigated by evaluating the corrosion resistances of 316L and 304L copper brazed stainless steels.

REFERENCES

[1] https://www.remeha.co.uk/Legislation-support/Energy-efficiency/Why-is-energy-efficiency-important. [Accessed 02.01.2020].

[2] https://www.worcester-bosch.co.uk/products/boilers/explained. [Accessed 21.12.2019].

[3] https://smarterhouse.org/heating-systems/types-heating-systems. [Accessed 02.01.2020].

[4] Y. Gurler, "Numerical Investigation of Structural Behaviour of Brazed Plate Heat Exchanger," in *36. CADFEM ANSYS Simulation Conference*,, Leipzig, 2018.

[5] G. F. Hewitt, G. L. Shires and T. R. Bott, Process Heat Transfer, New York: CRC Press, Begell House, 1994.

[6] Y. Gurler, "Design and Mechanical Behaviour of Brazed Plate Heat Exchangers (M. Sc. Thesis)," Izmir Institute of Technology, Izmir, 2018.

[7] https://www.gea.com/tr/binaries/plate-heat-exchanger_tcm47-41906.png. [Accessed 22.12.2019].

[8] T. Uhlig, V. Fedorov, M. Elßner, G. Wagner and S. Weis, "Reduction of liquid metal embrittlement in copper-brazed stainless steel joints," in *19th Chemnitz Seminar on Materials Engineering*, Chemnitz, 2017.

[9] Bosch Thermotechnology Ltd., "LH01 Pressure Cycling Durability of Hydraulic Components and Parts in Domestic Water Circuit (Bosch Confidential Data)," Bosch Thermotechnology Ltd., Wernau, 2010.

[10] https://www.ajdesigner.com/phpwaterhammer/pressure_increase_equation.php. [Accessed 19.04.2020].

[11] Kiwa Nederland B.V., "Evaluation Guideline regarding the Product Certificate GASKEUR label CW/HRww (Comfort Hot Water-High Efficiency, Hot Water)," 2011.

[12] J. Schijve, “Fatigue of structures and materials in the 20th century and thestate of the art,” *International Journal of Fatigue,* vol. 25, 679–702, 2003.

[13] https://www.linearmotiontips.com/mechanical-properties-of-materials-stress-and-strain. [Accessed 19.01.2020].

[14] W. D. Callister, Materials Science and Engineering, An Introduction, New York: John Wiley & Sons, Inc., 2007.

[15] https://www.quora.com/Why-do-we-use-0-2-offset-in-aluminum-stress-strain-curve. [Accessed 19.01.2020].

[16] T. I. M. S. H. N. M. T. Takahiro Morishita, "Multiaxial fatigue property of Ti–6Al–4V using hollow cylinder specimen under push-pull and cyclic inner pressure loading," *International Journal of Fatigue,* vol. 87, 370-380, 2016.

[17] http://www.engineeringarchives.com/les_mom_offsetyieldmethod.html. [Accessed 17.05.2020].

[18] Y. Suezawa, “Effects of Surface Roughness on the Fatigue,” *Transactiens ef the Japan Welding Society, Vol. T,Ne. 2,* 1976.

[19] B. L. a. R. P. W. E. J. DOLLEY, "The effect of pitting corrosion on fatigue life," *Fatigue and Fracture of Engineering Materials and Structures,* 555-560, 2000.

[20] B. Parida, “Fatigue Testing,” in *Encyclopedia of Materials: Science and Technology*, New York, Elsevier, 2001, 2994-2999.

[21] https://www.testresources.net/applications/test-types/fatigue-test/. [Accessed 08.02.2020].

[22] A. A. Azeez, “Fatigue Failure and Testing Method,” HAMK University of Applied Science, Hämeenlinna, 2013.

[23] A. Ameed, "Study of Fatigue Fractography of Mild Steel Used in Automotive Industry," *Al-Khwarizmi Engineering Journal,* vol. 15, 82-88, 2018.

[24] A. F. R. R. S. H. O. F. Ralph I. Stephens, Metal Fatigue in Engineering, John Wiley & Sons, 2000.

[25] G. Glinka, “The Local Stress-Strain Fatigue Method,” efatigue.com, 2010.

[26] D. F. Socie, "Fatigue and Fracture (Basic Course)," Department of Mechanical Science and EngineeringUniversity of Illinois at Urbana-Champaign , Illinois, 2009.

[27] https://www.marlinwire.com/blog/is-316-stainless-steel-worth-the-extra-cost-over-304. [Accessed 11.04.2020].

[28] https://www.steeltank.com/Portals/0/Pressure Vessels/SSWseminarOct2012/Relative Cost 4 15 2012.pdf [Accessed 11.04.2020].

[29] R. Steiner, AISI Type 316L Stainless Steel, Ohio: American Society for Metals, 1990.

[30] P. D. Harvey, Engineering Properties of Steel, Ohio: American Society for Metals , 1982.

[31] W. Tillmann, T. Henning and L. Wojarski, “Vacuum brazing of 316L stainless steel based on additively manufactured and conventional material grades,” in *IOP Conf. Series: Materials Science and Engineering 373 012023*, Dortmund, 2018.

[32] M. P. Groover, Fundamentals of Modern Manufacturing, New Jersey: JOHN WILEY & SONS, INC, 2010.

[33] J. Kowalewski and J. Szczurek, “Issues in vacuum brazing,” ASM International, Dallas, 2006.

[34] M. M. Schwartz, Brazing, Ohio: ASM International, 2003.

[35] K. A. Mohammad1, A. Ali, B. B. Sahari and S. Abdullah, “Fatigue behavior of Austenitic Type 316L Stainless Steel,” *Materials Science and Engineering 36,* 2012.

[36] X. Zhao, “Fatigue Properties of 316L Stainless Steel,” *Applied Mechanics and Materials ISSN: 1662-7482, Vols. 204-208, 3786-3789,* 2012.

[37] G. Benjamin, U. Akira, S. Tatsuo, T. Masahiro and I. Yu, “Effect of Loading Frequency in Fatigue Properties and Micro-Plasticity,” *13th International Conference on Fracture 16-21,* 2013.

[38] S. H. Lambertsen, L. Damkilde, A. S. Kristensen and R. R. Pedersen, “Estimation of Fatigue Life of Laser Welded AISI304 Stainless Steel T-Joint Based on Experiments and Recommendations in Design Codes,” *World Journal of Mechanics,* 2013.

[39] J.-Y. Huang, J.-J. Yeh, S.-L. Jeng, C.-Y. Chen and R.-C. Kuo, “High-Cycle Fatigue Behavior of Type 316L Stainless Steel,” *Materials Transactions, Vol. 47, No. 2 409-417,* 2006.

[40] W. Jiang, J. Gong and S. Tu, “The effect of filler metal thickness on tensile strength for a stainless steel plate – fin structure has been studied by experiments and finite element method,” *Material and Design: 2387-2396,* 2010.

[41] y. Li, X. Zhang, D.Parfitt, S. Jones and B. Chen, “Characterization of microstructure, defect and high cycle fatigue behavior in a stainless steel joint processed by brazing,” *Material Characterization 151 542-552,* 2019.

[42] M. Koster, C. Kenel, A. Stutz, W. Lee, A. Lis, C. Affolter and C. Leinenbach, “Fatigue and Cyclic Deformation Behavior of Brazed Steel Joints,” *Materials Science & Engineering A 581 90-97,* 2013.

[43] A. Schmiedt, J. Simon, M. Matthias, T. Wolfgang and W. Frank, “Tensile and fatigue assessmentsof brazed stainless steel joints using digital image correlation,” *MATEC Web of Conferences 165, 06003,* 2018.

[44] ASTM International, “Standard Test Methods for Tension Testing of Metallic Materials Designation: E 8/E 8M – 08,” ASTM International, Pennsylvania, 2008.

[45] ASTM International, “Standard Practice for Strain-Controlled Fatigue Testing Designation: E 606 – 92 (Reapproved 1998),” ASTM International, Pennsylvania, 1998.

[46] https://www.nanoscience.com/techniques/scanning-electron-microscopy/components/. [Accessed 14.02.2020].

[47] S. Kalpakjian and S. R. Schmid, Manufacturing Engineering and Technology, Prentice Hall, Pearson, 2009.

[48] https://www.thoughtco.com/metallographic-etching-2340003. [Accessed 14.02.2020].

[49] ASTM International, "Standard Practice for Microetching Metals and Alloys," ASTM International, Pennsylvania, 2015.

[50] BS ISO, “Metallic materials — Fatigue testing — Statistical planning and analysis of data BS ISO 12107:2003,” BS ISO, 2003.

[51] G. L. S. Omesh Chopra, "Effect of LWR Water Environments on the Fatigue Life of Reactor Materials," United States Nuclear Regulatory Commission, Illinois, 2018.

[52] North American Stainless, “Long Products Stainless Steel Grade Sheet - AISI 304L,” North American Stainless, 2020.

[53] R. L. P. P. R. R. Angelo Fernando Padilha, "Stainless steels heat treatment (Chapter 12)," in *Steel Heat Treatment Handbook. Second Edition*, Taylor & Francis Group, 2006, 695-735.

[54] https://www.phase-trans.msm.cam.ac.uk/abstracts/annealing.twin.html. [Accessed 06.01.2020].

[55] Y. Jin, "Annealing twin formation mechanisms (Doctoral Thesis)," l’École nationale supérieure des mines de Paris , Paris, 2014.

[56] https://quality-one.com/weibull/. [Accessed 28.04.2020].

[57] ReliaSoft Corporation, "Accelerated Life Testing Reference," ReliaSoft, Arizona, 2015.

[58] I. Virkkunen, “Thermal Fatigue of Austenitic and Duplex Stainless Steels (DSc Thesis),” Helsinki University of Technology, Helsinki, 2001.